Maejo International Journal of Science and Technology
Volume 2, Issue 3 August – December 2008

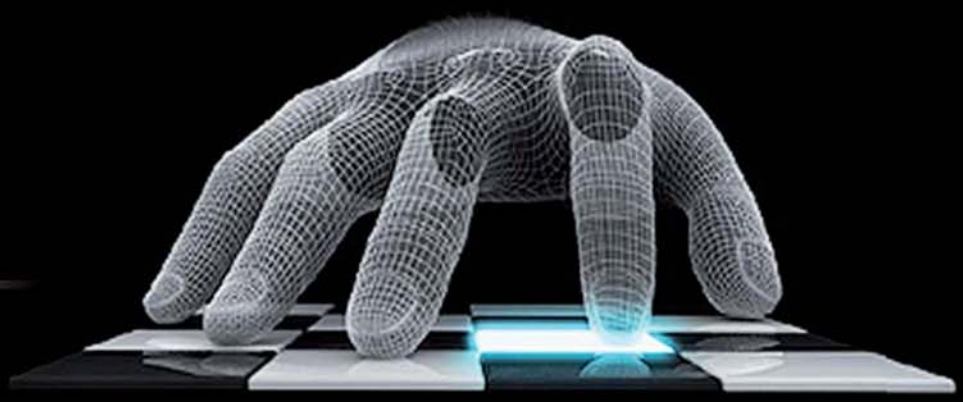

Coverage by Abstracting Service : This journal is covered by Science Citation Index Expanded (SciSearch), Journal Citation Reports/Science Edition, Zoological Record, SciFinder Scholar, Chemical Abstracts and DOAJ.

Available online at **www.mijst.mju.ac.th**

ISSN : 1905-7873

Maejo International Journal of Science and Technology
Volume 2 Issue 3 August – December 2008 ISSN : 1905-7873

Journal Information

Maejo International Journal of Science and Technology (ISSN 1905-7873 © 2008), the international journal for the rapid publication of all preliminary communication in Science and Technology is the first peer-refereed scientific journal of Maejo University (www.mju.ac.th). Intended as a medium for communication, discussion, and rapid dissemination of important issues in Science and Technology, articles are initially published online in an open access format, thereby giving authors the chance to communicate with a wide range of readers in an international community.

Publication Information

MIJST is published triannually. Articles are available online and can be accessed free of charge at http://www.mijst.mju.ac.th. Printed and bound copies of each volume are produced and distributed to authors and selected groups or individuals.

Abstracting/Indexing Information

MIJST is covered and cited by Science Citation Index Expanded (SciSearch®), Journal Citation Reports/Science Edition, Zoological Record, Directory of Open Access Journals (DOAJ), SciFinder Scholar, and Chemical Abstract Service (CAS).

Contact Information

Editorial office : Maejo International Journal of Science and Technology (MIJST), 1st floor, Orchid Building, Maejo University, San Sai, Chiang Mai 50290, Thailand
Tels : +66-53-87-3880, Fax : +66-53-87-3880
E-mail: duang@mju.ac.th

MAEJO INTERNATIONAL JOURNAL OF SCIENCE AND TECHNOLOGY

The International Journal for the Rapid Publication of Preliminary Communications in Science and Technology

http://www.mijst.mju.ac.th
ISSN 1905-7873

MAEJO INTERNATIONAL JOURNAL OF SCIENCE AND TECHNOLOGY
Volume 2, Issue 3 (August –December 2008)

CONTENTS

ISSN 1905-7873 © 2008 by Maejo University

MAEJO INTERNATIONAL JOURNAL OF SCIENCE AND TECHNOLOGY

Volume 2, Issue 3 (August –December 2008)

Author Index

ISSN 1905-7873 © 2008 by Maejo University

Instructions for Authors

Manuscript Preparation

Manuscripts should be prepared in English using a word processor. MS Word for Macintosh or Windows, and .doc or .rtf files are preferred. Manuscripts may be prepared with other software, provided that the full document (with figures, schemes and tables inserted into the text) is exported to a MS Word format for submission. Times or Times New Roman font is preferred. The font size should be 12 pt. and the line spacing "at least" 17 pt. The printing area is 17.5cm x 24.7cm (6.9" x 9.73"). For A4 paper, margins must be 1.5 cm on top, 3.5cm at the bottom and 1.75 cm on both left and right sides of the paper. For US letter-sized paper, margins must be 1.5 cm (0.59") on top, 1.74 cm (0.68") at the bottom and 2.05 cm (0.8") on both left and right sides. Although our final output is in .pdf format, authors are asked NOT to send manuscripts in this format as editing them is much more complicated.

Authors' full mailing addresses, homepage addresses, phone and fax numbers, e-mail addresses and homepages can be included in the title page and these will be published in the manuscripts and the Table of Contents. The corresponding author should be clearly identified. It is the corresponding author's responsibility to ensure that all co-authors are aware of and approve of the contents of a submitted manuscript.

A brief (200 word maximum) Abstract should be provided. The use in the Abstract of numbers to identify compounds should be avoided, unless these compounds are also identified by names.

A list of three to five keywords must be given, and placed after the Abstract. Keywords may be single words or very short phrases.

Although variations in accord with a manuscript's contents are permissible, in general all papers should have the following sections: Introduction, Materials and Methods, Results and Discussion, Conclusions, Acknowledgments (if applicable), and References.

Authors are encouraged to prepare figures and schemes in colour. Full colour graphics will be published free of charge.

Tables should be inserted into the main text, and numbers and titles supplied for all tables. All table columns should have an explanatory heading. To facilitate layout of large tables, smaller fonts may be used, but in no case should these be less than 10 pt. in size. Authors should use the Table option of MS Word to create tables, rather than tabs, as tab-delimited columns are often difficult to format in .pdf for final output.

Figures and schemes should also be placed in numerical order in the appropriate place within the main text. Numbers, titles and legends should be provided for all schemes and figures. These should be prepared as a separate paragraph of the main text and placed in the main text before the figure or scheme. Chemical structures and reaction schemes should be drawn using an appropriate software package designed for this purpose. As a guideline, these should be drawn to a scale such that all the details and text are clearly legible when placed in the manuscript (i.e. text should be no smaller than 8-9 pt.).

For bibliographic citations the reference numbers should be placed in square brackets, i.e. [ ], and placed before the punctuation, for example [4] or [1-3], and all the references should be listed separately and as the last section at the end of the manuscript.
(Download template file at www.mijst.mju.ac.th)

Format for References

Journal:

1. D. Buddhasukh, J. R. Cannon, B. W. Metcalf, and A. J. Power, "Synthesis of 5-n-alkylresorcinol dimethyl ethers and related compounds via substituted thiophens", Aust. J. Chem., 1971, 24, 2655-64.
Text:

2. A. I. Vogel, "A Textbook of Practical Organic Chemistry", 3rd Edn., Longmans, London, 1956.

Chapter in an Edited Text:

3. P. H Gore, in "Friedel-Crafts and Related Reactions" (Ed. G. A. Olah), Vol. 3, Interscience, London, 1964, Ch. 31.

Thesis / Dissertation:

4. W. phutdhawong, "Isolation of glycosides by electrolytic decolourisation and synthesis of pentinomycin", PhD. Thesis, 2002, Chiang Mai University, Thailand.

Patent:

5. K. Miwa, S. Maeda, and Y. Murata, " Purification of Stevioside by Electrolysis", Jpn. Kokai Tokkyo Koho 79 89,066 (1979).

Referees

A list of referees (with their affiliations and e-mail addresses) should be supplied, although they may not necessarily be approached. At least 3 persons (one or more non-native) should be in the list, and they should not come from the same institution.

English correction

This journal is published in English, so it is essential that for proper refereeing and quick publication all manuscripts be submitted in grammatically correct English and style. For this purpose we ask that non-native English authors ensure that their manuscripts are checked before submitting them for consideration. We suggest that for this purpose your manuscript be revised by an English speaking colleague before submission.

Submission

Manuscripts should be submitted to the editor by e-mail: duang@mju.ac.th

Maejo International Journal of Science and Technology

ISSN 1905-7873

Available online at www.mijst.mju.ac.th

Review

Recent trends in silicon carbide device research

Munish Vashishath[1,*] and Ashoke K. Chatterjee[2]

[1] Department of Electrical and Electronics Engineering, YMCA Institute of Engineering, Faridabad, India 121006

[2] Department of Electronics and Communication Engineering, Thapar Institute of Engineering and Technology, Patiala, India, 147004

[*] Author to whom correspondence should be addressed, e-mail: 1munish.vashishath@gmail.com

Received: 15 March 2008 / Accepted: 28 July 2008 / Published: 4 August 2008

Abstract: Silicon carbide (SiC) has revolutionised semiconductor power device performance. It is a wide band gap semiconductor with an energy gap wider than 2eV and possesses extremely high power, high voltage switching characteristics and high thermal, chemical and mechanical stability. The SiC wafers are available in 6H, 4H, 2H and 3C polytypes. Because of its wide band gap, the leakage current of SiC is many orders of magnitude lower than that of silicon. Also, forward resistance of SiC power devices is approximately 200 times lower than that of conventional silicon devices. The breakdown voltage of SiC is 8-10 times higher than that of silicon. In this paper, silicon carbide Schottky barrier diodes, power MOSFETs, UMOSFET, lateral power MOSFET, SIT (static inductiontransistor), and nonvolatile memories are discussed along with their characteristics and applications.

Keywords: silicon carbide, power MOSFET, SIT, nonvolatile memory

Introduction

Silicon carbide (SiC) is the only WBG (wide band gap) semiconductor that possesses a high-quality native oxide for use as an insulator in electronic devices. The main advantage of silicon carbide is that it can resist high field strengths and offers better heat conducting capacity than copper at room temperature. Due to high thermal conductivity and high breakdown electric field strength, SiC can be used at high temperature, high voltage, high frequency and high power applications. Table 1 gives the comparison of the electrical properties of SiC with other semiconductors, viz. Si, GaN and GaAs.

Table 1. Comparison of electronic properties of SiC with Si, GaAs and GaN

	Si	GaAs	GaN	6H-SiC	4H-SiC	3C-SiC
Bandgap (eV)	1.1	1.142	3.39	3	3.26	2.2
Breakdown field @ $10^{17}cm^{-3}$(MV/cm)	0.6	0.6	3.3	3.2	3.0	1.5
Electron mobility @$10^{16}cm^{-3}$ (cm^2/V-s)	1100	6000	1000	370	800	750
Hole mobility @$10^{16}cm^{-3}$ (cm^2/V-s)	420	320	200	90	115	40
Saturated electron drift velocity (cm/s)	10^7	10^7	$2.5x10^7$	$2x10^7$	$2x10^7$	$2.x10^7$
Intrinsic concentration, n_i (cm^{-3})	$1.5x10^{10}$	$1.9x\ 10^{-10}$	$2.1x10^6$	$2.3x\ 10^{-6}$	$8.2x\ 10^{-9}$	6.9
Thermal conductivity	1.5	0.55	1.3	4.9	4.9	5

(After R. Y. Lakhshman, MS Thesis, Mississippi State University, 2001, Ref. 8)

Thermal oxidation of SiC produces a layer of SiO_2 on the surface while the carbon atoms from the SiC form CO, which escapes as gas. Thus, it is possible to make all devices found in silicon IC technology in SiC, including high quality, stable MOS transistors and MOS integrated circuits. Examples of WBG semiconductors are: gallium nitride (GaN, EG=3.4eV), aluminum nitride (AlN, EG = 6.2eV) and silicon carbide (SiC, EG between 2.2-3.25 eV depending on the polytype used). SiC is so thermally stable that dopant impurities cannot be diffused at any reasonable temperature. Finally, SiC is the only compound semiconductor which can be thermally oxidised to form a high quality native oxide (SiO_2). Although SiC offers substantial advantages over silicon, it is still immature as a semiconductor material. The main limitations of the technology are in the area of crystal growth.

In 1955, a laboratory simulation process for growing SiC crystals was developed by J. A. Lely [1]. In the Lely process, the nucleation of individual crystals are uncontrolled and the resulting crystals are randomly sized hexagonal-shaped a-SiC platelets. In 1978, Tairov and Tsvetkov [2] introduced the growth of SiC single crystals by the vapour transport process.

In 1983, Ziegler [3] introduced the modified sublimation process for growing SiC single crystals. In 1987, a research group under R. F. Davis at North Carolina State University (NCSU) announced a modification to the original Lely sublimation process [4]. In this modified process, only one large crystal is grown and this crystal consists of a single polytype. In this process, which is the basis of current commercial systems, a charge of polycrystalline SiC is heated in a graphite crucible containing argon at 200 Pa.

In 1987, the students from the NCSU group founded a small company, Cree Research, to produce silicon carbide commercially. Single crystal SiC forms in the hexagonal lattice, with alternating hexagonal planes of silicon and carbon atoms. Each silicon atom bonds to four nearest-neighbouring carbon atoms and each carbon atom is attached to four nearest-neighbouring silicon atoms. Doping of silicon carbide can be done during epitaxial layer growth or after crystal growth by ion implantation.

But ion-implantation is normally used because of lower quality due to crystal damages created during ion bombardment than doped epilayers. The first step in making silicon carbide semiconductor devices is to grow the epitaxial layer using a process called chemical vapour deposition (CVD). The silicon carbide epilayers are produced in the CVD process by thermally decomposing silicon and carbon source gases (called precursors) onto boule-derived SiC substrates.

The SiC lattice consists of alternating planes of silicon and carbon atoms, and the stacking sequence of these planes defines different polytypes of the material identified by the repeating distance of the stacking sequence (e.g. 3C,4H & 6H). The lattice constant in the basal plane is virtually identical for all polytypes, but important electrical properties such as band gap energy, electron mobility and critical field differ significantly between the polytypes [5-7].

The electrical properties are changed by adding impurities and the impurity elements affect the electrical properties. The control over the impurity addition in CVD SiC epilayers is very limited. This leads to difficulties over the control of unintentional impurities, which makes it difficult to control and achieve the desired epilayer thickness. The other method of doping silicon carbide is selective doping after epitaxial layer formation. The selective doping is accomplished by ion implantation; the diffusion coefficients of aluminium and nitrogen are so low that diffusion in silicon carbide is impossible. Diffusion in SiC at high temperatures produces significant surface damage. Successful fabrication of implanted layers in SiC depends on the proper choice of implant anneal conditions. Implant activation typically requires annealing at temperatures between 1000 and 1700 ^{O}C.

Chemical etching is impractical owing to the high chemical stability of SiC and selective etching is accomplished by reactive ion etching (RIE) using fluorinated gases. SiC offers significant advantages for power electronics applications such as lamp ballasts, motor control, medical electronics, automotive electronics, high-density high-frequency power supplies and smart-power application-specific integrated circuits.

There are a number of possible crystal structures. These are 2H, 3C, 4H and 6H; but the most important are 3C, 4H and 6H. These structures differ by band gap energy, carrier mobility and breakdown field. For example, the energy gaps are 2.2, 3.26 and 3.0 eV for 3C, 4H and 6H-SiC respectively.

In this paper silicon carbide Schottky barrier diode, power MOSFET, lateral power MOSFET, static induction transistor and nonvolatile memory are discussed along with their characteristics, uses, structures and applications. Table 2 gives performance details of commercially available silicon carbidebased devices which are developed by Purdue Group, Cree Group, Rutgers/USCI and Denso Group.

Silicon Carbide Schottky Barrier Diode

Schottky barrier diodes (SBD) are unipolar devices, i.e. they do not inject minority carriers into a neutral region as do PN diodes. Since there is no minority charge storage, the turn of event is fast and the transient reverse current is small. As a result, the switching energy dissipated during turn-off is minimal. Hence, Schottky diodes eliminate the switching losses. SiC Schottky barrier diodes are attractive because the breakdown field of SiC is 8 to 10 times higher than for silicon. Hence, these are

Table 2. The best-reported SiC based power devices such as Schottky barrier diodes and power MOSFETS [83] fabricated and tested by different groups

Diode					
Sr. No.	**Fabricated Device**	**Blocking Voltage (KV)**	**Specific on resistance $m\Omega cm^2$**	**Figure of merit (MW/cm^2)**	**Device Fabricated By**
1	Schottky Barrier Diodes	4.9	43	558	Purdue Group
2	JBS Diode (4H)	5.96	24	1,480	Rutgers
3	Schottky Diode (4H)	10.8	97	1,202	Rutgers / USCI
4	MPS Diode (4H)	4.38	20.7	928	Rutgers / USCI
5	MPS Diode (4H)	1.5	10	225	Cree, Inc.
MOSFETs					
1	DMOSFET (6H)	.760	125	4.62	Purdue Group (1996)
2	DMOSFET	.350	18	6.81	NCSU (1997)
3	DMOSFET (4H)	2.4	42	137	Cree, Inc.
4	UMOSFET	1.41	275	7.2	Cree Group (1997)
5	IOP-UMOSFET (4H)	1.4	15.7	125	Purdue Group (1998)
6	UMOSAFET	.45	10.9	18.6	Denso Group (1997)

capable of operation at much higher temperatures than silicon devices. Purdue University fabricated the 1700V 4H-SiC Schottky barrier diode using both Ni and Ti as Schottky metals. Figure 1 shows the cross section of SBD. The N-layer is 10-13 microns thick.

The semiconductor under the edges of the Schottky contact is implanted with boron. Under reverse bias this produces a region containing a large density of deep levels that serve as charge trapping centres and accumulate a distributed charge that reduces the electric field crowding at the edges of Schottky contact [9]. The Schottky metal is covered with 1 micron of gold metallisation to reduce spreading resistance of the Schottky contact and the backside ohmic contact is formed by annealed nickel.

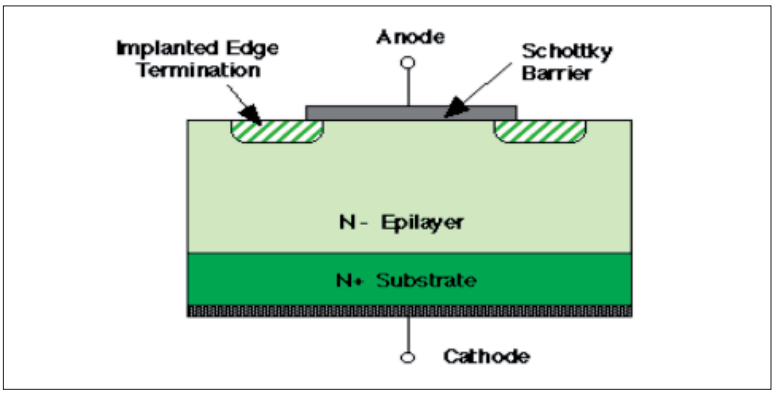

Figure 1. Cross section of SBD
(After A. Itoh et al., Ref. 9)

Figure 2 shows the forward and reverse (V-I) characteristics for the Ti and Ni contacted SBD. The barrier heights for Ti and Ni on 4H-SiC at room temperature are 0.8 eV and 1.3 eV respectively and the lower barrier Ti gives lower forward voltage drop but higher leakage current as compared to the Ni barrier. The reverse blocking voltages are 1500 and 1720 volts respectively.

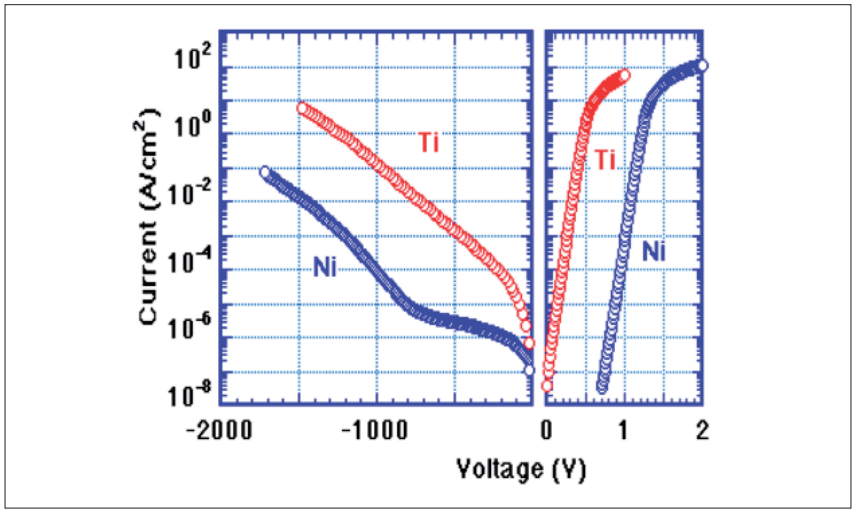

Figure 2. Forward and reverse (V-I) characteristics of SBD with Ti and Ni (After A. Itoh et al., Ref. 9)

Status of SiC based Schottky barrier diodes

In 1996, 4H-SiC Schottky barrier diodes having 1400 V with forward current densities over 700 A/cm^2 at 2 V were demonstrated [10]. In this paper, the Schottky rectifier consists of an N+ doped substrate (thickness ~11 mil) with back-side ohmic contact, a lightly doped (1x10^{16} cm^{-3}) epitaxial drift layer (thickness ~10 µm), and a top-side Schottky contact with a high-resistivity edge termination. The Schottky diode is fabricated by evaporating a high work function metal such as titanium, nickel, or gold, onto the epitaxial layer to form the Schottky contact and by depositing an ohmic contact metal onto the back of the N+ substrate.

In 1997, the results obtained with limited area amorphisation by argon ion-implantation at the periphery of 6H SiC Schottky barrier diodes were reported [11]. A variety of edge termination structures based upon the amorphised implanted region were studied during this work. The termination structures were fabricated using a three-mask process to create a high resistivity layer at the periphery of the device formed by using high dose argon ion-implantation with its position and area defined using a photoresist mask. It was established that, for obtaining a high breakdown voltage, the high resistivity layer should be in contact with the Schottky metal. It was demonstrated that only 50µm of the implant region is required at the periphery to obtain ideal plane parallel breakdown voltages. The leakage current at small reverse bias voltages was found to be directly proportional to the implant area.

In 2000, an accurate modeling and complete parameter extraction of the forward characteristics of the Ni/6H SiC Schottky barrier diodes (SBD) for high level current densities were presented [12]. The model took into account the high level injection effects of the excess majority carriers and current dependence of the series resistance. Direct extraction of the large bias SBD parameters was carried out. A very good agreement between the simulated forward curves using extracted parameters and measured data up to 500 A/cm^2 was obtained.

In 2001, the static and dynamic characteristics of large-area, high-voltage 4H-SiC Schottky barrier diodes were presented [13]. This device achieved the breakdown voltage greater than 1200 V and a forward current of 6 A, and enabled the use of SiC Schottky diodes in practical switching circuits.

In 2001, accurate modelling and parameter extraction for 6H-SiC Schottky barrier diodes with nearly ideal breakdown voltage were demonstrated [14]. Ni Schottky rectifiers on $2.7x10^{16}$ cm^{-3} n-type 6H-SiC epilayer using an effective edge termination based on an oxide ramp profile around the Schottky contact got experimented and simulated. Several anneals of the Schottky contacts were experimented. In particular, the diodes annealed at 900 ºC showed excellent reverse characteristics with a nearly ideal breakdown at about 800 V. In this work the device simulation was performed in MEDICI simulator.

In 2001, the use of thermally evaporated Ti Schottky barrier diodes on n type 6H SiC was fabricated [15]. They showed good rectification characteristics at room temperature. These diodes demonstrated a low reverse leakage current of below 1x10-4 A/cm^2. Using neon implantation to form edge termination improved the breakdown voltage up to 800 V.

In 2002, a new junction termination structure named guard ring assisted RESURF was proposed [16]. The structure maintained a stable and high breakdown voltage without being influenced by the deviation of impurity dose in the RESURF layer or by parasitic charge. The GRA-RESURF structure was adopted on 600-V range 4H-SiC Schottky barrier diodes and achieved high breakdown voltages with a good production yield in a wide range of implanted dose from $1x10^{13}$ to $5x10^{13}$ cm^{-2}. Comparison of various termination structures was also discussed in this paper.

In 2003, the breakdown voltage of 10 kV based on a 115μm n-type epilayer doped to $5.6x10^{14}$ cm^{-3} through the use of a multistep junction termination extension was demonstrated on 6H silicon carbide wafer [17]. A current density of 48 A/cm^2 was achieved with a forward voltage drop of 6V.

In 2004, the effect of different mechanism on the characteristics of silicon carbide characteristics was discussed [18]. In this paper, a number of experiments demonstrated that the Schottky barrier height for metal-SiC is different from the theoretical prediction. On the basis of non-uniform barrier height assumption for metal-SiC contact, a numerical simulation with 2D simulator MEDICI was performed in this paper. The simulation results showed that the model matches the experimental data very well. Patch defects make the Schottky-barrier height decrease. This may give a reasonable explanation for the non-ideal behaviours observed from many experiments. The effect of interface state density on Schottky barrier height was also discussed.

In 2005, high-voltage and low-loss 4H–SiC Schottky barrier diodes with a performance close to the theoretical limit using a Mo contact annealed at high-temperature were fabricated [19]. Hight-emperature annealing for the Mo contact was found to be effective in controlling the Schottky-barrier height at 1.2–1.3 eV without degradation of n-factor and reverse characteristics. Breakdown voltage of 4.15 kV, specific on-resistance of 9.07 $m\Omega cm^2$ and figure of merit of 1898 MW/cm^2 were achieved and also obtained were a 9 mm^2 Mo–4H–SiC SBD with breakdown voltage of 4.40 kV and specific onresistance of 12.20 $m\Omega cm^2$ in this paper.

In 2005, the performance of the commercially available and recently fabricated Schottky barrier diode of breakdown voltage of 1.2 kV was compared with the Si diodes at high temperature [20]. It was found that for a rated breakdown voltage of 1.2 kV, SiC Schottky diodes offer better performances in terms of switching time and recovery charge than PN-Si ultra-fast diodes, although they show slightly

higher forward voltage drops. Lower reverse leakage current was obtained using Ni instead of Ti for the Schottky contact.

In 2006, a new high voltage 4H-SiC SBD structure for monolithic microwave integrated circuit (MMIC) applications was proposed [21]. It employed one or more floating metal rings (FMR) which work in a similar fashion to guard rings. The influence of FMR structure on the breakdown voltage and cut-off frequencies of the SBD was studied by numerical device modeling. As compared to the one without ring, about 107% and 134% improvement in breakdown voltage while only about 17% and 25% decrease in cut-off frequencies was achieved in SBD with one and two rings.

Power MOSFET

Power switches can be considered as the heart of all power electronic systems. The increased power capabilities, ease of control, and reduced costs of power switches have made power electronic systems affordable in a large number of applications. The first power switches were thyristors and bipolar transistors. Thyristors were used in higher power systems because their ratings were scaled at a faster pace than bipolar transistors. Bipolar transistors were favoured for low and medium power applications because of their faster switching capability. The rating of these devices grew steadily until the late 1970s, the years in which the first power MOSFETs were introduced. Since the introduction of the first power MOSFETs, Si power MOSFETs have been immensely improved and have become the dominant device technology since 1980s for many applications for many reasons. First, MOSFET has a very high input impedance due to its MOS gate structure. Hence, it provides the simplest gate drive requirements. The creation of either inversion layers or accumulation layers under the MOS channel can be controlled using integrated circuits because of the small gate current that is required to charge and discharge the high input gate capacitance. Second, the MOSFET is a majority carrier device hence there is no minority charge storage involved in its operation. This results in faster switching operation. Third, compared to the bipolar transistors the MOSFETs have superior ruggedness and forward biased safe operating area which allows the elimination of snubber circuits for protection of the switch during operation in typical hard-switching applications. Fourth, as the majority carriers in silicon exhibit increasing resistivity with temperature, the thermal runaway behaviour is avoided in MOSFETs. MOSFET devices are formed as parallel combination of many thousands of individual MOSFET cells to take advantage of the thermal behaviour. Any device carrying excess current will heat up and become more resistive, diverting current into parallel paths. Excessive loss still produces thermal failure in MOSFET, but there is no unstable runaway effect if the parasitic BJT does not act. Due to these excellent characteristics, it would be desirable to utilise power MOSFETs for high voltage/power electronic applications. However, the blocking voltage capability of the MOSFET is based upon the ratings of the reverse body diode of the drift region. This blocking voltage is determined in part by the distance from source to drain. High blocking voltage capability implies high resistance because of geometry, so there is a trade-off between low drift region resistance and diode voltage capability.

Comparison of the figure of merits of Si and SiC polytypes determined by various scientists is given in Table 3. On the basis of Keyes' and Johnson's figure of merits, SiC has superior properties as compared to Si. They derived the figure of merits for high speed switches and high power discrete amplifiers. The figure of merits emphasises the electrical and thermal properties of various semiconducting materials for evaluating their power handling capability. Baliga derived two figures of merits. One is for low frequency and the other is for high frequency as well as high-power unipolar switches.

Table 3. Comparison of figures of merits SiC with Si [84]

Figure of Merits	Si	6H-SiC	4H-SiC	3C-SiC
Johnson's FOM	1	400	400	280
Keyes' FOM	1	5.1	5.1	5.8
Baliga FOM (Low Frequency)	1	240	560	140
Baliga FOM (High Frequency)	1	29	69	25

Silicon carbide based MOSFET can be used in high power applications and hence it requires a high breakdown voltage. The one-step field plate termination can enhance the breakdown voltage to 910 V, embedded mesa termination can increase it to 1350 V, and the embedded mesa with step field plating can give a breakdown voltage of 1100 V [22]. However, 6H-SiC DIMOSFETs in practice have attained a maximum blocking voltage of 760 V [23]. The specific on-resistance of the drift region of the MOSFET can be significantly reduced by enhancing the inversion channel mobility using pyrogenic reoxidation annealing [24], thereby reducing the power dissipation.

Power MOSFET can be classified under the following headings:

(i) Double implanted or DIMOSFET
(ii) UMOSFET
(iii) Lateral or LDMOSFET

Double implanted MOSFET

Power switching devices are reaching the upper limits imposed by low breakdown field of silicon, and high breakdown voltage can be achieved only by using a semiconductor with a higher breakdown field. SiC is unique among compound semiconductors since its native oxide is SiO^2, the same oxide as of silicon. This means that power devices used in silicon can all be fabricated in SiC. Here we will discuss double implanted MOS (DMOS) as shown in Figure 3. DMOS transistors are

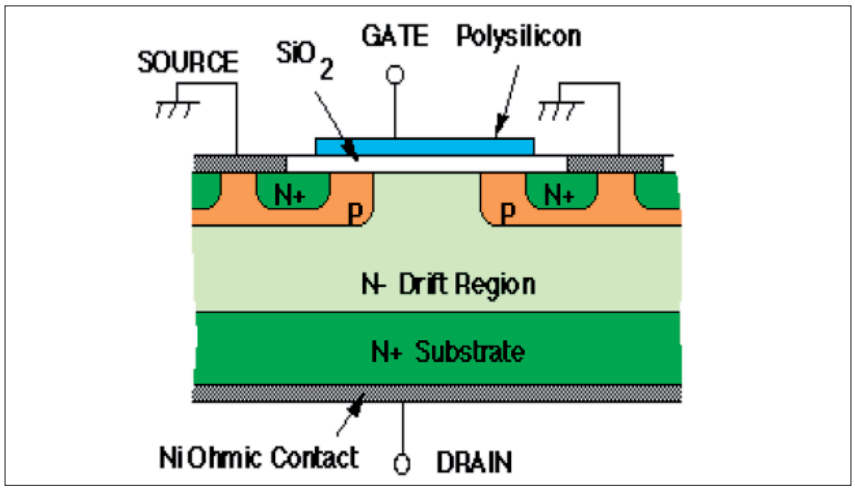

Figure 3. Double implanted MOSFET
(After J. N. Shenoy et al., Ref. 26)

common in silicon power device technology where the p-base and n^+ source regions are formed by diffusion of impurities through a common mask opening [25]. However, impurity diffusion is impractical in SiC because of the very low diffusion coefficients at any temperature. The Purdue group fabricated the first DMOS transistors in SiC using ion implantation to introduce dopants for the p-base and the n+ source [26-29]. The implanted DMOSFET requires that separate masks be used to define the p-base and the n+ source. The construction is a vertical structure with a drift layer built on a highly conductive n+ layer. The n-drift region is designed to give the forward blocking capabilities (Figure 3). The forward blocking capability is achieved by the pn junction between p-base region and n-drift region. During the device operation, a fixed potential to the p-base region is established by connecting it to the source metal by the break in the n+- source region. By short-circuiting the gate to the source and applying a positive bias to the drain, the p-base/n-drift region junction becomes reverse-biased and this junction supports the drain voltage by the extension of depletion layer on both sides. However, due to the higher doping level of the p-base layer, the depletion layer extends primarily into the n-drift region. On applying the positive bias to the gate electrode, the conductive path between the n+-source region and the n-drift region is formed. The application of positive drain voltage results in a current flow between drain and source through the n-drift region and conductive channel. The conductivity of the channel is modulated by the gate bias voltage and the current flow is determined by the resistance of various resistive components. The total specific on-resistance [30] is determined as

$$R_{on\text{-}sp} = Rn^+ + R_C + R_A + R_J + R_D + R_S \qquad (1),$$

where $R_{on\text{-}sp}$ is the specific on-resistance, Rn+ is the contribution from the n^+ -source, R_C is the channel resistance, R_A is the accumulation layer resistance, RJ is the resistance from the drift region between the p-base regions by virtue of the JFET pinchoff action, RD is the drift region resistance and RS is the substrate resistance. In a power MOSFET, the blocking voltage appears across the drift layer and so the drift-region resistance is considered to be the minimum possible theoretical value for the on-resistance of a MOSFET. For an ideal DIMOSFET, the resistances associated with the n+-source, the n-channel, the accumulation region and the n^+-substrate are usually neglected and the specific on-resistance of the power MOSFET is determined by the drift region alone. This assumption is not accurate at lower breakdown voltages where the drift region resistance RD is comparable to the other resistive components and these resistances should be included in calculating Ron-sp. However, at higher break down voltages, RD is significantly higher than other resistances and Ron-sp can be approximated by RD. The drift region analysis for an ideal DIMOSFET structure can be performed by taking the depletion layer in the drift region as an abrupt one-dimensional junction fabricated in a uniformly doped semiconductor. The doping level NB (cm-3) required to support a given breakdown voltage VB and the depletion width W(cm) [31] can be given by

$$N_B = \frac{\varepsilon E_C^2}{2qV_B} \qquad (2);$$

$$W = \frac{2V_B}{E_C} \qquad (3).$$

The specific on-resistance associated with the drift layer to support B V [32] is given by

$$R_{on-sp} = \frac{W}{qN_B\mu_n} \qquad (4).$$

Substituting (2) and (3) in (4), we get

$$R_{on-sp} = \frac{4V_B^2}{\varepsilon E_C^3 \mu} \qquad (5),$$

where ε is the permitivity in F/cm, E_C is the breakdown field in V/cm, q is the electronic charge in C and μ_n is the electron mobility in cm^2/V-sec [33]. From the equations, it has been confirmed that both the mobility μ_n and breakdown field E_C depend on N_B. The (V-I) characteristics of DIMOSFET are shown in Figure 4.

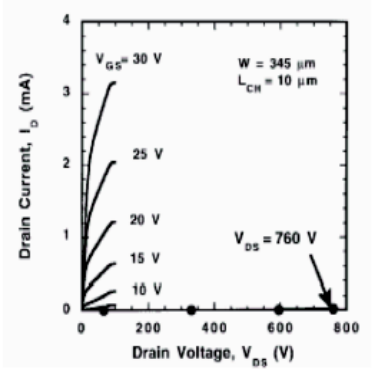

Figure 4. (V-I) characteristics of DIMOSFET
(After M. Bhatnagar and B. J. Baliga, Ref. 30)

SiC DIMOSFETs have been fabricated with the blocking voltage of 760V. To obtain the blocking voltage greater than 760 V for 6H-SiC depends on the drift region thickness, doping level, specific on-resistance and electric field strength. By adjusting all these parameters we propose to get the blocking voltage greater than 760V.

The safe operating area of MOSFET is divided into three regions: (i) maximum permissible drain current, (ii) maximum power dissipation limit, and (iii) maximum drain source voltage limit. The safe operating area of MOSFET does not contain any second breakdown as seen in the BJT. This is because of the majority carriers present in the MOSFET.

UMOSFET

The UMOSFET is formed by reactive ion etching, the electrical fields at the bottom corners being lower than that at the tip of the V- groove MOSFET. The substrate acts as the drain electrode. It is lightly doped and thick, constituting the lightly doped drain to ensure a high blocking voltage. The ptype base layer is grown by epitaxy and is grounded. As shown in Figure 5 the UMOS forms the pn junction and the MOS channel. In the blocking state the gate is grounded, which turns the MOS channel off. The large drain voltage is supported by the reverse-biased junction and the MOS capacitor. The electric fields in the pn junction and the MOS capacitor are shown to the right of the figure. It has been observed that the electric field in the oxide at the trench bottom is 2.5 times higher than the peak field in the semiconductor. Such high fields may lead to the damage of the oxide before the pn junction breaks

down. The field at the trench corners is even higher due to two-dimensional effects. Hence, in UMOSFETs the maximum blocking voltage depends on oxide breakdown and not on the semiconductor breakdown [34]. The maximum breakdown voltage provided by the device is 260V.

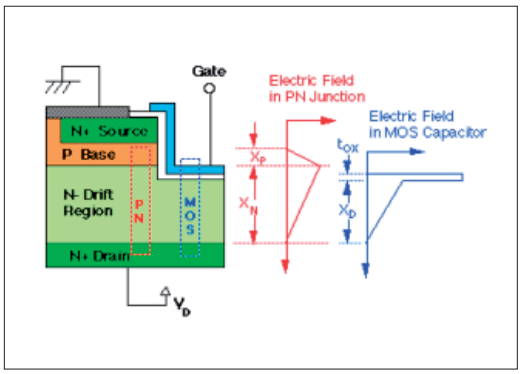

Figure 5. Cross section of 4H-SiC UMOSFET
(After J.Tan et al., Ref. 34)

In order to overcome the limitation of the device a new UMOSFET with integral oxide protection has been developed, which limits the electric fields in the trench which simultaneously reduces the on-resistance. The structure is shown in Figure 6 with electric fields in the blocking state. A new p-region is formed at the bottom of the trench by ion-implantation and reduces the electric field at the oxide/semiconductor interface to zero. A new n-type layer (known as current spreading layer) grown epitaxilly between the n-drift region and the p-type base layer prevents the pinch-off of the conducting channel in the on state. The layer also facilitates lateral current flow into the drift region. Figure 7 shows (V-I) characteristics of IOP-UMOSFET. The features of IOP-UMOSFET are as follows:

- The blocking voltage of the device is 1.4KV;
- The breakdown is nondestructive and the oxide failure does not occur;
- The specific on-resistance is 15.7 mΩcm^2; and
- The figure-of-merit $VB^2/_{Ron\text{-}sp}$ is 125 MW/cm^2, the highest value ever reported for a power MOSFET in any material system and 25 times higher than the theoretical limit for silicon power MOSFETs.

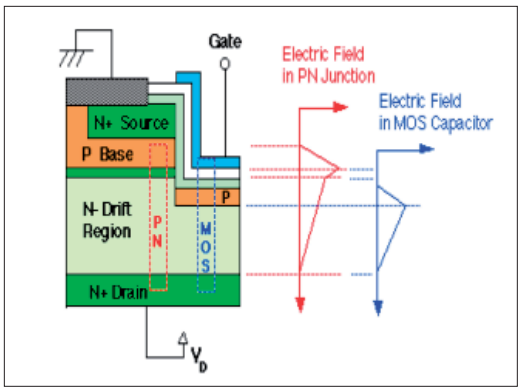

Figure 6. Cross section of 4H-SiC IOP-UMOSFET
(After J. Tan et al., Ref. 34)

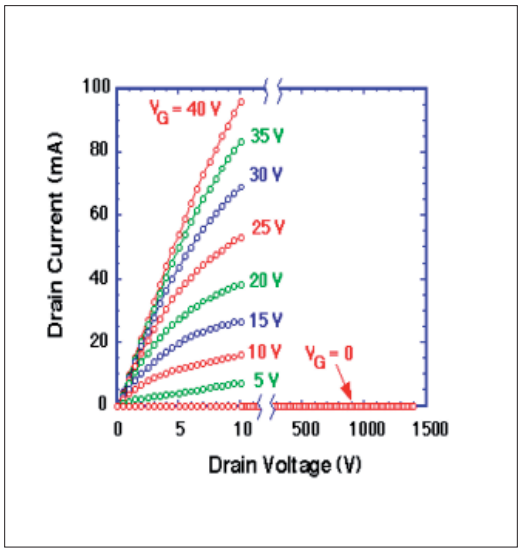

Figure 7. (V-I) Characteristics of IOP-UMOSFET
(After J. Tan et al., Ref. 34)

Lateral MOSFET

Before the advent of power devices of SiC, MOSFETs and thyristors had been fabricated as vertical structures with the substrate acting as an anode. In the off state, the voltage was blocked by a reverse-biased pn junction. In order to achieve high blocking voltage, the drift region should be lightly doped and thick. For a given device thickness, there was a maximum possible blocking voltage regardless of doping. For SiC lateral MOSFETs with a 10 μm drift region, the maximum possible voltage is 1600V. In order to overcome the limitations of vertical-type MOSFETs we use the lateraltype MOSFET [35]. The structure of lateral DMOSFET is as shown in Figure 8. From the figure it can been observed that the insulating substrate is of SiC. In the blocking state, the depletion layer spreads mainly into the lightly-doped drift region. Once the depletion region reaches the insulating substrate, it continues spreading toward the drain. Here, the maximum voltage is not limited by the thickness of the layer. Figure 9 shows the current voltage characteristics of lateral DMOSFET. From the characteristics, it is observed that the device withstands a maximum drain voltage of 2.6 kV. From the above discussion we can say that the device should be implemented laterally rather than vertically because there is no necessity for an increase of surface area required for the device.

Problems in characterising the oxides in SiC MOSFET and MOS reliability

Silicon carbide MOS interface is more complex than that on Si due to the presence of carbon in the compound and the non-cubic crystal structure. The wide bandgap of SiC makes it difficult to measure the interface state density using MOS techniques at room temperature. This is due to the fact that interface states are more than about 0.6 eV from the majority carrier band exchange charge. Several MOS measurement techniques may be used for silicon carbide. Precautions must be taken to ensure that the interface states are actually responding. There are two effective methods which are used for measuring the interface state density and these are the simultaneous hi-lo CV technique and the ac conductance technique.

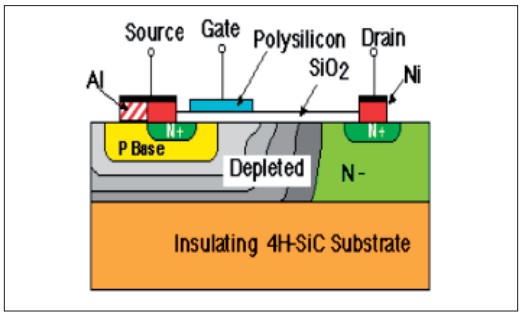

Figure 8. Cross section of lateral MOSFET
(After J. Spitz et al., Ref. 35)

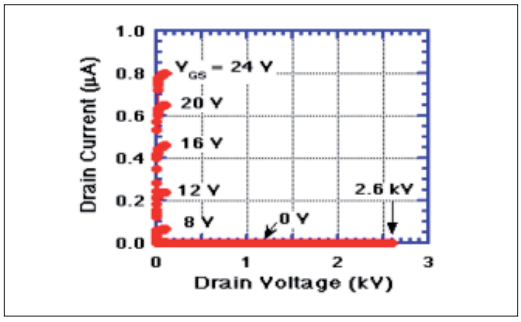

Figure 9. (V-I) Characteristics of lateral DMOSFET at room temperature
(After J. Spitz et al., Ref. 35)

SiC has a high-quality thermal oxide (SiO_2), thus it is possible to fabricate MOS-based power switching devices having extremely high input impedance. The limiting factor in these devices is likely to be the reliability of the thermally grown oxide. In order to achieve acceptable device reliability, the maximum field in the oxide may need to be limited. Unless this occurs, the high-field capability of SiC cannot be fully utilised. The reliability is evaluated using a MOS capacitor structure. Oxides are thermally grown by wet oxidation at 1150 °C using a baseline procedure that yields the interface state densities around $1.5x10^{11}$ eV^{-1} cm^{-2} and the fixed oxide charge densities around $9x10^{11}$ cm^{-2}.

Status and issues regarding the analysis and development of SiC based MOSFETs

In late 1980s, it was observed that power silicon devices were approaching their theoretical limits and that these limits could be significantly extended by fabricating power devices in the materials with higher breakdown electric fields, such as silicon carbide [36]. For vertically oriented majority carrier devices, the theoretical minimum value of the resistance-area product under punch- through condition is:

$$R_{on-sp} = \left(\frac{3}{2}\right)^3 \frac{V_B^2}{\mu_n \varepsilon_S E_C^3} = \frac{3.375 V_B^3}{\mu_n \varepsilon_s E_C^3} \qquad (6)$$

where $R_{on\text{-}sp}$ is the specific on-resistance in Ωcm^2, μ_n is the electron mobility perpendicular to the surface, ϵs is the permittivity of the semiconductor, E_c is the critical field for avalanche breakdown perpendicular to the surface, and V_B is the designed blocking voltage of the drift region. Although it varies with doping, the critical field E_c in SiC is almost an order of magnitude higher than in silicon. Even allowing for the lower electron mobility, the specific resistance in SiC at a given blocking voltage is about 400 times than that in silicon.

In 1994, silicon carbide MOS characteristics were explained in a paper by Brown et al. [37]. This paper produced data which characterise the SiC/SiO_2 interface and explain one of the previously unexplained abnormalities observed in the characteristics of SiC MOSFETs. The outstanding distinction between the MOS characteristics on p and n type SiC wafers obviously indicates that the difference is probably caused by the fact that the p type wafers are Al doped and the n type wafers are N doped. The redistribution of impurities that occurs during the thermal oxidation of SiC and Si behaves in a similar fashion. N type dopants are rejected by the oxide during growth whereas p type dopants are incorporated into the oxide. Hence, the Al dopant in the oxide is likely to be the causes of the p type SiO_2/SiC interface characteristics [37].

The first MOSFETs in SiC were reported in the late 1980s and the first power MOSFETs in 1994 [38]. The power devices were the vertical-trench MOSFETs or UMOSFETs. UMOSFETs are attractive because the base and source regions are formed epitaxially without the need for ion implantation and associated high temperature annealing. In UMOSFETs, the MOS channel is formed on the sidewalls of trenches created by RIE. However, SiC UMOSFETs were reported to have two serious problems: (a) A high electric field occurs in the gate oxide caused by higher electric fields in the SiC drift region. This problem occurs at the trench corners leading to catastrophic failure of the gate oxide at higher drain voltages, thus restricting the maximum operating voltage to less than 40% of ideal breakdown voltage, and (b) The low inversion layer mobility along the trench sidewalls results in high specific on-resistance, which nullifies the advantage of low drift region in SiC. By 1995, UMOSFETs fabricated on the carbon face of SiC had achieved the breakdown voltage of about 260V.

In 1996, the advantages and limitations of 4H-SiC power UMOSFET structure were demonstrated by US Air Force (WPAFB, Dayton Ohio) and Office of Naval Research, Arlington, Virginia [39]. According to this report, the use of p+ polysilicon gate leads to a higher breakdown voltage as the Fowler Nordheim injection from the gate electrode is reduced. It was also concluded that the insulator reliability is the limiting factor and therefore the high temperature operation of these devices may not be practical.

In 1997, Denso Corporation Japan introduced UMOSFET. This UMOSFET produced a blocking voltage of 450V, a specific resistance of 10.9 $m\Omega cm^2$, and $VB^2/_{Ron\text{-}sp}$ of 18.6 MW/cm^2 [40]. In the same year, Northrop Grumman Science and Technology Centre introduced and fabricated the 4HSiC UMOSFETs at the blocking voltages of 1.1kV and 1.4 kV [40-41], as well as the 4H-SiC DIMOSFETs at a blocking voltage of 900V [42].

In 1998, Purdue University reported a SiC accumulation-channel UMOSFET with new structural features that shield the trench oxide from high electric fields in the blocking state [43-44]. The new features consisted of p-type region formed in the trench bottom by self-aligned ion implantation and a thin n-type epilayer incorporated between the n-drift region and the p-type base.

A way to avoid the problem with oxide breakdown at the trench corners is to eliminate the trenches. This was accomplished in 1996 with the introduction of planar implanted DMOSFETs [43- 44,27]. Since impurity diffusion is impractical in SiC, the base and source regions are formed by selective ion implantation using aluminum or boron for the p-type base and nitrogen for the n+ source. Because p-type implants are conducted at temperatures between1600 and 1700 ^{o}C, the self-aligned implant process using polysilicon gates is not practical in SiC. Hence, the realignment tolerances must be allowed between two sources and gate. This should also alter the alignment of the underlying base material. Due to these disadvantages, the elimination of the trench corners resulted in a threefold improvement in the device blocking voltage to 760V. This blocking voltage is achieved using 6H-SiC [43-44,27].

In 1998, the 4H-SiC UMOSFET was fabricated with a breakdown voltage of 1.4 kV and a specific on-resistance of 311 mΩcm^2 by the CREE Research Inc [44]. The fabricated device required the impurity concentration of the drift region of 1x10^{15}/cm^3 and required n- thickness of 15μm. For the prototype module, three kinds of 2.0 kV UMOSFETs with different chip areas (0.7x0.7, 1.5x1.5, and 3.0x3.0 mm^2) were designed. All were fabricated in CREE Research Inc by using 4H-SiC wafers. In this report the relationship between the breakdown voltage and the specific on-resistance was presented by various groups which were involved in the fabrication of silicon carbide based power devices.

In 1999, the usefulness of silicon carbide for the device application was explained [45]. In the same year, the theoretical and numerical analysis of SiC JFET and MOSFET at 6.5 kV was presented [46]. According to this report, to improve the on-state/breakdown performance of the JFET, buried layers in conjunction with a highly doped buffer layer have been used. Trench technology has been employed for the MOSFET. The devices are simulated and optimised using MEDICI simulator. In order to obtain a 6.5 kV breakdown voltage, the n-drift region length is 60μm long with a doping concentration of 2x10^{15} cm^{-3}. The distance between the gate and the source diffusions is 0.6 μm. For a trench MOSFET, the p-well doping is 5x10^{17} cm^{-3} and its length is equal to 3.8 μm. The doping concentration of the n-drift region has to be decreased to 1.7x10^{15} cm^{-3}. In order to obtain the proposed breakdown voltage, the n-drift layer length is 60μm long. The gate oxide thickness for the simulated structure is 0.2μm.

In 1999, high-voltage lateral MOSFETs on 6H and 4H SiC wafers were fabricated with 400-475 V breakdown voltage using the RESURF principle [47]. A MOS electron inversion layer mobility of about 50 Ωcm^2/V-sec was obtained on 6H-SiC wafers. This mobility is high enough such that the specific on-resistance of the 6H-SiC MOSFETs is limited by the resistance of the drift layer. The measured FET specific on-resistance Ron-sp ranges from 0.25 to 0.7750 Ωcm^2 depending on the device structure. However, this resistance is much higher than predicted because the sheet resistance of the drift layer is an order of magnitude higher than expected for the implant doses used. This paper also concluded that by redesigning the devices with appropriate drain edge terminations and by reducing gate overlap over the drift region, a substantial increase in breakdown voltage is expected.

In 2000, the characterisation of SiC epitaxial channel MOSFETs was demonstrated. Silicon carbide epitaxial channel MOSFETs were fabricated on 6H SiC substrates with N+ epitaxial source and drain electrodes. The electrical characteristics were modelled in the sub-pinch off depletion and accumulation modes of operation. A buried channel mobility of 230 cm^2/V-sec and an accumulation mode surface mobility of 45 cm^2/V-sec were extracted at room temperature under a 50% activation of channel donor impurities [48].

In 2001, high-voltage lateral RESURF metal oxide semiconductor field effect transistors in 4H–SiC were experimentally demonstrated with a breakdown voltage of 900 V and a specific on-resistance of 0.5 Ωcm^2. Lighter RESURF doses and/or thicker gate oxides were required in SiC lateral MOSFETs to achieve highest breakdown voltage capability. In this paper [49], lateral RESURF MOSFETs were fabricated on p/p^+ 4H–SiC substrates with epitaxial thickness and doping of 10μm and 4-5x10^{15} cm^{-3} respectively. The source/drain regions were implanted with phosphorus to create a box profile of junction depth of 0.5μm and total dose of 5x10^{15} cm^2. The RESURF region was also realised with a box profile implant of the same junction depth with nitrogen as the dopant. The implants were activated at 1200 ^{0}C in argon ambient.

In 2001, a new 800V lateral MOSFET with dual conduction paths was presented and demonstrated [50]. The feature of this new device was a buried P-type layer that divides the N-type drift region into two parallel conduction paths. The dual conduction paths provide an on-state resistance reduction of 33% as compared to a state-of-the-art double RESURF MOSFET. Charge balance is maintained among the layers to ensure high blocking voltage capability. The manufacturing process was relatively simple and provided excellent control of the charge in each layer by using ion implantation steps rather than epitaxial layers. A new BiCMOS Power IC process featuring this novel device was used to manufacture the cost-effective integrated power supply chips.

In 2001, a 4H-SiC RF power MOSFET was fabricated and characterised for the first time [51]. The improved performance of this device was facilitated by a two-metal-layer process which optimises the conflicting requirements of the acceptable inversion-layer mobility and the low contact resistance. The cut-off frequency of the device with 1μm gate length was in excess of 7 GHz. The breakdown voltage of the newly fabricated MOSFET was found to scale with the drift length. A breakdown voltage of 950 V was achieved in MOSFETs with specific on-resistance of 24 Ωmm^2. The parasitic resistances were reasonably small due to dopant activation and post metallisation anneals. The sheet resistances ofthe N source/drain and N drift regions were measured to be 300 Ω/sq and 3400 Ω/sq respectively. The resistivity of the ohmic contact was 1.5x10^{-5} Ωcm^2.

In 2002, a novel analytical model of a SiC MOSFET was presented [52]. In this paper, by using known experimental results, a semi empirical relation for carrier mobility (μ) dependence on electric field intensity, dopant concentration and temperature was formulated. Based on this relation, appropriate analytical mathematical-physical model for simulation of current-voltage characteristics, transconductance and conductance of MOSFET were developed. All models were formulated taking into account, among other effects, the dependence of threshold voltage on temperature and impurity concentration in the channel, as well as the effect of the channel narrowing. Using the proposed model a simulation algorithm was designed and a simulation of the MOSFET performance was performed.

In 2002, a 10 A, 2.4 kV power DIMOSFET in 4H-SiC was reported and the characteristics of large area (3.3x3.3 mm^2), high-voltage 4H-SiC DiMOSFETs were demonstrated [53]. The MOSFETs showed a peak MOS channel mobility of 22 cm^2/V-sec and a threshold voltage of 8.5 V at room temperature. The DIMOSFETs exhibited an on-resistance of 42 $m\Omega cm^2$ at room temperature and 85 $m\Omega cm^2$ at 200 ºC. Stable avalanche characteristics at approximately 2.4 kV were observed. An on current of 10 A was measured on a 0.103cm^2 device. High switching speed was also demonstrated. In this paper, the MOS channel length defined by the p-well and n implants was 1.5μm. Electrons flowed laterally from the n source through a MOS channel on the implanted p-well, then flowed vertically through the JFET region formed by two adjacent p-well regions and then through the lightly doped n drift region into the drain. The cell pitch was 16 μm and the packing density of the gate periphery was 1250 cm/cm^2. A 20-μm thick drift layer with a doping concentration of 2.5x10^{15} cm^{-3} was chosen for a 2000 V blocking voltage design. This paper also suggested that the devices are capable of high-voltage, high-frequency and low-loss switching applications.

In 2002, a two-zone, lateral RESURF field 6H-SiC MOSFET with a breakdown voltage as high as 1300 V and a specific on-resistance of 160 m Ωcm^2 was fabricated [54]. These MOSFETs exhibited stable and reversible breakdown indicating an avalanche breakdown in SiC that had not been reported in earlier lateral SiC MOSFETs. In this paper, the device was fabricated on p/p^+ 6H-SiC wafers with epitaxial thickness and doping of 10μm and $7x10^{15}$ cm^{-3} respectively. The specific on-resistance of the MOSFET is lower than any lateral MOSFET reported in silicon or SiC with similar breakdown voltage.

In 2003 and 2004, numerical device simulations on a 4H –SiC vertical MOSFET were presented [55-56]. The simulations mainly focused on reverse blocking voltage, threshold voltage and on-state resistance. The simulated gate MOSFET had a gate oxide thickness of 50nm, a source depth of 0.2 micron and a p-well depth of 1 micron. The channel length was of 1micron.

In 2004, a comparison of modern SiC power devices was demonstrated [57]. In this paper an analysis of the static and dynamic behaviour of a 2 kV SiC MOSFET and IGBT was presented. By comparing the circuit performances it was observed that IGBT is two times faster than MOSFET.

In 2005, a design and fabrication of a 1600V 4H-SiC UMOSFET with a dual buffer layer structure was demonstrated. The fabricated device exhibited 50mΩcm^2 of specific on-resistance with ~1μm of the channel length that could be further reduced to <1μm. In this paper, the n-type drift layer was ~25μm thick with 3-$5x10^{15}$ cm^{-3} of doping concentration. Two n-type buffer layers were grown on top of the drift layer. The first buffer layer was ~3μm thick and 1-$2x10^{16}$ cm^{-3} doped with nitrogen. The second layer was ~0.5μm thick, 0.5-$1x10^{17}$ cm^{-3} doped with nitrogen followed by the final p-type, ~2μm thick base layer with 0.8-$1x10^{17}$ cm^{-3} doped with aluminum. The N^+ layer was formed by high energy up to 700 KeV nitrogen implantations to obtain ~1μm channel length [58]. UMOSFET trench gates were perpendicular to the primary flat of the SiC wafers to achieve high inversion channel mobility.

In 2005, an on-state performance of trench oxide-protected SiC UMOSFETs on 115μ m-thick n-type 4H-SiC epilayers designed for blocking voltages up to 14 kV was demonstrated [59]. In this paper, a current density of 137A/cm2 and a specific on-resistance of 228 mΩcm^2 were achieved at a gate bias of 40 V. The effect of current spreading on the specific on-resistance for finite-dimension devices was investigated. A 115μm-thick, $7.5x10^{14}$ cm^{-3} n-type epilayer was first grown on n+ 4H-SiC substrate, cut 8^o off axis and followed by a 0.4 μm, $2x10^{17}$ cm^{-3} n-type current spreading epilayer and a 1.5 μm, $2x10^{17}$ cm^{-3} p-type epilayer to form the base region of the UMOSFET. Source contacts were formed by implanting $4x10^{15}$ cm^{-2} nitrogen at 650 ^oC using a Ti-Au mask. Gate trenches approximately 2 μm deep were formed by reactive ion etching using a Ni mask. Sacrificial oxidations were performed to smooth the trench sidewalls. The active area of the device was .018cm2 and required a current 2.5 A. The device required a current density of 137A/cm^2. The blocking layers of doping and the thickness used here were theoretically capable of blocking 14 kV and had actually been demonstrated to block 10 kV. However, problems with the edge terminations in the devices limited the blocking voltage to just over 5 kV [59].

In 2005, a 1330 V, 67mΩcm2 4H-SiC RESURF lateral MOSFET was investigated [60]. The figure of merit of the presented device was 26 MW/cm2. This figure of the merit was the best among the reported lateral MOSFETs.

In 2006, 4H-SiC DMOSFETs of breakdown voltages of 1.2 kV and 1.8 kV were fabricated [61]. For 1.2 kV, an epilayer with a doping concentration of $6x10^{15}$ cm^{-3} and a thickness of 12 μm could be used. For 1.8 kV 4H SiC DMOSFET the device had a gate oxide of 500Å. The gate oxide electric field was limited to approximately 3 MV/cm. The active area of this device was 0.0936 cm^2. An onresistance of 85 mΩ (Ron-sp = 8 mΩcm2) and a drain current of 50 A (534 A/cm^2) at a forward drop of 5.7 V were measured at room temperature.

In 2006, silicon carbide as energy efficient wide band gap devices was discussed [62]. For RF applications, GaN HEMTs allowed the use of highly efficient Class E circuit topologies demonstrating a high power of 63 W at 2 GHz with 75% power added efficiency. SiC Schottky diodes were allowing up to a 25% reduction in losses in power supplies for computers and servers when used in the power factor correction circuit. Even higher efficiencies could be obtained when the SiC Schottkys were combined with a SiC MOSFET as the switch, resulting in yet another 22% reduction in losses. For motor control, SiC Schottky allowed a >35% reduction in losses as demonstrated for a 3 HP motor drive [62].

In 2007, a compact circuit simulator model was developed and used to describe the performance of a 2kV 4H SiC power DIMOSFET [63]. This model also made a comparison with the widely used 400V, 5A Si power MOSFET. The model's channel current expressions are unique in that they include the channel regions at the corners of square and hexagonal cells that turn on at lower gate voltages and the enhanced linear region transconductance. This model also actively describes the static and dynamic performance of both the Si and SiC devices. In this paper [63] the detailed device comparisons show that both the on-state performance and switching performance at 25 °C are similar between the 400V Si and 2kV SiC MOSFETs with a difference that the SiC device requires twice the gate drive voltage. The main difference between the devices is that the SiC has a five times higher voltage rating without an increase in the specific on-resistance.

Static Induction Transistor

Due to high breakdown field, silicon carbide is an ideal semiconductor for the fabrication of high power microwave devices operating in the 1-10 GHz range. Static induction transistors have power levels of 470 W at 600 MHz and 38 W at 3 GHz. Due to a high thermal conductivity of SiC, it removes the heat from the substrate during microwave operation. Figure 10 shows the cross section of the SiC static induction transistor (SIT). From the cross section it can be observed that the SIT is a majority carrier unipolar device in which the flow of the electrons from source to drain is controlled by a saddleshaped two-dimensional potential barrier in the semiconductor between the metallic gates. If the doping level and lateral dimensions are chosen correctly, the height of barrier potential will be modulated both by the gate and drain. Since the current increases exponentially as the barrier is lowered, the output characteristics of SIT are like a triode. SIT is important as a microwave device at low frequencies. The maximum drain voltage is 250 V, the on-current at the knee is about 80mA/mm and the blocking gain is approximately 10.

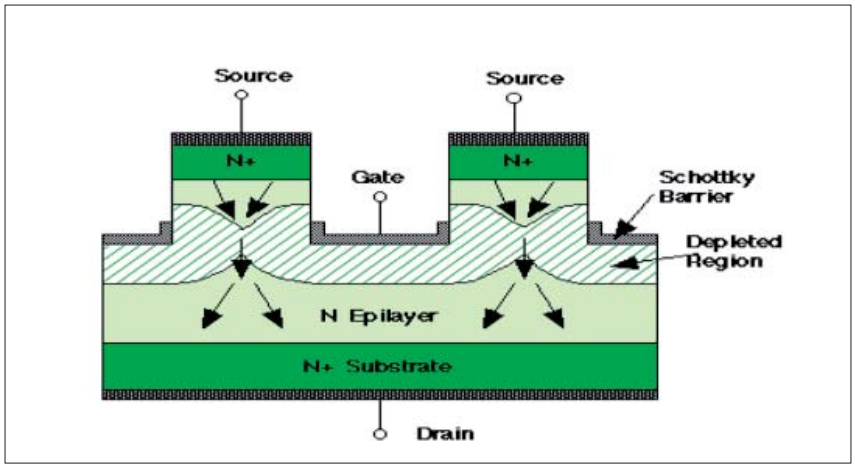

Figure 10. Cross section of static induction transistor (SIT)
(After R. C. Clarke et al., Ref. 64)

Status and issues regarding the analysis and development of SiC based SIT

In 1995, 6H-SiC static induction transistors (SITs) were demonstrated, using SiC-specific semiconductor processing technologies such as VPE, reactive ion etching and self aligned sidewall Schottky gates [64]. Under test conditions, 6H-SiC SITs developed 38 W of output power at 175 MHz, a power added efficiency of 60%, and an associated gain of 10 dB. The maximum channel current was 300 mA, and the maximum blocking voltage was 200 V. SIT requires two extremes of doping, a thick 5µm unintentionally-doped drift layer of $1x10^{16}$ cm^{-3} concentration and a very highly doped ($lx10^{19}$ cm^{-3}), 0.2µm-thick contact layer. The growth chemistry for SiC employs propane as a source of carbon and silane as a source of silicon, transported via hydrogen carrier gas to an inductively heated (1450°C) graphite susceptor [64].

In 1995 also, SITs were demonstrated on 4H SiC [65]. SiC-specific semiconductor processing technologies such as epitaxy, reactive ion etching, and sidewall Schottky gates were employed. Under pulsed power test conditions, 4H-SiC SITs developed a maximum output power of 225 W at 600 MHz, a power added efficiency of 47% and a gain of 8.7 dB. The maximum channel current was 1 A/cm and the maximum blocking voltage was 200 V.

In 1997, solid state DTV transmitters were demonstrated [66]. These transmitters used silicon bipolar, MOS or silicon carbide SIT transistors in the RF power amplifiers. The solid state transmitters achieved the highest power levels by using the latest LDMOS and silicon carbide RF transistors. In 1998, ion implanted SITs in 4H SiC for the microwave power generation in L and S bands were demonstrated. The ion implanted SITs were measured with 35W and 300W output powers at L and Sbands [67]. In 1999, analysis and design of C-band SITs in 4H SiC was demonstrated. Experimental devices were fabricated on n-type epitaxial wafers of 4H-SiC obtained from Cree Research [68].

In 2000, a multiple self-aligned fabrication process was developed for recessed gate microwave SITs in silicon carbide. This process was demonstrated by fabricating 4H-SiC SITs having fT of 7 GHz [69]. In 2001, a SiC-SIT with SAO structure was fabricated by using aluminum implantation for p gate on 4H n-type SiC [70]. It was found that the SAO structure could be fabricated as expected by observing the cross sectional structure. A very low specific on-resistance of 39 $m\Omega cm^2$ was successfully obtained. By reducing a unit cell, lower on-resistance could be expected.

In 2002, a vertical channel type static induction transistor with the novel gate structure was introduced [71]. A highest blocking voltage of 2000 V in the case of vertical channel type silicon carbide SITS and a low on-resistance of 70mΩcm^2 were realised. Turn-off characteristics were investigated and a very fast turn-off time of 20 ns at high temperature of 200 ˚C under dc voltage of 1000 V was successfully demonstrated. Large current turned-off properties were also demonstrated by a parallel connection of two small SITS. In the same year, a silicon carbide based self-aligned and ion implanted SIT for 150 W having S-band operations got demonstrated [72].

In 2003, the effect of interface charges on the operation of 4H silicon carbide SITs was presented [73].

In 2005, a recessed gate silicon carbide SIT was demonstrated [74]. A developed new approach was used to solve the breakdown voltage and the specific on-resistance and trade-off problem, and consequently an extremely high power capability was achieved. Simulations were fully performed to analyse the influence of critical design parameters on the device power performance. They showed that the basic trade-off was successfully eliminated if the depth of a JFET diffusion layer was greater than 1.35 times the gate trench depth due to the effective suppression of the JFET resistance. Consequently, the proposed device architecture showed much higher power capability than the conventional structure, suggesting that the device power performance be maximised by implementing the JFET diffusion layer in a conventional SiC SIT with a narrow half-width of the source region [74].

In 2006, ultra low on-resistance silicon carbide SITs with buried gate structures (SiC-BGSITs) were successfully developed through an innovative fabrication process [75]. A submicron buried p+ gate structure was fabricated by a combination of submicron trench dry etching and epitaxial growth on a trench structure. The breakdown voltage VB and specific on-resistance $R_{on\text{-}sp}$ of the fabricated SiCBGSIT were 700V at a gate voltage $V_G = -12$ V, and 1.0 mΩcm^2 at a current density of $J_D = 200$ A/cm^2 and $V_G = 2.5$ V respectively. This $R_{on\text{-}sp}$ was the lowest on-resistance for 600V-class power switching devices, including other SiC devices and GaN HEMTs. The fabricated BGSIT with Nch was 1.3x10^{16} /cm3. The device active area and Wch were 200x200 μm^2 and 0.9 μm respectively. The drain current ID reached 0.08 A, corresponding to a current density JD of 200 A/cm^2 at a drain voltage $V_D = 0.2$ V and $V_G = 2.5$ V. From these parameters, the calculated $R_{on\text{-}sp}$ was as low as 1.0 mΩ cm^2. The $R_{on\text{-}sp}$ calculated by the device simulator of the same dimension as the fabricated device was 1.1 mΩcm^2, which was almost the same as the measured Ron-sp. From the characteristics, we can observe the decrease of the drain-current I_D at $V_D > 6$ V. This phenomenon probably comes from the decrease of the carrier mobility by the self-heating effect and implies the thermal and electrical hardness of such a device at high current density.

In 2007, a buried gate SIT in 4H-SiC with ultra low on-resistance was presented [76]. A result of device simulation showed the appropriate parameters for the device design. For BGSIT with wide Wch, an ultra-low Ron-sp of 1.1 mΩcm^2 was obtained with normally-on characteristic, while a clear saturation I_{DS}-V_{DS} characteristic and a slightly high $R_{on\text{-}sp}$ of 1.4 mΩcm^2 were obtained with quasi normally-off characteristic for BGSIT with narrow W_{ch}. In order to realise normally-off characteristic, Wch must be reduced more. However, it must be realised without increase of on-resistance.

Nonvolatile Memory

The wide bandgap of SiC results in an extremely low value of the intrinsic carrier concentration at room temperature, which is lower than that due to silicon. The leakage current of SiC is negligible. Hence the dynamic memory cells in SiC have storage times of many years at room temperature. Figure 11 shows the cross section of SiC vertically integrated bipolar NVRAM cell at left along with Nchannel MOSFET control logic at right. The NVRAM cell consists of an NPN bipolar access transistor connected to a pn junction storage capacitor. Storage times are plotted as a function of temperature. If these data are extrapolated to lower temperatures, they predict a room temperature storage time of over one million years and give the concept of a truly nonvolatile memory [77].

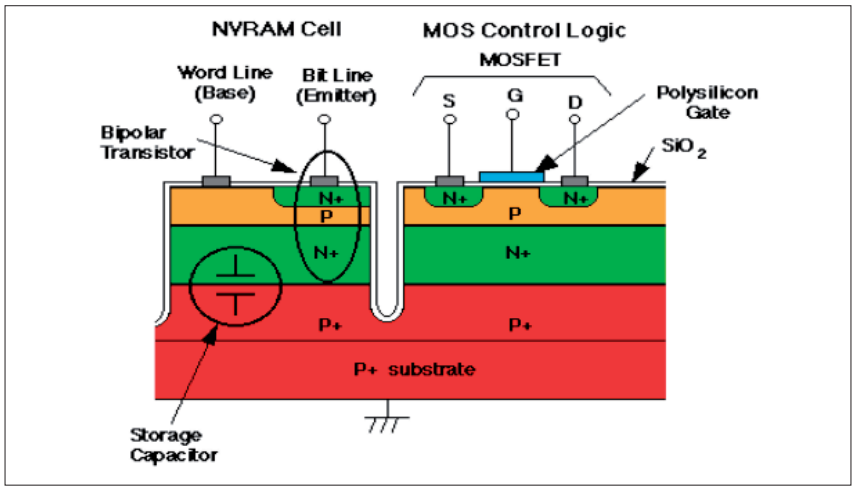

Figure 11. Cross section of nonvolatile memory
(After J. A. Copper, Jr. et al., Ref. 77)

Status and issues regarding the analysis and development of SiC based nonvolatile memory In a paper on dynamic charge storage in 6H silicon carbide presented in 1992 [78], pn-junction storage capacitors were fabricated in 6H silicon carbide. The charge decay was dominated by surface generation at the mesa edges and the storage time strongly depended on the method of surface passivation. Charge recovery was thermally activated. Devices passivated by dry oxidation and by wet oxidation exhibited activation energies of 0.66 and 1.48 eV respectively. As a figure of merit, extrapolation of the dry-oxide data gave a room-temperature storage time of 10^6 s, while the same operation on the wet-oxide data gave a value of 10^{14} s.

In 1994, a vertically integrated bipolar storage cell in 6H silicon carbide for nonvolatile memory applications was reported [79]. The vertical1y integrated 6H-SiC bipolar memory cell had an extrapolated room-temperature storage time of 10^6 s. Electrical writing of the cell was demonstrated.

Since no applied bias was needed during the storage state, the bipolar cell had a potential for use as a nonvolatile memory.

In the same year, the first monolithic NMOS digital integrated circuits in 6H-SiC were presented [80]. The logic gates were implemented in enhancement-mode NMOS using ion implanted MOSFETs with non-self-aligned metal gates. Inverters, NAND and NOR gates, XNOR gates, D-latches, RS flipflops, binary counters, and half adders were fabricated and characterised. All circuits operated properly from room temperature to over 300°C.

In 2001, N_2O and NO nitridation by either annealing or direct growth of gate oxides on 4H SiC were analysed [81]. The analysis was based on binding energies from x-ray photoelectron spectroscopy and depth profiles of nitrogen at the SiO_2-SiC interface from secondary ion mass spectrometry. A clean SiO_2-SiC interface was found in both NO and N_2O annealed/grown samples as opposed to the interface annealed in Ar which exhibited complex sub-oxides and oxide-carbon compounds.

In 2002, nonvolatile memory characteristics of MOS capacitors were presented [82]. The MOS capacitors were fabricated on N-type 4H SiC substrate with nitrided oxide-semiconductor interface. The charge-retention time was in the order of 4.6×10^9 years as determined by thermally activated (275- 355ºC) capacitance transient measurements and extrapolation to room temperature. The estimated activation energy of the charge generation processes was 1.6 eV. The results and the analysis demonstrate that 4H SiC MOS capacitors can be used as a memory element in nonvolatile RAMs.

Conclusions

At present SiC devices appear to compete in the semiconductor market as high voltage, high power switching devices. In this paper we estimate that SiC can be used as a power device and in the development of the nonvolatile memory. It has also been examined that SiC devices can also be operated at microwave frequencies. However, in order to become economically feasible, several critical materials and processing issues still need to be solved.

References

1. J. A. Lely, "Darstellung von einkristallen von siliziumcarbid und beherrschung von art and menge der eingebauten verunreinigungen," *Ber. Dt. Kerm. Ges.,* **1955**, *32*, 229-231.
2. Y. M. Tairov and V. F. Tsvetkov, "Investigations of growth processes of ingots of silicon carbide single crystals," *J. Cryst. Growth,* **1978**, *43*, 209-212.
3. G. Ziegler, P. Lanig, D. Theis, and C. Weyrich, "Single crystal growth of SiC substrate material for blue light emitting diodes," *IEEE Trans. Electron Devices*, **1983**, 30, 277-281.
4. C. H. Carter, Jr., L. Tang and R. F. Davis, "Growth and characterization of silicon carbide crystal", 4th National Review Meeting on the Growth and Characterization of Silicon Carbide, Raleigh, NC, USA, **1987**, pp.15-28.
5. M. Ostling and N. Lundberg, "Low ohmic cobalt silicide contacts to p-type 6H-SiC", IEEE Device Research Conf., Santa Barbara, CA, USA, June **1996**, pp.157-157.
6. S. Sridevan, P. K. Mclarty, and B. J. Baliga, "On the presence of aluminum in thermally grown oxides on 6H-silicon carbide [power MOSFETs]", *IEEE Electron Device Lett.*, 1996, 17, 136-138.
7. J. W. Palmour, Cree Research, private communication, **1996**.
8. R. Y. Lakshman, "A Process for hydrogenation of silicon carbide crystals", *MS. Thesis,* 2001, Mississipi State University, USA.

9. A. Itoh, T. Kimoto, and H. Matsunami, "Excellent reverse blocking characteristics of high-voltage 4H-SiC Schottky rectifiers with boron-implanted edge termination", *IEEE Electron Device Lett.,* **1996**, *17*, 139-141.
10. C. Weitzel, J. Palmour, C. Carter, K. Moore, K. Nordquist, S. Allen, C. Thero, and M. Bhatnagar, "Silicon carbide high-power devices", *IEEE Trans. Electron Devices,* **1996**, *43*, 1732-1741.
11. D. Alok and B. J. Baliga, "SiC device edge termination using finite area argon implantation", *IEEE Trans. Electron Devices,* **1997**, *44*, 1013-1017.
12. G. Brezeanu, M. Badila, B. Tudor, and B. Millan, "Accurate modeling of Ni/6H SiC Schottky barrier diode (SBD) forward characteristics at high current densities", Int. Conference on Semiconductor, Sinaia, Romania, October **2000**, Vol.1, pp. 193-196.
13. D. T. Morisette, J. A. Cooper, Jr., M. R. Melloch, G. M. Dolny, P. M. Shenoy, M. Zafrani, and J. Gladish, "Static and dynamic characterization of large area high-current-density SiC Schottky diodes", *IEEE Trans. Electron Devices,* 2001, *48*, 349-352.
14. B. Gheorghe, M. Badila, B. Tudor, J. Millan, P. Godignon, F. Udrea, G. A. J. Amaratunga, and A. Mihaila, "Accurate modeling and parameter extraction for 6H-SiC Schottky barrier diodes (SBDs) with nearly ideal breakdown voltage", *IEEE Trans. Electron Devices*, 2001, 48, 2148-2153.
15. Z. Liu, S. Wang, F. Yu, Y. Zhang, and H. Zhao, "Ti Schottky barrier diodes on n-type 6H-SiC", 6th Int. Conference on Solid State and Integrated Circuit Technology, Beijing, China, October 2001, Vol. 2, pp. 1183-1186.
16. K. Kinoshita, T. Hatakeyama, O. Takikawa, A. Yahata, and T. Shinohe, "Guard ring assisted RESURF: A new termination structure providing stable and high breakdown voltage for SiC power devices", 14th Int. Symposium on Power Semiconductor Devices and ICs, Santa Fe, NM, USA, June 2002, pp. 253-256.
17. J. H. Zhao, P. Alexandrov, and X. Li, "Demonstration of the first 10-kV 4H-SiC Schottky barrier diodes", *IEEE Trans. Electron Device Lett*., 2003, 24, 402-404.
18. Y. Zhang, Y. Zhang, Y. Wang, and R. Liang, "The effect of different mechanism on the characteristics of SiC Schottky barrier diode", 4th Int. Workshop on Junction Technology, Beijing, China, March 2004, pp. 171-174.
19. T. Nakamura, T. Miyanagi, I. Kamata, T. Jikimoto, and H. Tsuchida, "A 4.15 kV, 9.07mΩcm^2 4H–SiC Schottky barrier diode using Mo contact annealed at high temperature", *IEEE Trans. Electron Device Lett*., 2005, 26, 99-101.
20. X. Jordan, D. Fournier, M. Vellvehi, A. P Crez, R. Perez, P. Godignon, and J. Millin, "Comparative evaluation of high current SiC Schottky diodes and Si PN junction diodes", Spanish Conference on Electron Devices, Tarragona, Barcelona, Spain, February 2005, pp.87-90.
21. C. H. Zhou, X. R. Luo, X. C. Deng, J. P. Zhang, Z. J. Li, and B. Zhang,"High breakdown voltage 4H-SiC Schottky barrier diodes with floating metal rings for MMIC applications", 8th Int. Conference on Solid-State Integrated Circuit Technology, Shanghai, China, October 2006, pp. 944-946.
22. S. Hu and K. Shan, "A new edge termination technique for SiC power devices", *Solid State Electronics*, 2004, 48, 122-123.
23. J. A. Cooper, M. R. Melloch, R. Singh, A. Aggarwal, and J. W. Palmour, "Status and prospect for SiC MOSFET", *IEEE Trans. Electron Devices*, 2002, 49, 658-664.
24. R. Kosugi, S. Suzuki, M. Okamoto, S. Harada, J. Senzaki, and K. Fukuda, "Strong dependence of the inversion channel mobility of 4H and 6H SiC (0001) MOSFETs on the water content in pyrogenic re-oxidation annealing", *IEEE Electron Device Lett*., 2002, 23, 136-138.
25. S. M. Sze, "Physics of Semiconductor Devices," 2nd Edn., John Wily & Sons, New York, 1985.

26. J. N. Shenoy, J. A. Cooper, and M. R. Melloch, "High-voltage double-implanted MOS power transistors in 6H-SiC", IEEE Device Research Conference, Santa Barbara, CA, USA, June **1996**, pp. 202-204.
27. J. N. Shenoy, J. A. Cooper, and M. R. Melloch, "High-voltage double-implanted power MOSFET's in 6H-SiC," *IEEE Trans. Electron Device Lett*., **1997**, 18, 93-95.
28. P. M. Shenoy and B. J. Baliga, "The planar 6H-SiC ACCFET: A new high-voltage power MOSFET structure," *IEEE Trans. Electron Device Lett*., **1997**, 18, 589-591.
29. M. Ruff, H. Mitlehner, and R. Helbig, "SiC devices: Physics and numerical simulation", *IEEE Trans . Electron Device*, **1994**, 41, 1040-1054.
30. M. Bhatnagar and B. J. Baliga, "Comparison of 6H-SiC, 3C-SiC and Si for power devices", *IEEE Trans. Electron Devices*, **1993**, 40, 645-655.
31. K. Shenai, R. S. Scott, and B. J. Baliga, "Optimum semiconductors for high power electronics," *IEEE Trans. Electron Devices*, **1989**, 36, 1811-1823.
32. B. J. Baliga, "Trends in power semiconductor devices," *IEEE Trans. Electron Devices*, **1996**, 43, 1717-1731.
33. R. B. Hillborn and H. Kang, "Charge Carrier Concentration and Mobility in n-Type 6H Polytypes of SiC", University of South Carolina Press, 1973, pp. 337-339.
34. J. Tan, J. A. Cooper, Jr., and M. R. Melloch, "High-voltage accumulation-layer UMOSFETs in 4H SiC", *IEEE Electron Device Lett*., 1998, 19, 487-489.
35. J. Spitz, J. A. Cooper, and M. R. Melloch, "High-voltage lateral DMOSFETs in 4H-SiC", *IEEE Electron Device Lett.,* 1998, 19, 100-102.
36. B. J. Baliga, "Power semiconductor device figure of merit for high-frequency applications", *IEEE Electron Device Lett.,* 1989, 10, 455-457.
37. D. M. Brown, M. Ghezzo, J. Kretchmer, E. Downey, J. Pimbley, and J. Palmour, "SiC MOS interface characteristics", *IEEE Trans. Electron Devices*, 1994, 41, 618-620.
38. J. W. Palmour, J. A. Edmond, H. S. Kong, and C. H. Carter, Jr., "Vertical power devices in silicon carbide," Int. Conference on Silicon Carbide and Related Materials, Santa Barbara, USA, 1994, p. 499.
39. A. K. Agarwal, R. R. Siergiej, S. Seshadri, M. H. White, P. G. McMullin, A. A. Burk, L. B. Rowland, C. D. Brandt, and R. H. Hopkins, "A critical look at the performance advantages and limitations of 4H-SiC power UMOSFET structures", 8th Int. Symposium on Power Semiconductor Devices and ICs, Maui, HI, USA, May 1996, pp. 119-122.
40. A. K. Agarwal, J. B. Cascady, L. B. Rowland, W. F. Valek, M. H. White, and C. D. Brandt, "1.1KV 4H-SiC Power UMOSFET's," IEEE Trans. Electron Device Lett., 1997, 18, 586-588.
41. Y. Sugawara and K. Asano, "1.4 kV 4H-SiC UMOSFET with low specific on resistance," Int. Symposium on Power Semiconductor Devices and ICs, Kyoto, Japan, 1998, pp.119-122.
42. J. B. Casdy, A. K. Agarwal, L. B. Rowland, W. F. Valek, and C. D. Brandt, "900V DMOS and 1100 V UMOS 4H-SiC power FET's," IEEE Devices Research Conference, Fort Collins, USA, June 1997, pp. 32-33.
43. J. B. Casady, A. K. Agarwal, L. B. Rowland, S. Seshadri, P. A. Sanger, and C. D. Brandt, "Silicon carbide MOSFET technology", IEEE Int. Symposium on Compound Semiconductor, San Diego, USA, 1997, pp. 359-362 .
44. Y. Sugawara and K. Asan, "1.4kV 4H-SiC UMOSFET with low specific on- resistance", 10th Int. Symposium on Power Semiconductor Devices and ICs, Kyoto, Japan, June 1998, pp.119-122.
45. C. M. Johnson, N. G. Wright, S. Ortolland, D. Morrison, K. Adachi, and A. O'Neill, "Silicon carbide power devices: hopeful or hopeless?", IEE Colloquium on Recent Advances in Power Devices, London, UK, 1999, pp. 10/1-10/5.

46. A. Mihaila, F. Udrea, R. Azar, J. Liang, G. Amaratungal, A. Rusu, and G. Brezeanu, "Theoretical and numerical investigation of SiC JFET and MOSFET at 6.5kV", Semiconductor Conference, Sinaia, Romania, October **1999**, pp.191-194.
47. N. S. Saks, S. S. Mani, A. K. Agarwal, and M. G. Ancona, "A 475-V high-voltage 6H-SiC lateral MOSFET", *IEEE Electron Device Lett*., 1999, 20, 431-433.
48. W. E. Wagner, III and M. H. White, "Characterization of silicon carbide epitaxial channel MOSFETs", *IEEE Trans. Electron Devices*, 2000, 47, 2214-2220.
49. S. Banerjee, K. Chatty, T. P. Chow, and R. J. Gutmann, "Improved high-voltage lateral RESURFMOSFETs in 4H–SiC", *IEEE Electron Device Lett*., 2001, 22, 209-211.
50. D. R. Disney, A. K. Paul, M. Darwish, R. Basecki, and V. Rumennik, "A new 800V lateral MOSFET with dual conduction paths", Int. Symposium on Power Semiconductor Devices and ICs, Osaka, Japan, 2001, pp. 399-402.
51. D. Alok, E. Arnold, R. Egloff, J. Barone, J. Murphy, R. Conrad, and J. Burke, "4H-SiC RF power MOSFETs", *IEEE Electron Device Lett*., 2001, 22, 577-578.
52. R. Ramovi, M. Jevti, J. Hadzi-Vukovi, and D. Randjelov, "A novel analytical model of a SiC MOSFET", 23rd Int. Conference on Microelectronics (MIEL 2002), Nis, Yugoslavia, May 2002, Vol. 2, pp. 447-450.
53. S. H. Ryu , A. Agarwal, J. Richmond, J. Palmour, N. Saks, and J. Williams, "10 A, 2.4 kV Power DiMOSFETs in 4H-SiC", *IEEE Electron Device Lett*., 2002, 23, 321-323.
54. S. Banerjee, T. P. Chow, and R. J. Gutmann, "1300-V 6H-SiC Lateral MOSFETs with two RESURF zones", *IEEE Electron Device Lett.,* 2002, 23, 624-626.
55. M. Hasanuzzaman, S. K. Islam, and L. M. Tolbert, "Model simulation and verification of vertical double implanted (DIMOSFET) transistor in 6H-SIC", *Int. J. Modeling and Simulation,* 2003, 4, 1-4.
56. M. Avram, G. Brezeanu, and D. P. Poenar, "The comparison of modern SiC power devices", IEEE Int. Conference on Industrial Technology, Hammamet, Tunisia, December 2004, Vol.1, pp.504-509.
57. L. Chen, O. J. Guy, M. R.Jennings, S. P. Wilks, and P. A. Mawby, "Simulation study of 1.2kV 4H-SiC DIMOSFET structures", 7th Int. Conference on Solid-State and Integrated Circuits Technology, Beijing, China, October 2004, Vol.3, pp. 2341-2344.
58. Q. Zhang, M. Gomez, C. Bui, and E. Hanna, "1600V 4H-SiC UMOSFETs with dual buffer layers", 17th Int. Symposium on Power Semiconductor Devices and IC's", Santa Barbara, CA, USA, May 2005, pp. 211-214.
59. Y. Sui, T. Tsuji, and J. A. Cooper, Jr., "On-state characteristics of SiC power UMOSFETs on 115 μm drift layers", *IEEE Electron Device Lett*., 2005, 26, 255-257.
60. T. Kimoto, H. Kawano, and J. Suda, "1330 V, 67 $m\Omega cm^2$ 4H-SiC (0001) RESURF MOSFET", *IEEE Electron Device Lett*., 2005, 26, 649-651.
61. A. Agarwal, M. Das, B. Hull, S. Krishnaswami, J. Palmour, J. Richmond, S. H. Ryu, and J. Zhang, "Progress in silicon carbide power devices", 64th Device Research Conference, Pennsylvania, USA, June 2006, pp. 155-158.
62. J. W. Palmour, "Energy efficient wide bandgap devices", Compound Semiconductor Integrated Circuit Symposium 2006, San Antonio, TX, USA, November 2006, pp. 4-7.
63. T. R. McNutt, A. R. Hefner, H. A. Mantooth, D. Berning, and S. H. Ryu, "Silicon carbide power MOSFET model and parameter extraction sequence", *IEEE Trans. Power Electronics*, 2007, 22, 353-362.

64. R. C. Clarke, R. R. Siergiej, A. K. Agarwal, C. D. Brandt, A. A. Burk, Jr., A. Morse, and P. A. Orphanos, "30W VHF 6H-SiC Power static induction transistor", IEEE/Cornell Conference on Advanced Concepts in High Speed Semiconductor Devices and Circuits, Ithaca, NY, USA, August 1995, pp. 47-55.
65. R. C. Clarke, R. R. Siergiej, A. K. Agarwal, C. D. Brandt, A. A. Burk, Jr., A. Morse, and P. A. Orphanos, "High power 4H SiC static induction transistors", Int. Electron Devices Meeting, Washington, DC, USA, December 2005, pp. 353-356.
66. C. Davis, J. Hawkins, and C. Einolf, Jr.,"Solid state DTV transmitters", *IEEE Trans. Broadcasting*, 1997, 43, 252-260.
67. A. K. Agarwal, L. S. Chen, G. W. Eldridge, R. R. Siergiej, and R. C. Clarke, "Ion-implanted static induction transistors in 4H-SiC", 56th Device Research Conference, Charlottesville, VA, USA, June 1998, pp. 94-95.
68. J. P. Henning, A. Przadka, M. R. Melloch, and J. A. Cooper, Jr., "Design and demonstration of C-band static induction transistors in 4H silicon carbide", 57th Device Research Conference, Santa Barbara, CA, USA, June 1999, pp. 26-28.
69. J. P. Henning, A. Przadka, M. R. Melloch, and J. A. Cooper, Jr., "A novel self-aligned fabrication process for microwave static induction transistors in silicon carbide", *IEEE Electron Device Lett*., 2000, 21, 578-580.
70. H. Onose, T. Yatsuo, A. Watanabe, T. Yokota, T. Ishikawa, I. Sanpei, T. Someya, and Y. Kobayashi, "Design consideration for 2 kV SiC-SIT", 13th Int. Symposium on Power Semiconductor Devices and IC's", Osaka, Japan, June 2001, pp. 179-182.
71. H. Onose, A. Watanabe, T. Someya, and Y. Kobayashil, "Switching properties of 2 kV SiC- SIT", 14th Int. Symposium on Power Semiconductor Devices and IC's, Santa Fe, NM, USA, June 2002, pp. 134-135.
72. T. J. Knight, R. C. Clarke, R. R. Barron, J. A. Ostop, B. A. Morick, J. R. Gigante, W. J. Malkowski, A. W. Morse, G. DeSalvo, and K. J. Petrosky, "A silicon carbide self-aligned and ion implanted static induction transistor (SAI-SIT) for 150 watt S-band operation", 60th Device Research Conference, Santa Barbara, California, USA, June 2002, pp.179-180.
73. J. Fuerherm, Y. A. Zeng, and M. H. White, "A study of interface charges on the operation of 4H silicon carbide (SiC) static induction transistors", Int. Symposium on Semiconductor Device Research, Washington, DC, USA, December 2003, pp. 134-135.
74. Y. C. Choi, H. Y. Cha, M. Chandrasekhar, L. F. Eastman, and M. G. Spencer, "A new approach to maximizing the power handling capability in recessed-gate silicon carbide static induction transistors", IEEE 36th Power Electronics Specialist Conference, Orlando, FL, USA, 2005, pp. 2171-2174.
75. Y. Tanaka, M. Okamoto, A. Takatsuka, K. Arai, T. Yatsuo, K. Yano, and M. Kasuga, "700-V, 1.0-mΩcm^2 Buried gate SiC-SIT", *IEEE Electron Device Lett*., 2006, 27, 908-910.
76. Y. Tanaka, M. Okamoto, A. Takatsuka, K. Arai, T. Yatsuo, K. Yano, and M. Kasuga, "Buried gate static induction transistors in 4H-SiC (SiC-BGSITs) with ultra low on-resistance, 19th Int. Symposium on Power Semiconductor Devices and ICs, Jeju, Korea, May 2007, pp. 93-96.
77. J. A. Cooper, Jr., J. W. Palmour, C. T. Gardner, M. R. Melloch, and C. H. Carter, Jr., "Bulk and perimeter generation in 6H-SiC diodes," Int. Semiconductor Device Research Symposium, Charlottesville, VA, USA, December 1991, pp. 110-112.
78. J. A. Cooper, Jr., M. R. Melloch, W. Xie, J. A. Palmour, and C. H. Carter, Jr., "Dynamic charge storage in 6H-silicon carbide: prospects for high-speed nonvolatile RAM's," *IEEE Trans. Electron Devices,* 1992, 39, 2646-2647.

79. W. Xie, J. A. Cooper, Jr., M. R. Melloch, J. W. Palmour, and C. H. Carter, Jr, "A vertically integrated bipolar storage cell in 6H silicon carbide for nonvolatile memory applications", *IEEE Electron Device Lett*., 1994, 15, 212-214.
80. W. Xie, J. A. Cooper, Jr., and M. R. Melloch, "Monolithic NMOS digital integrated circuits in 6H-SiC", *IEEE Electron Device Lett*., 1994, 15, 455-457.
81. P. Jamet and S. Dimitrijev, "Physical properties of N2O and NO-nitrided gate oxides grown on 4H SiC," *Appl. Physics Lett*., 2001, 79, 323–325.
82. K. Y. Cheong and S. Dimitrijev, "MOS capacitor on 4H–SiC as a nonvolatile memory element", *IEEE Electron Device Lett*., **2002**, 23, 404-406.
83. J. Spitz, J. A. Cooper, and M. R. Melloch, "Lateral power MOSFETs", http://www.ecn.purdue.edu/wbg/DeviceResearch/LDMOSFETs/Index.html, Purdue WBC, Purdue University, West Lafayette, IN, USA, July **1997**.
84. www.ece.rutgers.edu/~jzhao, **1992**.

Maejo International Journal of Science and Technology

ISSN 1905-7873
Available online at www.mijst.mju.ac.th

Full Paper

Embryonic development, hatching, mineral consumption, and survival of Macrobrachium rosenbergii (de Man) reared in artificial seawater in closed recirculating water system at different levels of salinity

Krasindh Hangsapreurke[1, 6,*], Thon Thamrongnawasawat [2], Sorawit Powtongsook [4], Pratak Tabthipwon[5], Prajuab Lumubol[2], and Boonyarath Pratoomchat [3]

[1] Faculty of Fisheries Technology and Aquatic Resources, Maejo University, Sansai, Chiangmai, Thailand
[2] Graduate School, Kasetsart University, Bangkok, Thailand
[3] Department of Marine Science, Faculty of Fisheries, Kasetsart University, Bangkok, Thailand
[4] Marine Biotechnology Research Unit, c/o Department of Marine Science, Chulalongkorn University, Bangkok, Thailand
[5] Department of Aquaculture, Faculty of Fisheries, Kasetsart University, Bangkok, Thailand.
[6] Department of Aquatic Science, Faculty of Science, Burapha University, Bangsaen, Chonburi, Thailand

Corresponding author, e-mail : krasindh@yahoo.com

Received: 22 January 2008 / Accepted: 29 July 2008 / Published: 20 August 2008

Abstract : This experiment aims to study the effect of different levels of salinity (5, 15 and 25 ppt) using artificial sea water on the embryonic development and hatching percentage of the eggs of unripe berried female giant freshwater prawns (Macrobrachium rosenbergii) with an average size of 14.3+0.6 cm TL. After incubation through the heart beating stage (grayish black eggs), the brooders in each salinity were separately transferred to the hatching tank with 15 ppt saline water for the second part of the study. After hatching, the healthy larvae from the brooders which were previously incubated in 3 levels of salinity were collected for the larviculture experiment. The closed recirculating water system with trickling filter unit packed with fiberglass and bioballs was used as incubation and larviculture units. The metamorphosis period and survival rate were examined. The rearing water from each larviculture aquarium was collected for determination of sodium, magnesium, potassium, calcium and chloride ions. The result showed that the percentage of ripe berried females (with heart beating stage embryos) were not significantly different ($p>0.05$) between 5 and 15 ppt salinity but their values were significantly higher ($p<0.05$) than that obtained in 25 ppt salinity. The hatching rate of eggs from berried females incubated in 5 ppt salinity was significantly higher ($p< 0.05$) than those obtained in 15 and 25 ppt salinity while the hatching rate in 15 ppt salinity was also significantly higher ($p< 0.05$) than that in 25 ppt salinity. There were no significant differences ($p>0.05$) in the survival rate of post larvae

and metamorphosis period among the treatments. The first post larvae stage occurred on the 26th day. During 30 days of larviculture, the survival rate of all treatments was 100% until the 19th day, after which it suddenly decreased. When the concentrations of the ions in the rearing water were determined in all treatments, it was found that the concentration of magnesium ions rapidly declined ($p<0.01$) while those of sodium and potassium ions decreased gradually ($p<0.05$). No change was observed in the calcium and chloride ion concentration throughout the experiment ($p>0.05$). The low survival rate during the final stage of larviculture might be due to the depletion of the previously mentioned ions especially that of magnesium.

Keywords: Macrobrachium rosenbergii, giant freshwater prawns, mineral consumption, artificial sea water, salinity, larval production

Introduction

The giant freshwater prawn, Macrobrachium rosenbergii (de Man) is a highly esteemed food for Thais. In former time, these prawns were highly abundant in rivers, lagoons, freshwater reservoirs and brackish water areas [1-2] . However, a very drastic reduction of the wild stock has been observed because of water pollution and overfishing which could have been due to the increasing demand of freshwater prawns in the global market. To provide for the global market demand many giant freshwater prawn farms have been established. Since the discovery of the importance of salinity as a basic requirement for the larval survival of M. rosenbergii [1] numerous hatcheries have developed techniques to mass-produce the post-larvae at a commercial scale.

In 2000, the world production of giant freshwater prawns was estimated at 118,501 MT and was valued at $ 410,001,000 [3]. Thailand's production in 2002 was approximately 15,000 MT [4] or an estimated 12.6% of world production. The giant freshwater prawn is an important economic aquatic animal that can be cultured in all freshwater areas throughout Thailand. The central area is the most prominent for hatcheries which have been expanding to other areas. However, because of the high demand, production is still not enough. Although some areas are not suitable for culture because of low temperatures in winter time, some studies have reported success by increasing the temperature of the water by 3-4° C through covering the earthen ponds with plastic film [5]. Furthermore, some researchers have studied the effect of culture season and stocking density for giant freshwater prawn culture in the northern part of Thailand and found out the best conditions for the area where temperature decreases in the winter time [6]. These findings led to the expansion of culture areas in the North and Northeast which are far from the source of larvae production. In the past, it was possible to transport larvae from the source to anywhere because of low transportation cost. Unfortunately, because of the continuing increase in the transportation cost for saline water and shrimp larvae, increased production is becoming less feasible. Furthermore, lower survival rate of larvae can occur due to stress from long hours of transportation, hence the growing need for local hatcheries. However, these hatcheries still need to transport concentrated seawater from the source, which still commands high transportation cost and in turn makes it difficult for local hatcheries to continue larval production.

Therefore, it is necessary to find an alternative source of saline water to lower the cost of operation. Artificial sea water should be the best choice but information in its use is lacking. To address this problem, the use of commercial artificial sea water under closed circulating saline water system with trickling filter unit packed with fiberglass and bioballs has been investigated in this study. The major ions were also examined throughout culture period. Furthermore, the embryonic development and hatching of the berried females eggs were monitored under different levels of salinity using artificial sea water to observe its effect on the larval production.

Materials and Methods

The experiment was divided into two parts. The first part involved the effect of artificial sea water at 5, 15 and 25 ppt (parts per thousand) salinity on the embryonic development and hatching percentage of the eggs of berried females (M. rosenbergii). After incubation until the heart beating stage (grayish black eggs), the brooders in each salinity were separately transferred to the hatching tank which had a salinity of 15 ppt. After hatching, the healthy larvae from each brooder assigned in three different salinity levels were collected for the larviculture experiment. The second part focused on studying the mineral consumption of the prawn larviculture in a closed recirculating water system using artificial sea water. The metamorphosis period and survival rate were examined.

Source of water and brooders

Artificial sea salt powder (Marinium®) from Mariscience International Co. Ltd. was used. Salinity was adjusted to desirable levels using Jenway conductivity meter (model 4200). The unripe berried females (embryonic stage of gastrula) at an average size of 14.3+0.6 cm in total length (TL) from a commercial farm in Chiangrai province were used.

Incubation and larviculture system

A closed recirculating water system employing glass aquariums with trickling filter unit packed with fibreglass and bioballs was used for incubation and larviculture. All aquariums were rectangular with a dimension of 29.5 x 60.0 x 38.0 cm and covered tightly with a plastic lid. Three compartments were included in each aquarium. The first compartment (29.5 x 44.5 x 38.0 cm) with a fine mesh net cage was provided for larval rearing area. The fine mesh net cage of 15 x15 x13 cm was used for 1- to 10- day-old larvae, while the cage of 20 x 20 x 20 cm was used for >10-day-old larvae. The second compartment (14.3 x 17.5 x 38.0 cm) was provided with a trickling filter unit. The inside of the compartment contained 2 layers of fibreglass at the top and 720 bioballs at the bottom. The last compartment (11.7 x 14.3 x 38.0 cm) was installed with a water pump (capacity 600 L/hr) for water circulation (Figure 1).

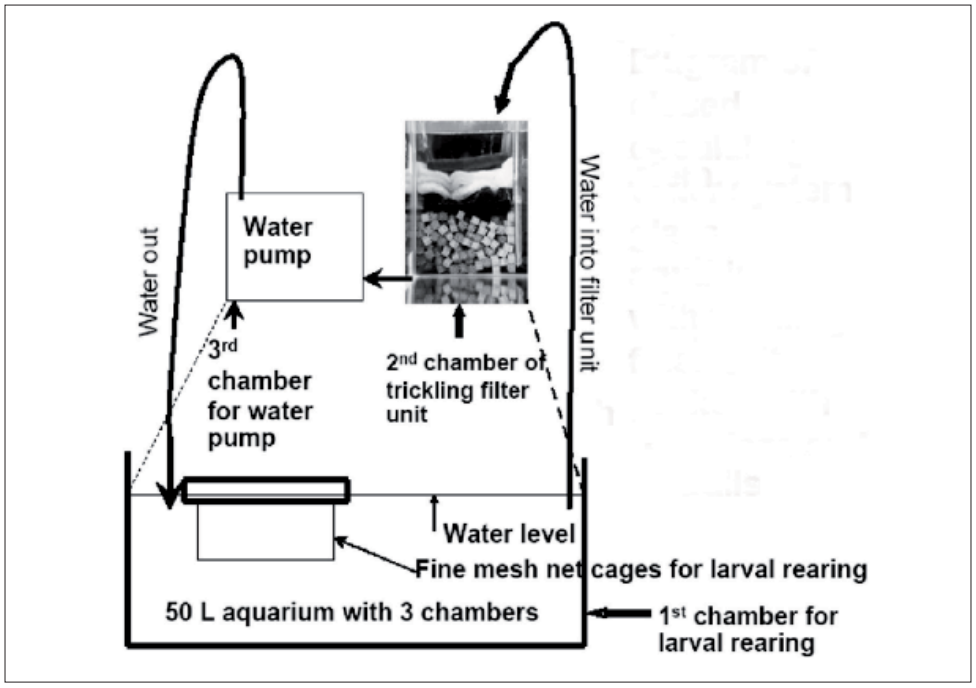

Figure 1. Diagram of the closed recirculating water system aquarium

Egg incubation

The berried females at gastrula stage were held in the 50-L closed recirculating water system aquariums at a density of six females/aquarium. The experiment was performed in triplicate per salinity. Acclimatisation to 5, 15 and 25 ppt artificial sea water was done prior to the experiment proper. During incubation they were fed with sliced fresh squid.

Ten eggs from each female were sampled daily to examine the embryonic stage. The developmental period from gastrula stage to heart beating stage (grayish black colour) was individually recorded. The major ions, viz. sodium, magnesium, potassium, calcium and chloride from the incubation water of each salinity values were determined.

The water in each incubation aquarium was sampled at the beginning and the 10th day of incubation.

Preparation of larvae and larviculture

The ripe berried females from different salinity levels were separately stocked in 100-L fibreglass tanks which contained 15 ppt artificial sea water until hatching. The healthy larvae from the brooders were then randomly sampled (80 larvae/L.) and put in each 50-L aquarium containing artificial sea water at 15 ppt salinity for the larviculture experiment. The closed recirculating water system with trickling filter unit packed with fibreglass and bioballs was used. The lavae were fed with newly-hatched Artemia nauplii at a density of five individuals/ml twice a day throughout the experiment. There was no water change, but the debris was removed regularly. The larval development was checked daily at 8.00 am.

Sampling of rearing water and mineral determination

The rearing water from each larviculture aquarium was collected at the start and three times a week thereafter throughout the experiment. One ml from each water sample was drawn (using an automatic pipette) for determination of sodium, magnesium, potassium, calcium and chloride ions by high performance energy dispersive X- ray fluorescence spectrophotometry (Oxford ED2000) [7-8]

Water quality

Water temperature and pH were checked daily using a Horiba (Model D-21) pH-metre. Nitrite and ammonia were checked every two days using a Hanna C203 multi-parameter specific ion metre. DO was checked daily using a Jenway (9002 Model) DO metre.

Data analysis

All data were analysed by regression analysis, ANOVA and Tukey's using SPSS program.

Results and Discussion

Embryonic development

After the unripe berried females were incubated in various levels of salinity for 10 days, it was observed that the percentages of the ripe berried females in 5 ppt and 15 ppt salinity during 7-10 days were not significantly different ($p>0.05$), but their values were significantly higher than those in 25 ppt salinity ($p< 0.05$) (Figure 2). Sodium, magnesium, potassium, calcium, and chloride ions in the 3 levels of salinity are shown in Table 1. It was clear that the concentrations of those ions were positively correlated with the degree of salinity.

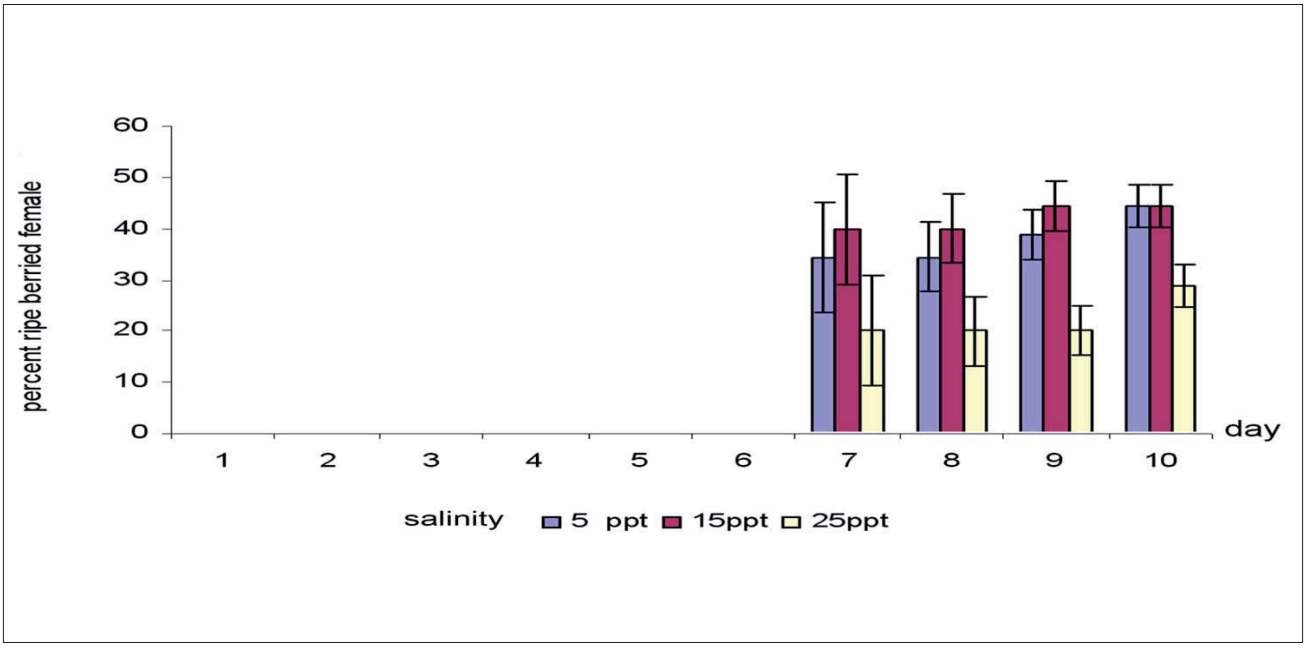

Figure 2. Percentage of ripe berried females after incubation in different levels of salinity during 7-10 days

Table 1. Concentration (mM/L) of Na, Mg, K, Ca and Cl ions in artificial sea water (5, 15 and 25 ppt salinity) at the 1st and 10th day of incubation

Ions	5 ppt (mM/L)		15 ppt (mM/L)		25 ppt (mM/L)	
	Day 1	Day 10	Day 1	Day 10	Day 1	Day 10
Na	64.26 ± 8.45^{a}	46.02 ± 2.11^{b}	199.36 ± 4.03^{a}	155.07 ± 16.95^{b}	287.21 ± 7.22^{a}	243.22 ± 6.7^{b}
Mg	6.95 ± 0.45^{a}	3.66 ± 0.44^{b}	23.93 ± 1.29^{a}	18.95 ± 0.72^{b}	36.57 ± 0.47^{a}	36.61 ± 0.33^{a}
K	2.43 ± 0.19^{a}	2.35 ± 0.10^{a}	5.24 ± 0.45^{a}	5.00 ± 0.40^{a}	7.73 ± 0.56^{a}	7.39 ± 0.17^{a}
Ca	1.96 ± 0.04^{a}	1.94 ± 0.16^{a}	4.82 ± 0.83^{a}	5.13 ± 0.81^{a}	7.82 ± 0.64^{a}	7.95 ± 0.25^{a}
Cl	2.43 ± 0.19^{a}	2.35 ± 0.10^{a}	5.24 ± 0.45^{a}	5.00 ± 0.40^{a}	7.73 ± 0.56^{a}	7.39 ± 0.17^{a}

Note: Means in the same row with different superscripts differ significantly ($p < 0.05$).

The embryonic development of berried females was significantly affected by salinity. Significantly higher percentages of ripe berried females were observed in 5 and 15 ppt salinity. New [9] reported that the suitable salinity for egg incubation was ≤15 ppt. Damrongphol et al. [10] also reported that the embryonic development in vitro was dramatically altered by the concentrations of Na, K and Cl ions in the medium during egg incubation. Their findings (169.2 mM of NaCl and 3.6 mM of KCl) were comparable to, though somewhat lower than ours in the 15 ppt salinity. This phenomenon further supports Ling's findings [11] that the berried females have to migrate to a brackish water area to release the larvae. Furthermore, Singh [12] reported that the isosmotic point for this prawn is 17.5-18.0 ppt. It was indicated that the embryos should need an isosmotic balance for optimum development. The 15 ppt in this experiment seemed to be the most suitable. However, a high percentage of ripe berried females also occurred at 5 ppt, which means that it is also possible to incubate the eggs at 5 ppt salinity although it is considered hyposmotic for the major minerals. This agrees with the findings of Brohmanonda and Sahavacharin [13] who earlier reported that the wild berried females were consistently caught in waters with 3-6 ppt salinity, which was also used for their incubation. Furthermore, New and Singholka [14] reported that some hatcheries placed the berried females in 0-5 ppt saline water during egg incubation prior to transfer to 12 ppt saline water for hatching without osmotic shock. Currently, some hatcheries in Thailand observe that keeping berried females in water of 3-5 ppt salinity can stimulate and improve embryonic development. This clearly indicates that the isosmotic point concept is not a limitation for M. rosenbergii, although it still needs some ions especially Na^{+}, K^{+} and Cl^{-} for development. Egg development and hatching was not possible with deionised water [15]. Also, a hyperosmotic medium was not suitable for the egg development which was negatively affected by an extremely high concentration of ions.

During the 10-day incubation period, it was apparent that sodium ions declined at all salinity levels, but magnesium ions declined only at 5 and 15 ppt salinity. It is possible that the embryos need sodium and magnesium from the environment for their normal development [10]. This experiment has shown that the salinity range of 5-15 ppt was suitable for egg incubation and larval rearing, and that the salinity at 5 ppt should be the most optimum for M. rosenbergii egg incubation. A salinity of 15 ppt has also been used commercially by some Thai farmers for a long time. The salinity at 25 ppt is apparently too high for the incubation of M. rosenbergii eggs since the isosmotic point of the prawn is between 17.0-17.5 ppt [12]. Sandifer et al. [16] reported that the prawn could not survive longer than 24 hours if introduced abruptly into sea water of salinity greater than 18 ppt.

Hatching rate

The hatching rate from berried females incubated in water of 5 ppt salinity was significantly higher ($p< 0.05$) than that in 15 ppt and 25 ppt salinity while the hatching rate in 15 ppt salinity in turn was significantly higher ($p< 0.05$) than that in 25 ppt salinity (Figure 3).

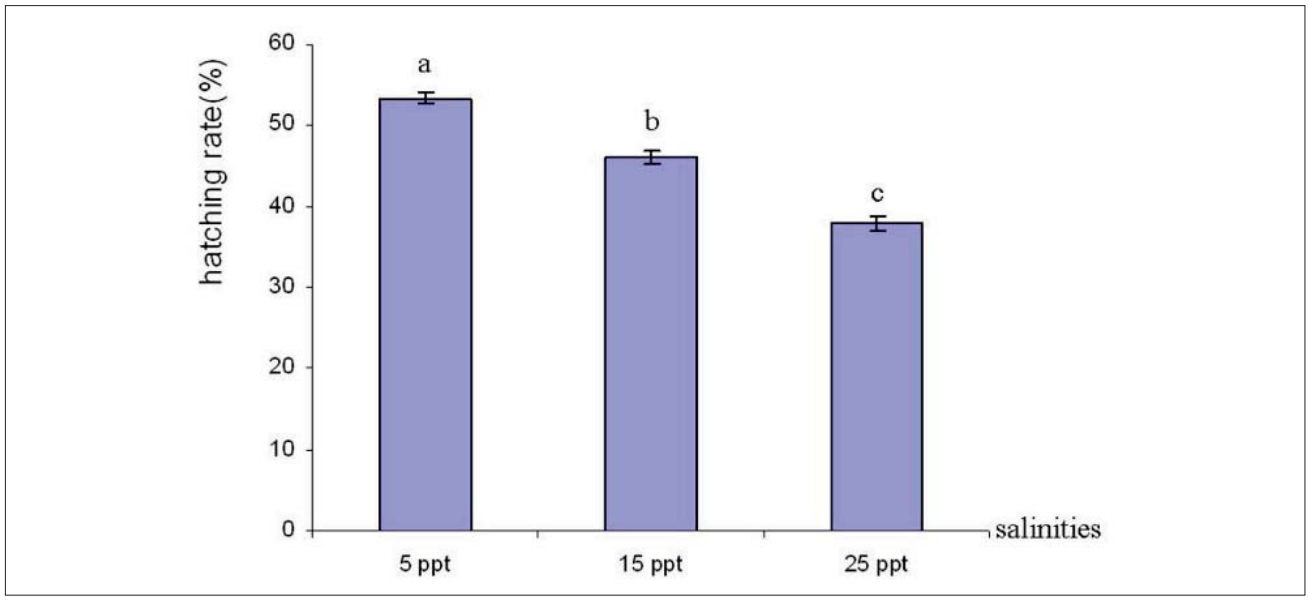

Figure. 3 Hatching rate from berried females incubated in 5, 15 and 25 ppt salinity (± SE)

After 10 days of incubation, all ripe berried females were separately transferred to 15 ppt saline water for hatching. The hatching rate of females incubated in 5 ppt salinity was significantly highest. This agrees with the findings of New [9] that higher hatchability occurs in females incubated in ≤15 ppt salinity. This result is further supported by Brohmanonda and Sahavacharin [13] who also reported a 58% hatching rate at 3-6 ppt salinity. The concentration of the major ions at low salinity (3-5 ppt) apparently improved egg incubation. The survival rate and metamorphosis period of the larvae during the egg incubation at 3 different levels of salinity were not significantly different ($p>0.05$) when cultured in 15 ppt salinity. This indicates that the influence of different salinity during the egg incubation is not the limiting factor for the nursery in artificial sea water at 15 ppt salinity under the closed recirculating system. The result does not agree, however, with the practice of commercial hatcheries in Thailand who believe that higher production occurs when low salinity (3-5 ppt) was used for the egg incubation.

Ion fluctuation during larviculture

As illustrated in Figure 4, during the 30 days of larviculture, magnesium ion concentration rapidly declined ($p<0.01$) while potassium and sodium ion concentration decreased gradually ($p<0.05$). Calcium ion concentration did not change throughout the experiment ($p>0.05$). On the other hand, chloride ion concentration increased but not significantly ($p>0.05$).

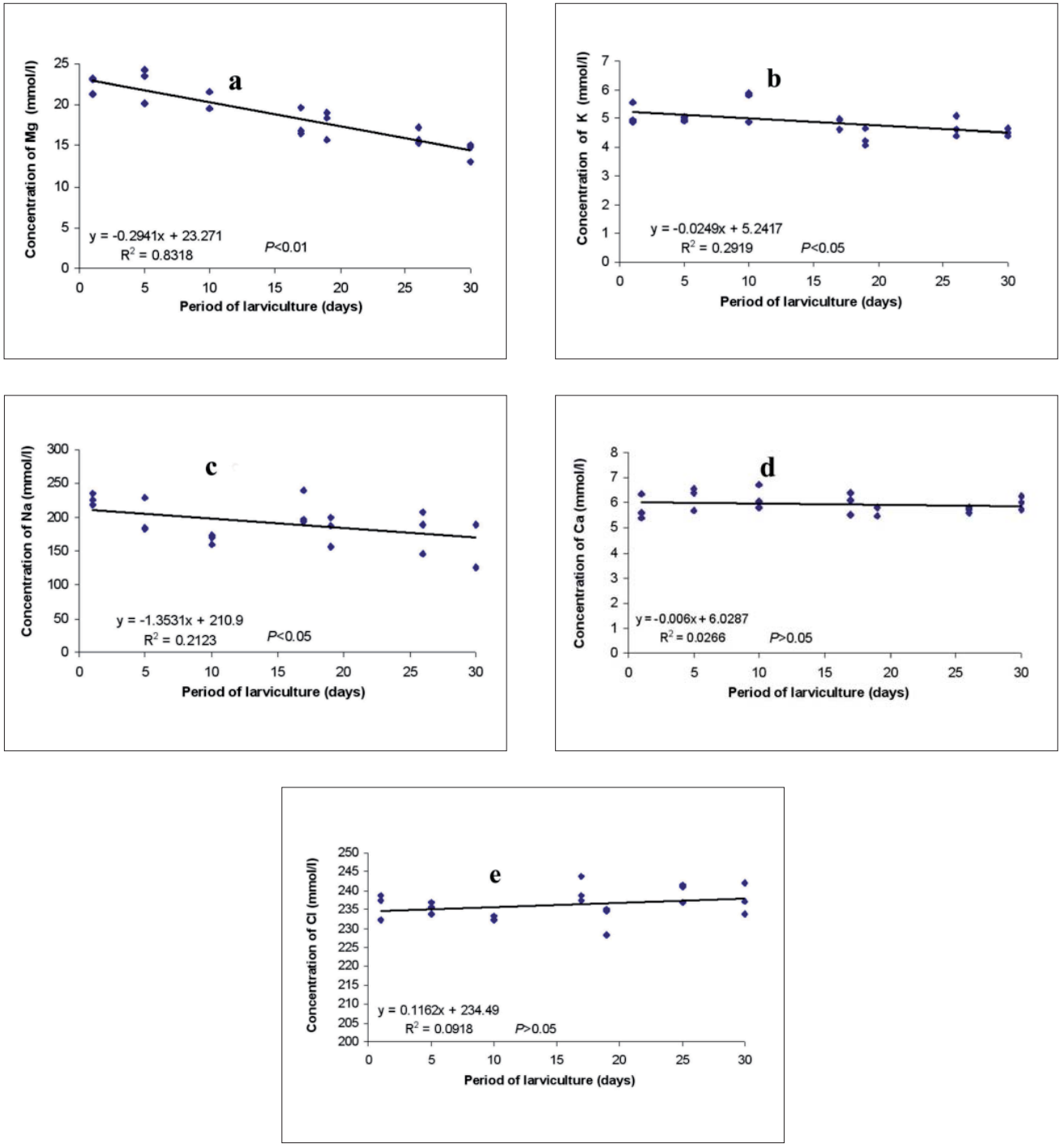

Figure 4. Ion concentrations of magnesium (a), potassium (b), sodium(c), calcium (d) and chlorine (e) in rearing water during 30 days in the closed recirculating system

Survival rate

In trying to reduce the utilisation of saline water in *M. rosenbergii* larviculture by using artificial sea water in place of concentrated sea water under the closed recirculating water system, the survival rate (Figure 5) in our experiment was 18-27% (14-22 PL/L), which was higher than the findings of Tansakul [17] who obtained 15% from nursing in a static water system using artificial sea water at 12 ppt salinity and a density of 10 larvae/L and 12.5% water changing every five days. This is comparable to the result of Ang [18], who obtained 17-50 PL/L in a recirculation system, and also comparable with the report of Menasveta and Piyatiratitivorakul [19] who investigated the closed recirculating system with a separate sub-sand filter unit and a sub-sand filter inside the rearing tank. They could achieve 15.9-18.7% survival rate with a density of 20 larvae/L. Thapa [20] observed a 23% survival rate in an open circulating water system containing rock salt with a density of 50 larvae/L. However, it was noted that the initial stocking density of larvae was significantly lower than that used in our experiment. The survival rate obtained from this study, however, was still lower than that from the commercial farms in Thailand (35-40%) with a culturing density of 80-100 larvae/L using an open system. This indicates that though the system in this experiment is acceptable for *M. rosenbergii* larviculture it seems to need further improvement.

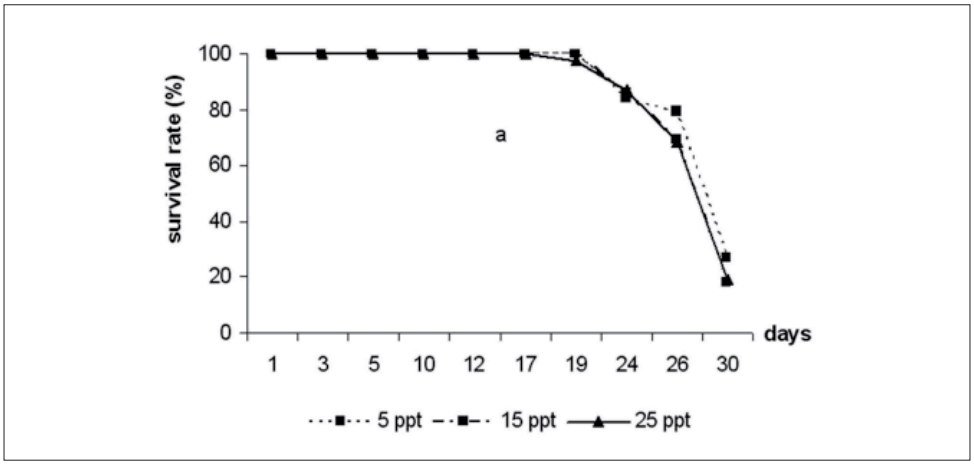

Figure 5. Survival rates of the larvae produced from brooders incubating their eggs in 5 ppt, 15 ppt and 25 ppt salinity during 30-day experiment

The survival rate decreased rapidly after 19 days of culture in this experiment. It might have been caused by the negative effect of continuous depletion of magnesium, potassium and sodium ions in the culture medium. Magnesium ions decreased more than twofold during the study. It should be noted that magnesium is an essential element for cuticle formation and for the neurosystem [7,21,22] while potassium is necessary for the osmoregulatory system and membrane potential [18,22]. The optimum levels of magnesium and potassium ions for M. rosenbergii larvae are 16.45 and 7.67 mM/L respectively [22]. Zang et al. [23] reported that ions such as Na^+, K^+, Ca^{2+}, Mg^{2+}, Cl^-, Br^-, HCO_3^-, and possibly SO_4^{2-} are essential for M. rosenbergii rearing and suggested that the Mg^{2+}/Ca^{2+} ratio should be between 1.8-2.0. It is clear that Mg^{2+}/Ca^{2+} ratio in this experiment was 1.51±0.16 from the start and decreased to 0.61±0.09 after 20 days. This means that the survival rate of the larvae in our experiment might have been affected by this condition. Sodium, magnesium and calcium are also necessary for supporting the normal embryonic development, hatching, and survival of the newly hatched larvae [10]. With these findings, the supplementation of magnesium, sodium and potassium is needed in the culture medium to maintain a suitable concentration throughout the culture period. Calcium ions and calcium/magnesium ion ratio should also be maintained although they are of minor factor for the survival rate.

The average concentrations of ammonia and nitrite during the 30-day experiment were 0.08 and 0.03 ppm respectively, which were very low. The recommended range of total ammonia and nitrite are less than 1.0 and 0.25 ppm respectively [24]. The mortality was therefore not caused by ammonia and nitrite which were produced by the larvae and live feed. The closed recirculating system in our experiment had no impact on the metamorphosis of the larvae because the first day of the post larval stage occurred at the 26th day, which was similar to the result from the commercial production [25].

Conclusions

Unripe females of Macrobrachium rosenbergii incubated in saline water with 5 ppt salinity produced the highest hatching compared to those obtained with 15 and 25 ppt salinity. Embryonic and larval development of the freshwater prawns consume minerals from the rearing water. The larvae consume magnesium, sodium and potassium ions for their metamorphosis during the rearing process.

It was found that artificial sea water from commercial sea salt powder can be used to prepare artificial saline water in place of concentrated sea water from salt farms. Moreover, the use of closed recirculating water system with trickling filter unit packed with fibreglass and bioballs can efficiently reduce saline water usage. This system should therefore be suitable for hatcheries in the northern or north-eastern part of Thailand or in areas that are far away from the coast. There is thus a high possibility to apply this system to the commercial production of M. rosenbergii larvae in the future. However, maintenance of magnesium and potassium concentrations in the culture medium during larval rearing process should be addressed.

Acknowledgements

This research was financially supported by the National Research Council of Thailand (NRCT). We acknowledge the Mariscience International Company Limited for providing commercial sea-salt powder (Marinium®), and Kasetsart University (Sriracha Campus) for allowing us to use the X-ray fluorescence spectrophotometer. We appreciate the assistance of Mr. Krirk Wongsontam for operating the X-ray fluorescence spectrophotometer.

References

1. S. W. Ling and A. B. O. Merican, "Notes on the life and habitats of the adults and larval stages *of Macrobrachium rosenbergii (de Man)", Indo-Pacific Fisheries Council Proceedings,* Karachi, Pakistan, 6-23 Jan.1961, pp. 55-60.
2. T. A. Qureshi, S. M. Basha, and R. Biwas, "Larval rearing of Indian river prawn Macrobrachium *malcolmsomii through synthetic seawater", Oostende Bellgium European Aquaculture Society,* **1993**, 19, 158-224.
3. FAO, "FAO Year Book fisheries statistic", *Aquaculture Production,* **2000**, 90, 1-78.
4. Department of Fisheries, "Fisheries Statistic of Thailand 2002", Fishery Information Technology Center, Department of Fisheries, Ministry of Agriculture and Cooperatives, 2004, 91 pp.

5. N. Whangchai, T. Ungsethaphand, C. Chimanat, K. Mengumphan, and S. Uraiwan, "Performance of giant freshwater prawn *Macrobrachium rosenbergii* (de Man) reared in earthen ponds beneath plastic film shelters", *Chiang Mai J. Sci.* , **2007**, 34, 89-96.
6. R. D. Baysa and N. Whangchai, "Effect of culture season and stocking density on growth and production of giant freshwater prawn *Macrobrachium rosenbergii* (de Man) raised in northern Thailand", *Mj. Int. J. Sci. Tech.,* **2007**, 1, 216-221.
7. B. Pratoomchat, P. Sawangwong, and J. Machado, "Organic and inorganic compound variations in haemolymph, epidermal tissue and cuticle over the molt cycle in *Scylla serrata* (Decapoda)", *Comp. Biochem. Physiol.,* 2002, 131, 243-255.
8. B. Pratoomchat, P. Sawangwong, and J. Machado, "Effects of controlled pH on organic and inorganic composition in haemolymph, epidermal tissue and cuticle of mud crab *Scylla serrata", J. Exp. Zool,* 2003, 295, 47-56.
9. M. B. New, "Freshwater prawn culture : a review", *Aquaculture,* 1990, 88, 99-143.
10. P. Damrongphol, P. Jaroensastraraks, and B. Poolsanguan, "Effect of various medium compositions on survival and hatching rates of embryos of the giant freshwater prawn *Macrobrachium rosenbergii* cultured *in vitro", Fish. Sci.,* 2001, 67, 64-70.
11. S. W. Ling, "The general biology and development of *Macrobrachium rosenbergii* (de Man)", *FAO Fisheries Report,* 1969, 57, 589-606.
12. T. Singh, "The isosmotic concept in relation to the aquaculture of the giant prawn *Macrobrachium rosenbergii," Aquaculture,* 1980, 20, 251-256.
13. P. Brohmanonda and S. Sahavacharin, "Results of experimental culture of giant freshwater prawn larvae *Macrobrachium rosenbergii* (de Man) at Songkhla Marine Fisheries Station", Division of Research and Investigations, Department of Fisheries, 1970, 23 pp.
14. M. B. New and S. Singholka, "Freshwater prawn farming", A manual for the culture of *Macrobrachium rosenbergii,* FAO Fisheries Technical Paper 225 (Rev .1), FAO Rome, 1995.
15. P. Damrongphol, N. Engchuan, and B. Poolsanguan, "Simple in vitro culture of embryos of the giant freshwater prawn *Macrobrachium rosenbergii", J. Sci. Soc. Thailand,* 1990, 16, 17-24.
16. P. A. Sandifer, J. S. Hopkins, and T. I. J. Smith, "Observations on salinity tolerance and osmoregulation in laboratory-reared *Macrobrachium rosenbergii* postlarvae (Crustacea: Caridea)", *Aquaculture,* 1975, 6, 103-114.
17. R. Tansakul, "Progress in Thailand rearing larvae of the giant prawn *Macrobrachium rosenbergii", Aquaculture,* 1983, 31, 95-98.
18. K. J. Ang, "A recirculated biostream hatchery system for larval culture of *Macrobrachium rosenbergii* (de Man)", in "Abstract of World Aquaculture 1996" (Ed. L. R. Cresswell), World Aquaculture Society, 1996, 202-203.
19. P. Menasveta and S. Piyatiratitivorakul, "A comparative study on larviculture techniques for the giant freshwater prawn *Macrobrachium rosenbergii* (de Man)", *Aquaculture,* 1980, 20, 139- 249.
20. A. B. Thapa, "Effect of different sources of salt water and ionic concentrations on larval nursing of giant freshwater prawn *Macrobrachium rosenbergii* (de Man)", *MSc. Thesis,* 2002, Kasetsart University, Thailand.
21. B. Pratoomchat, P. Sawangwong, R. Guedes, M. L. Reis, and J. Machado, "Cuticle ultrastructure changes in the crab *Scylla serrata over the molt cycle", J. Exp. Zool.,* 2002, 293, 414-426.
22. C. Visudtibhan, "Effect of different levels of magnesium ion and potassium ion on the survival *Macrobrachium rosenbergii* (de Man) post larvae in the rock salt water", *MSc. Thesis,* 1993, Kasetsart University, Thailand.

23. Z. Zang, X. Dai, J. Zhang, and Z. Zhu, "Effect of Mg^{2+}, Ca^{2+} and Mg^{2+}/Ca^{2+} contents on survival rates of *Macrobrachium rosenbergii* larvae reared in mixed water", *Oceanologia et Limnologia Sinica,* 1995, 26, 552-557.
24. K. V. Jayachandran, "Palaemonid Prawns: Biodiversity, Taxonomy, Biology and Management", Science Publishers Inc., Cochin (India), 2001.
25. S. Pitipornchai, Personal communication, 2007.

Maejo International Journal of Science and Technology

ISSN 1905-7873

Available online at www.mijst.mju.ac.th

Short Report

Effect of trifluralin on production of male bicellular cells in "Sai Num Phueng" mandarin (Citrus reticulata), calamondin (Citrofortunella mitis), and "Paen" lime (Citrus aurantifolia)

Sahha Toolapong

Horticulture Department, Faculty of Agricultural Production, Mae Jo University, San Sai, Chiang Mai, 50290, Thailand

e-mail: sahha@mju.ac.th

Received: 4 April 2008 / Accepted: 3 September 2008 / Published: 4 September 2008

Abstract: The doubling of male cellular cells of the flowers of mandarin (cultivar "Sai Num Phueng"), calamondin, and lime (cultivar "Paen") by using different concentrations (0.05, 0.10, 0.20, and 0.40%) of trifluralin, which were directly applied to the 35-40 cm length of flush twigs, was studied. The citrus twigs, upon increasing the trifluralin concentration, produced a correspondingly high number of flowers with male bicellular cells (except calamondin that showed an opposite trend), as well as a high number of the male bicellular cells themselves. The normal and male bicellular cells, however, appeared to be similar in size.

Keywords: Citrus reticulata, Citrus aurantifolia, Citrofortunella mitis, trifluralin, microtubules, male bicellular cells

Introduction

Trifluralin (α,α,α-trifluoro-2,6-dinitro-N,N-dipropyl-p-toluidine) is a man-made chemical that is generally used as a soil-treating herbicide (a pre-emergent) to control many annual grasses and broadleaf weeds [1,2]. Jackson and Steller [3] found that trifluralin and orizalin applications caused disappearance of spindle micro-tubules and cell plates that were usually present at the centre of living root-tip cells from germinating seeds of corn and wheat, while mitochondria and plastids were abnormal in shape. Suwanaketnikom [4] mentioned that the micro-tubules are protein structures present in all eukaryotic cells of higher plants, and that some herbicides can cause a non-formation of micro-tubules in plant cells, having a similar action as colchicine which causes an absence of spindle fibres during cell division.

Citrus is an economic sub-tropical fruit crop of the world with a great commercial potential and is also considered to be an important crop in Thailand. However, their naturally high number of seeds per fruit is not what growers, consumers and processors want, which are citrus cultivars that produce either fewer seeds or are seedless. Double male cellular cells are therefore valuable for citrus breeding programs which involve crossing of the male parent having bicellular cells with a haploid female parent, and which can be obtained through treatment with a chemical, e.g. colchicine or a derivative of dinitroaniline (trifluralin, orizalin, etc.).

Materials and Methods

A 44.5% emulsifiable solution of trifluralin (obtained from Japan) was used. The new flush twigs of mandarin (Citrus reticulata, Sai Num Phueng cultivar), calamondin (Citrofortunella mitis), and lime (Citrus aurantifolia, Paen cultivar), each 35-40 cm in length with natural flowery initiation, were wrapped with cotton and plastic sheets (Figure 1) soaked in different concentrations (0.05, 0.10, 0.20, and 0.40%) of trifluralin for 5 days. The citrus flowers (pre-bloom stage) were then collected and kept in 70% ethanol. Later, the number of citrus flowers producing male bicellular cells, and the number and size of the normal and bicellular cells were observed under the microscope using an orcein staining solution.

Results and Discussion

After being applied with different concentrations of trifluralin, the treated pre-bloom flowers from the new flush twigs of mandarin, calamondin and lime were observed under 400x microscopic magnification. It was found that the number of citrus flowers producing male bicellular cells could be increased by increasing the applied chemical concentrations (Tables 1 and 3), except for calamondin wherein the increase in trifluralin concentration resulted in the reduction of the number of flowers having male bicellular cells (Table 2). However, as the chemical concentration applied was increased, the number of the male bicellular cells of all the three citrus flowers also increased (Tables 1-3 and Figure 2). According to Ladlie et al. [5], This is because the central arrangement of the chromosomes is affected by trifluralin and colchicine as shown by their natural failure to form spindle micro-tubules during cell division. Moreover, colchicine may have interfered with the process of cell division, which results in the 'doubling' of chromosome numbers [6]. Jackson and Steller [3] found a reduced number of micro-tubules, especially the cell plates which were located at the centre of the endosperm cells of African blood lily (Haemanthus Katherinae) after application of 50 ppm of trifluralin for 15 minutes to 2 hours. After 3 hours there was a complete disappearance leading to the automatic cessation of the telophase phase. Meanwhile, Fedtk [7] said that the absence of the spindle micro-tubules affected nuclear division and chromosome separation, but Betts and Morrison [8] reported that during the mitotic root-tip cell division, the number of chromosomes was changed and enlargement of the nucleoli occurred after application of trifluralin and matribuzin. The male normal and bicellular cells of the citrus flowers in the present case were similar in sizes (Tables 1-3).

Table 1. Production of male bicellular cells (MBCs) from mandarin flowers after trifluralin application

Trifularin concentration (%)	Number of				Cell size (mm)	
	Flowers	Flowers with MBCs (%)	Cells observed	MBCs (%)	Normal	MBCs
0	10	0 (0)	57	0 (0)	0.089 X 0.090	-
0.05	10	0 (0)	54	0 (0)	-	0.098 X 0.083
0.10	10	2 (20)	65	2 (3.08)	-	0.073 X 0.080
0.20	10	5 (50)	90	5 (5.56)	-	0.081 X 0.098
0.40	10	8 (80)	78	8 (10.23)	-	0.080 X 0.103

Table 2. Production of male bicellular cells (MBCs) from calamondin flowers after trifluralin application

Trifluralin concentration (%)	Number of				Cell size (mm)	
	Flowers	Flowers with MBCs (%)	Cells observed	MBCs (%)	Normal	MBCs
0	10	0 (0)	80	0 (0)	0.078 X 0.094	-
0.05	10	6 (60)	91	5 (5.50)	-	0.075 X 0.085
0.10	10	4 (40)	81	10 (12.35)	-	0.070 X 0.085
0.20	10	3 (30)	74	14 (18.92)	-	0.080 X 0.100
0.40	10	1 (10)	84	17 (20.24)	-	0.085 X 0.105

Table 3. Production of male bicellular cells (MBCs) from lime flowers after trifluralin application

Trifluralin Concentration (%)	Number of				Cell size (mm)	
	Flowers	Flowers with MBCs (%)	Cells observed	MBCs(%)	Normal	MBCs
0	15	0 (0)	60	0 (0)	0.074 X 0.086	-
0.05	8	0 (0)	72	0 (0)	-	0.074 X 0.088
0.10	6	2 (33.33)	54	3 (5.56)	-	0.070 X 0.089
0.20	6	3 (50.00)	63	7 (11.11)	-	0.075 X 0.090
0.40	5	5 (100)	71	10 (14.08)	-	0.074 X 0.087

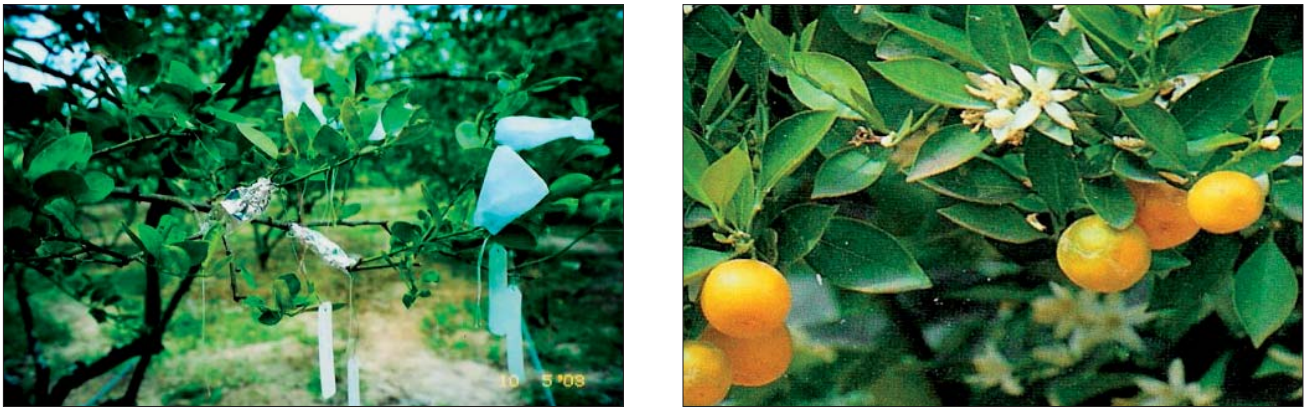

Figure 1. Application of trifluralin on "Paen" lime (left), and flowers and fruits of calamondin (right)

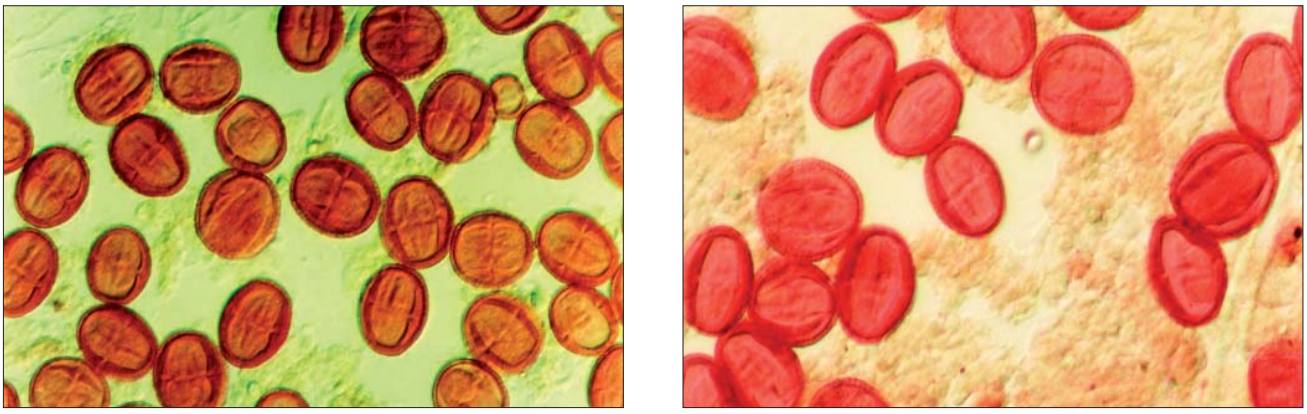

Figure 2. Male bicellular cells of calamondin (left) and "Paen" lime (right)

References

1. J. Tor, C. Xu, J. Stucki, M. Wander, and G. K. Sims, "Trifluralin degradation under microbiologically induced nitrate and Fe. (III) Reducing conditions", US Department of Agriculture, Agricultural Research Service, United Nations, Urbana IL 61801, 1998.
2. R. J. Reigart and J. R. Roberts, "Recognition and Management of Pesticide Poisonings", 5th Edn., U. S. Environmental Protection Agency, Office of Pesticide Programs, Washington, D.C., 1999.
3. W. G. Jackson and D. A. Steller, "Regulation of mitosis. IV. An in vitro and ultrastructure study of effects of trifluralin", Can. J. Bot., 1973, 51, 1513-1516.
4. R. Suwanaketnikom, "Herbicide and plant physiology" (in Thai), Agronomy Department, Faculty of Agriculture, Kasetsart University, Bangkok, 1988.
5. J. S. Ladlie, W. F. Meggitt, and D. Penner, "Effect of trifluralin and matribuzin combination on soybean tolerance to matribuzin", Weed Sci., 1977, 25, 88-93.
6. P. Mooney, M. Watson, and A. Harty, "Developing new seedless citrus triploid cultivars", HortResearch, Kerikeri Research Centre, New Zealand, 1997.
7. C. Fedtke, "Biochemistry and Physiology of Herbicide Action", Springer-Verlag, New York, 1982.
8. M. F. Betts and I. N. Morrison, "Fall and spring applications of trifluralin and matribuzin in Faba beans (Vicia faba)", Weed Sci., 1979, 27, 691-695.

Maejo International Journal of Science and Technology

ISSN 1905-7873
Available online at www.mijst.mju.ac.th

Full Paper

Image-based fingerprint verification system using LabVIEW

Ajat S. Arora 1 and Sunil K. Singla 2,*

[1] Department of Electrical and Instrumentation Engineering, Sant Longowal Institute of Engineering and Technology, Longowal, Punjab, India
[2] Department of Electrical and Instrumentation Engineering, Thapar University, Patiala, Punjab, India

*Corresponding author, e-mail: sunilksingla2001@yahoo.com

Received: 4 April 2008 / Accepted: 1 September 2008 / Published: 5 September 2008

Abstract: Biometric-based identification/verification systems provide a solution to the security concerns in the modern world where machine is replacing human in every aspect of life. Fingerprints, because of their uniqueness, are the most widely used and highly accepted biometrics. Fingerprint biometric systems are either minutiae-based or pattern learning (image) based. The minutiae-based algorithm depends upon the local discontinuities in the ridge flow pattern and are used when template size is important while image-based matching algorithm uses both the micro and macro feature of a fingerprint and is used if fast response is required. In the present paper an image-based fingerprint verification system is discussed. The proposed method uses a learning phase, which is not present in conventional image-based systems. The learning phase uses pseudo random sub-sampling, which reduces the number of comparisons needed in the matching stage. This system has been developed using LabVIEW (Laboratory Virtual Instrument Engineering Workbench) toolbox version 6i. The availability of datalog files in LabVIEW makes it one of the most promising candidates for its usage as a database. Datalog files can access and manipulate data and complex data structures quickly and easily. It makes writing and reading much faster. After extensive experimentation involving a large number of samples and different learning sizes, high accuracy with learning image size of 100 × 100 and a threshold value of 700 (1000 being the perfect match) has been achieved.

Keywords: biometrics, fingerprint, LabVIEW, datalog files, segmentation, pseudo random subsampling

Introduction

Biometric-based personal authentication (verification/identification) systems use physiological (e.g. fingerprint, face, hand geometry, etc.) or behavioural (e.g. speech, handwriting) traits of a person. Biometric systems are becoming increasingly popular, compared to traditional systems because of their ability to provide more security. In practice there are three different methods to check the identity of a person [1,2]; these are:

- Ownership: something you have (key, smart card, etc.)
- Knowledge: something you know (PIN, password, etc.)
- Biometrics: something you are or something you do (fingerprints, face, voice, etc.)

The conventional methods (ownership and knowledge) of checking someone's identity actually suffers from two common problems [2,3]:

- Their inability to differentiate between an authorised person and an imposter who fraudulently acquires the access privilege of the authorised person
- Their being lost, stolen, copied (ownership) or forgotten, guessed (knowledge) Only the third method, i.e. biometrics, can identify you as you and is much more secured than the conventional methods.

Fingerprint is one of the most promising methods among all the biometric techniques and has been used for personal authentication for a long time. A fingerprint consists of raised friction ridges separated by recessed valleys of skin [4,5]. The locations and angular orientation of the ridge endings and ridge bifurcations within the fingerprint uniquely characterise the fingerprint. Presently, it is used for commercial applications as well as by law enforcement agencies. In practice fingerprint systems are of two types [1,2], viz. fingerprint identification and fingerprint verification.

Fingerprint Identification: This kind of system compares the biometric information of a person to all entities on a database. A person does not assert his/her identity to that system; instead the person just gives the biometric information. The system then tries to match this data to all the entities in the database and drives whether a match can be made. This type of system is known as identification system. This system gives the information: "Who the person is."

Fingerprint Verification: A verification system authenticates a person's identity by comparing the captured fingerprint information to one specific entry on a database that corresponds to that person. By comparing one-to-one the system decides whether the identity claimed by the individual is true or not. A verification system is also known as a one-to-one system.

The fingerprint has gained widespread public acceptance due to its convenience and reliability. It takes little time and effort to acquire one's fingerprint so its recognition is considered among the least intrusive of all biometric verification techniques. Fingerprint verification algorithms are of minutiaebased and image-based [6]. For minutiae-based fingerprint algorithm, only a small part of the finger image is required for verification. Normally, ridge ending and ridge bifurcation are taken into consideration. According to the empirical study, two individuals will not have eight or more common minutiae [7,8]. It would be ideal to use this algorithm where space restrictions impacted the use and deployment of biometrics, but this type of system requires a high-quality fingerprint image. Also, minutiae-based approach requires extensive preprocessing operation and it is also required to reduce the number of false minutiae erroneously detected in noisy fingerprint images [9]. Image-based matching

algorithm uses both the micro and macro features of a fingerprint. The size of the image required for authentication must be larger as compared to minutiae-based algorithm, so the memory requirement is more. However, this algorithm is computationally more efficient because it can be directly applied to the gray-scale fingerprint image without or with very little preprocessing. Moreover, unlike the minutiaebased system, the image-based fingerprint verification system is capable of dealing with bad-quality images from which the minutiae cannot be extracted reliably, and also with fingerprints that suffer from non-uniform shape distortion [10]. Instead of using only the minutiae locations the image-based system uses the gray-level information which provides much richer and more discriminatory information than only the minutiae locations.

Present Work

In the present work an image-based algorithm for fingerprint verification is discussed as it is faster than the minutiae-based algorithm. The proposed algorithm has been developed using LabVIEW (Laboratory Virtual Instrument Engineering Workbench) 6i software. The proposed verification algorithm consists of two steps: enrollment of the user and authentication of the user.

In the enrollment process new users are enrolled in the system. Each user has to enter his/her name and password along with biometric information, i.e. the fingerprint. The flow chart of enrollment type module is shown in Figure 1. For the enrollment of the user a data record is to be maintained in the database containing the name and the password of the user. If simple text files are used the name and password get stored together as a single string. Using LabVIEW datalog files [11] (which are exclusively available in LabVIEW to maintain database of records) the information regarding the user is stored in the form of clusters. Datalog files make writing and reading much faster. They also simplify data retrieval because the original blocks of data can be read as a record without having to read all records that precede it in the file. Random access is fast and easy with datalog files because all it needs is to access the record as a record number. This module is designed in such a way that no two users should be of the same name although a user can have any password. If the same name is entered that already exists in the database the algorithm will demand a new name to be entered. The next step is to store the reference biometric information of the person concerned. The reference/query image may contain the information which is not required. In order to eliminate such undesirable information, a preprocessing step, i.e. segmentation, is performed. Segmentation is the process of separating the foreground region in the image from the background one. The foreground region corresponds to the clear fingerprint area containing the ridges and valleys, which is the area of interest. The background corresponds to the region outside the border of the fingerprint area which does not contain any valid fingerprint information. The segmentation is performed by calculating the variance. A foreground region has a high variance value while a background region has a low one. The image is divided into an 8 × 8 window and its variance calculated. If the variance is below a particular value then that is a background. If it is above a particular value then it contains the biometric information. The variance k of the window of size $W \times W$ is given by:

$$\sigma^2(k) = \frac{1}{W^2}\sum_{i=0}^{W-1}\sum_{j=0}^{W-1}\left(I(i,j) - M(k)\right)^2$$

where $M(k)$ = mean of block k
$I(i, j)$ = value at pixel (i, j)
σ = standard deviation

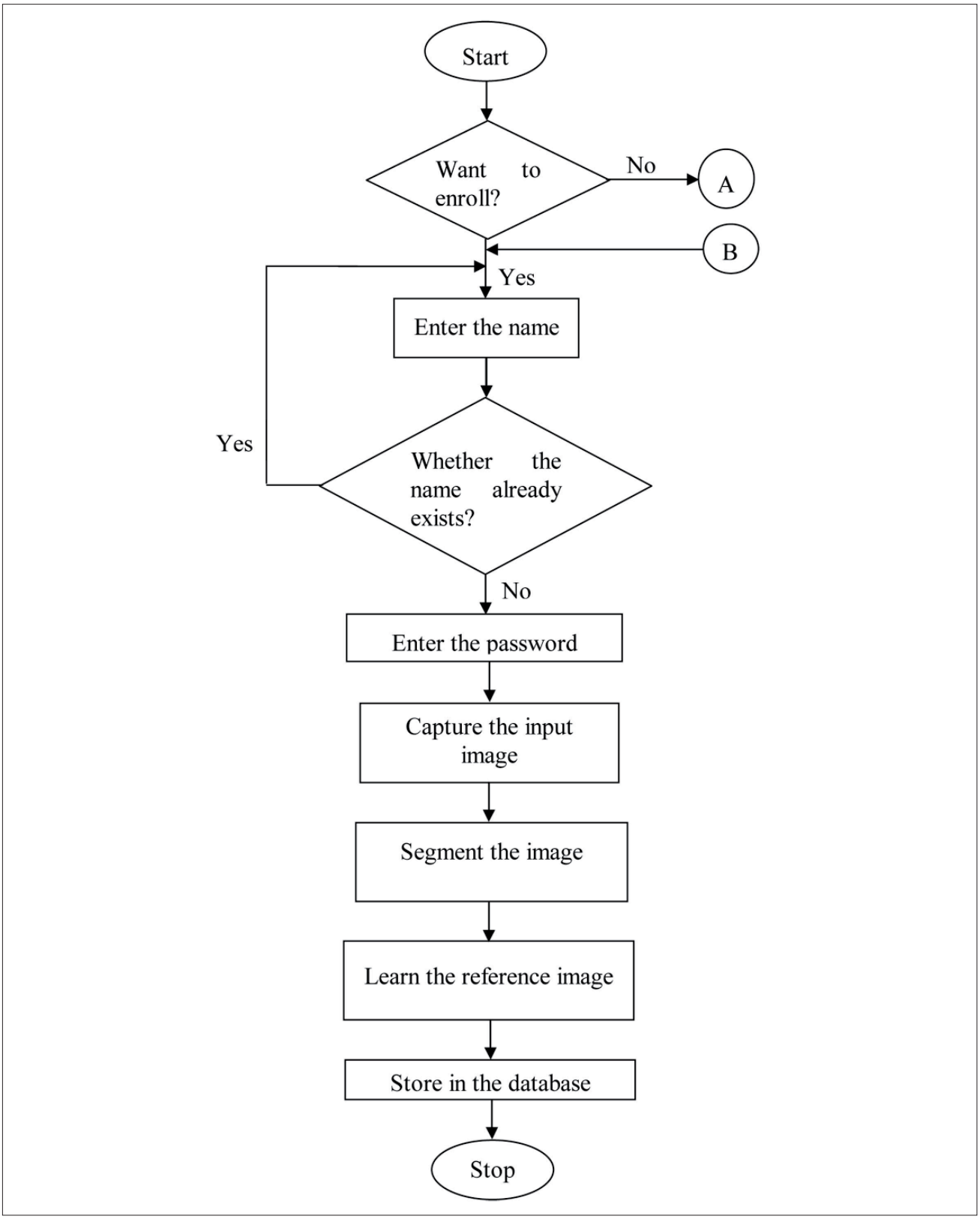

Figure 1. Flowchart of enrollment process

From the segmented image a template is extracted. The size of the extracted template is very critical for the accuracy of the system. Too small template may not provide enough distinction; on the other hand if the entire fingerprint is taken as a template then the elastic deformation of the query image may cause serious errors. Experiments have been conducted by considering the template sizes of 50 × 50, 100 × 100 and 200 × 200 pixels extracted from the centre of the image. The extracted template is fed to the image acquisition (IMAQ) learn pattern virtual instrument (VI). This VI creates a description of the template of the reference image that is to be compared with the data of the query image during the matching stage. In the learning phase a pseudo random sub-sampling is performed in which pixels are analysed by checking their surrounding neighborhood for uniformity and each pixel is classified according to how large the uniformity of its surrounding neighborhood is (e.g. 3 × 3, 5 × 5 and soon) [12]. This step will reduce the amount of calculations in the matching stage. The features of the reference image are extracted using the edge detection operation and the information is stored in a file along with the circular intensity profile of the reference image used in finding the rotated version of the image in the search/query image.

In the verification step (Figure 2), the name and password of the user is first checked. If they are incorrect the system gives a message: "You are not an enrolled user", and stops. If this stage is passed then the system demands for the fingerprint image in question and, after the preprocessing step, compares the two images (one in the reference pallet and the other the preprocessed image in question) with the help of the image acquisition (IMAQ) match pattern virtual instrument (VI), which matches the two images and calculates the threshold value. If the threshold value lies within the accepted limit the system will accept the identity of the user; otherwise, it will reject it.

Database

In the present work the fingerprint images from FVC2002/Db1_a database has been used to obtain the results. The database has been created by:

- Translating the fingerprint images by 1 pixel in both X and Y direction
- Rotating the fingerprint images by 1 degree
- Both translating and rotating the images by 1 pixel and 1 degree

The images are translated and rotated up to ± 15 pixels and ± 15 degrees. Figure 3 shows the original image (1_1 of FVC2002/Db1_a), its translated, rotated and translated plus rotated versions. In this way for every selected image of FVC2002/Db1_a, 90 images (30 translated, 30 rotated and 30 translated plus rotated) are obtained.

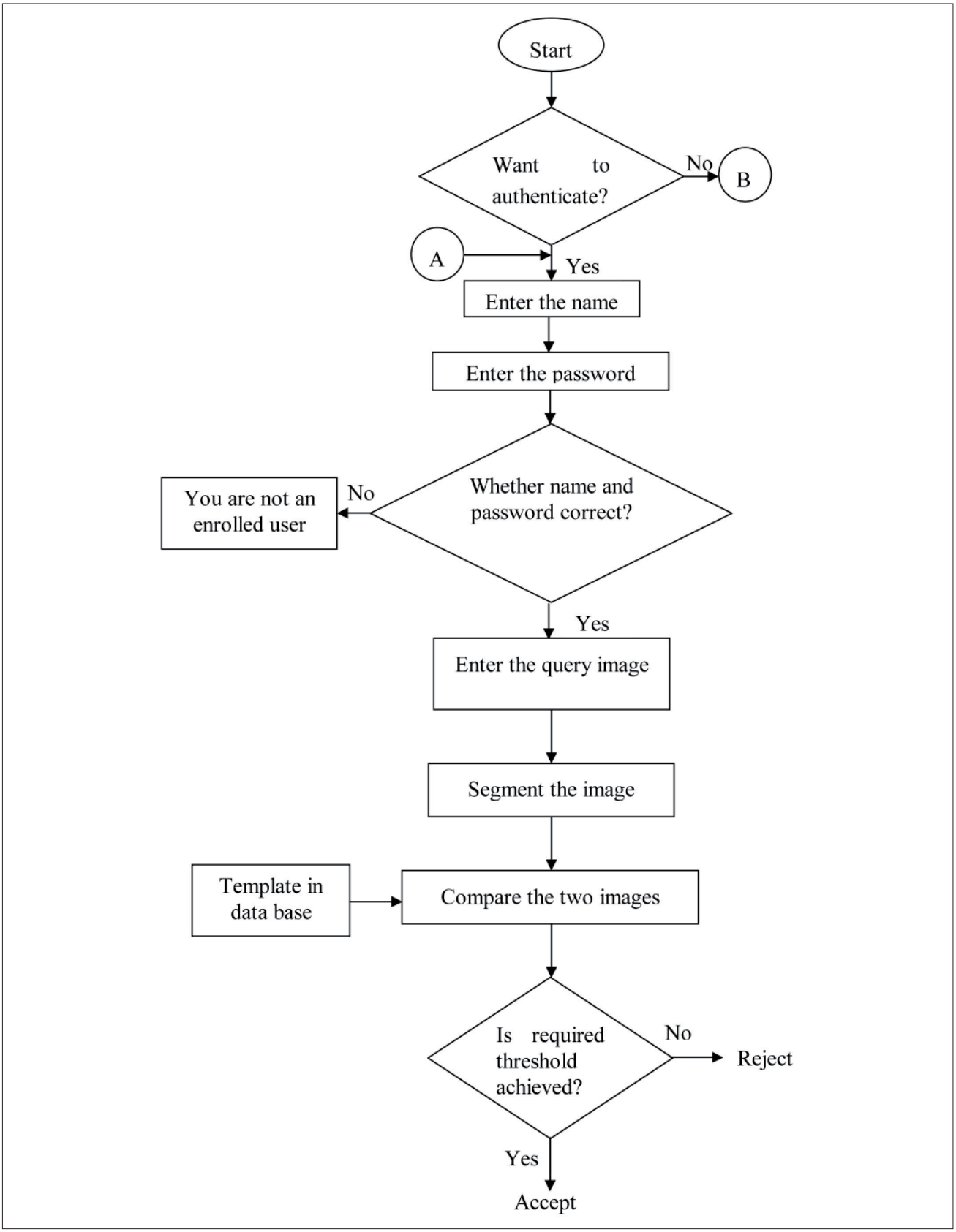

Figure 2. Flow chart of verification process

Figure 3. (a) Original image; (b) translated image in X and Y direction; (c) rotated image; (d) rotated plus translated image

Results and Discussion

Two performance measures, namely false rejection rate (FRR) and false acceptance rate (FAR) were calculated for different images for comparison of results with different thresholds and window sizes. Experiments were performed by considering template size of 50 × 50, 100 × 100 and 200 × 200 pixels extracted from the centre of the image. Figure 4 shows the extracted images of template size 50 × 50, 100 × 100 and 200 × 200 pixels respectively, extracted from the centre of the image 1_1 of FVC2002/Db1_a database.

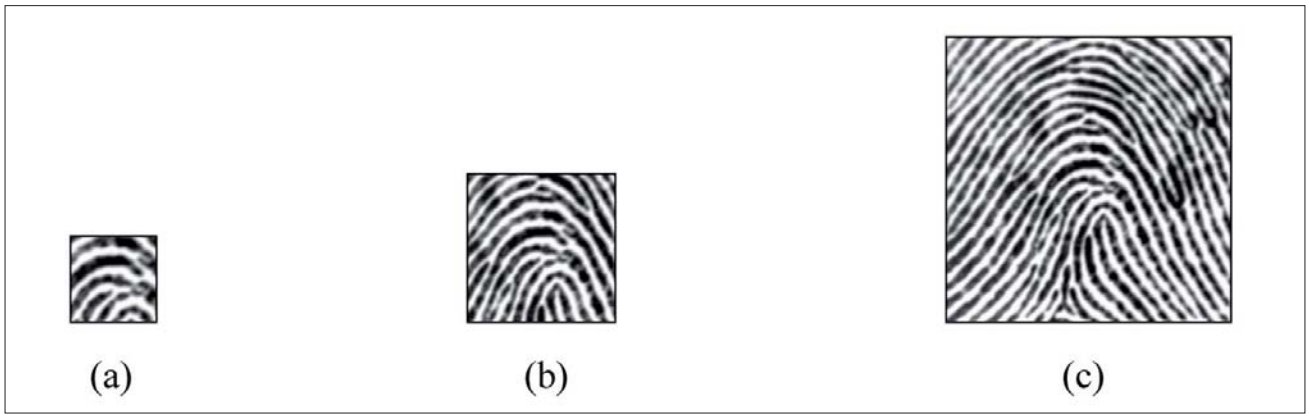

Figure 4. Template size of (a) 50 × 50 pixels, (b) 100 × 100 pixels, and (c) 200 × 200 pixels extracted from the centre of image 1_1

False rejection rate (FRR)

For the images which were only translated from the original image, no false rejection was found for any reference template size at any threshold value. However, when the images were rotated or translated plus rotated, the following results were obtained for different template learning images (Tables 1-6, and Figures 5-10). Tables 1-3 show % false rejection for different learning image sizes when only rotation was applied to the images, while Tables 4-6 represent the same when both rotation and translation were applied to the images. Figures 5-10 are the graphical representation of the different results obtained for the various learning image sizes.

Table 1. FRR for rotation-only learning images, size 200 × 200 pixels

Threshold	Image No.													
	1_1	2_1	3_1	4_1	5_1	6_1	7_1	10_1	11_1	12_1	13_1	14_1	15_1	16_1
700	0%	13%	37%	13%	0%	13%	0%	13%	13%	0%	7%	0%	7%	0%
750	3%	13%	37%	13%	0%	13%	0%	13%	17%	7%	7%	3%	7%	3%
800	3%	13%	40%	17%	0%	13%	0%	13%	30%	20%	7%	3%	7%	13%
850	3%	13%	50%	47%	0%	23%	0%	13%	37%	37%	17%	7%	20%	20%
900	10%	23%	73%	73%	7%	37%	7%	27%	43%	63%	60%	37%	37%	27%

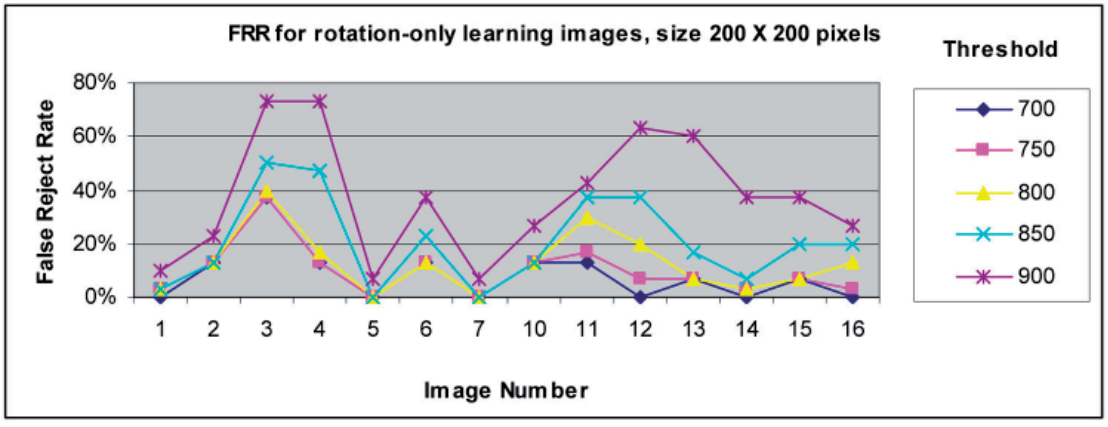

Figure 5. FRR for rotation-only learning images, size 200 × 200 pixels, at various thresholds

Table 2. FRR for rotation-only learning images, size 100 × 100 pixels

Threshold	Image No.													
	1_1	2_1	3_1	4_1	5_1	6_1	7_1	10_1	11_1	12_1	13_1	14_1	15_1	16_1
700	0%	0%	3%	0%	0%	0%	3%	13%	0%	0%	0%	0%	0%	0%
750	0%	0%	3%	0%	0%	7%	7%	13%	0%	0%	0%	0%	0%	0%
800	0%	3%	13%	0%	0%	13%	20%	13%	0%	0%	0%	0%	3%	0%
850	0%	3%	27%	3%	0%	17%	43%	13%	10%	0%	0%	0%	17%	17%
900	7%	20%	37%	3%	33%	37%	87%	17%	30%	10%	3%	7%	53%	57%

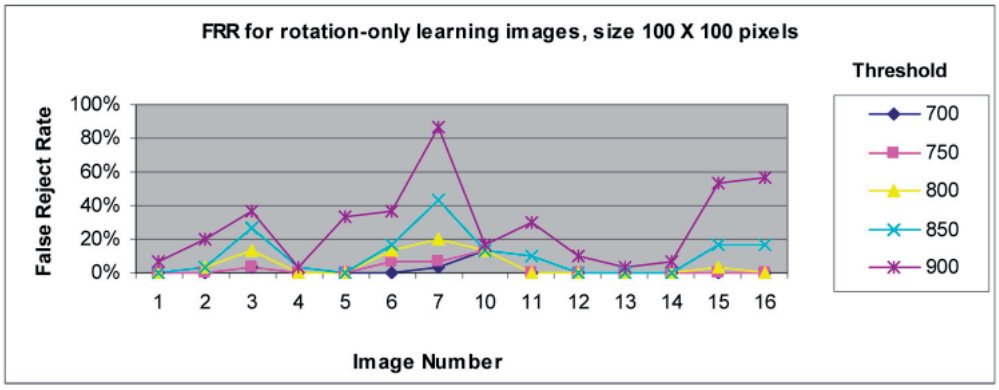

Figure 6. FRR for rotation-only learning images, size 100 × 100 pixels, at various thresholds

Table 3. FRR for rotation-only learning images, size 50 × 50 pixels

Threshold	Image No.													
	1_1	2_1	3_1	4_1	5_1	6_1	7_1	10_1	11_1	12_1	13_1	14_1	15_1	16_1
700	0%	0%	0%	0%	0%	0%	0%	0%	0%	0%	0%	0%	0%	0%
750	0%	0%	0%	0%	0%	0%	0%	0%	0%	0%	0%	0%	0%	0%
800	0%	0%	0%	0%	0%	0%	0%	0%	0%	0%	0%	0%	0%	0%
850	0%	0%	0%	0%	0%	0%	0%	0%	0%	0%	0%	0%	10%	3%
900	0%	17%	0%	0%	0%	0%	0%	0%	0%	0%	0%	0%	33%	10%

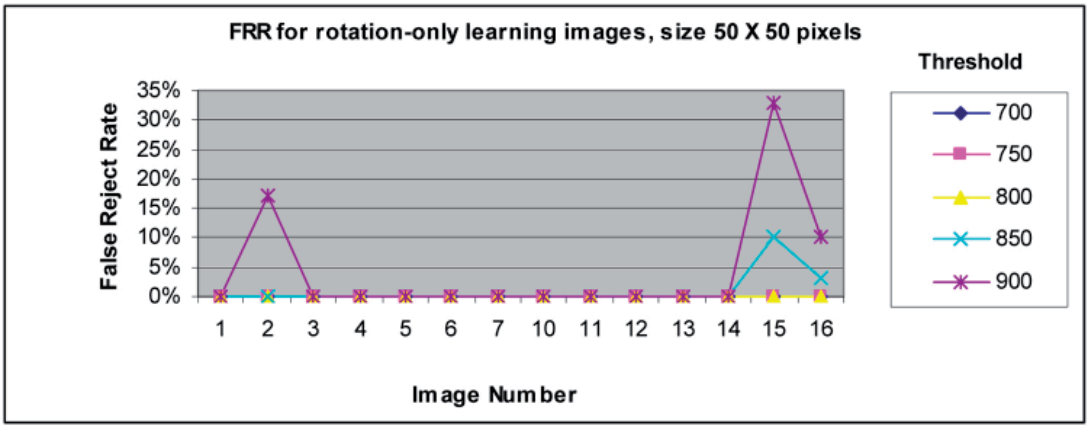

Figure 7. FRR for rotation-only learning images, size 50 × 50 pixels, at various thresholds

Table 4. FRR for rotation-and-translation learning images, size 200 × 200 pixels

Threshold	Image No.													
	1_1	2_1	3_1	4_1	5_1	6_1	7_1	10_1	11_1	12_1	13_1	14_1	15_1	16_1
700	0%	13%	27%	13%	0%	13%	0%	13%	13%	0%	7%	0%	7%	0%
750	3%	13%	27%	13%	0%	13%	0%	13%	17%	7%	7%	3%	7%	3%
800	3%	13%	30%	17%	0%	13%	0%	13%	30%	20%	7%	3%	10%	13%
850	3%	13%	40%	47%	0%	23%	0%	13%	37%	40%	17%	7%	20%	20%
900	10%	23%	67%	73%	7%	33%	7%	23%	50%	53%	60%	33%	37%	27%

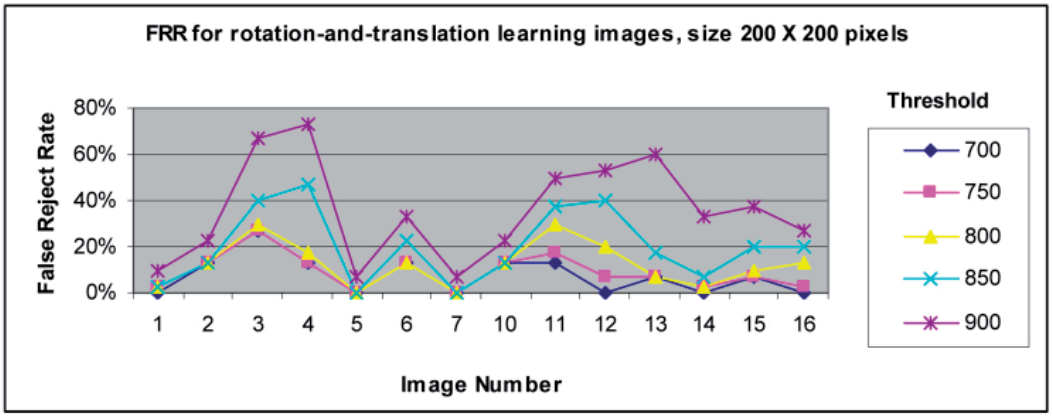

Figure 8. FRR for rotation-and-translation learning images, size 200 × 200 pixels, at various thresholds

Table 5. FRR for rotation-and-translation learning images, size 100 × 100 pixels

Threshold	Image No.													
	1_1	2_1	3_1	4_1	5_1	6_1	7_1	10_1	11_1	12_1	13_1	14_1	15_1	16_1
700	0%	0%	0%	0%	0%	0%	3%	13%	0%	0%	0%	0%	0%	0%
750	0%	3%	0%	0%	0%	7%	3%	13%	0%	0%	0%	0%	0%	0%
800	0%	7%	10%	0%	0%	10%	17%	13%	0%	0%	0%	0%	3%	0%
850	3%	7%	20%	3%	0%	13%	43%	13%	10%	0%	0%	0%	20%	17%
900	10%	23%	27%	3%	33%	30%	83%	17%	30%	10%	7%	10%	53%	57%

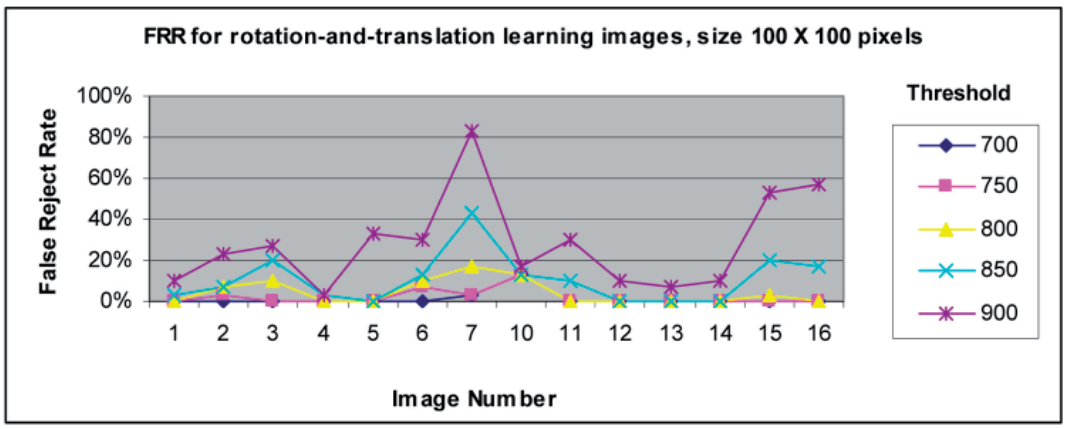

Figure 9. FRR for rotation-and-translation learning images, size 100 × 100 pixels, at various thresholds

Table 6. FRR for rotation-and-translation learning images, size 50 × 50 pixels

Threshold	Image No.													
	1_1	2_1	3_1	4_1	5_1	6_1	7_1	10_1	11_1	12_1	13_1	14_1	15_1	16_1
700	0%	0%	0%	0%	0%	0%	0%	0%	0%	0%	0%	0%	0%	0%
750	0%	0%	0%	0%	0%	0%	0%	0%	0%	0%	0%	0%	0%	0%
800	0%	0%	0%	0%	0%	0%	0%	0%	0%	0%	0%	0%	3%	0%
850	0%	0%	0%	0%	0%	0%	3%	3%	0%	0%	0%	0%	17%	3%
900	0%	20%	3%	0%	0%	0%	3%	7%	0%	0%	3%	0%	37%	10%

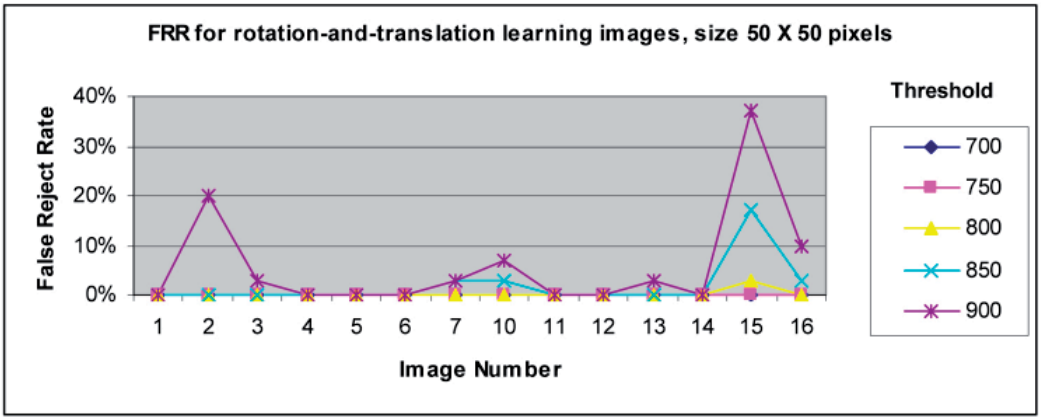

Figure 10. FRR for rotation-and-translation learning images, size 50 × 50 pixels, at various thresholds

False acceptance rate (FAR)

No false acceptance was found for the learning image sizes of 100 × 100 and 200 × 200 pixels up to threshold of 700. However, for the learning image size of 50 × 50 pixels the following results were observed (Table 7 and Figure 11). Table 7 represents % false acceptance at various thresholds for the learning image size of 50 × 50 pixels while Figure 11 is the graphical representation of the results from Table 7.

Table 7. FAR for learning images, size 50 × 50 pixels

Threshold	Image No.													
	1_1	2_1	3_1	4_1	5_1	6_1	7_1	10_1	11_1	12_1	13_1	14_1	15_1	16_1
700	0%	25%	90%	50%	3%	68%	70%	75%	88%	100%	13%	5%	23%	0%
750	0%	10%	75%	30%	0%	40%	60%	68%	53%	90%	8%	0%	3%	0%
800	0%	5%	53%	5%	0%	13%	30%	33%	35%	80%	8%	0%	0%	0%
850	0%	0%	28%	3%	0%	8%	15%	10%	13%	60%	0%	0%	0%	0%
900	0%	0%	3%	0%	0%	0%	5%	0%	0%	25%	0%	0%	0%	0%

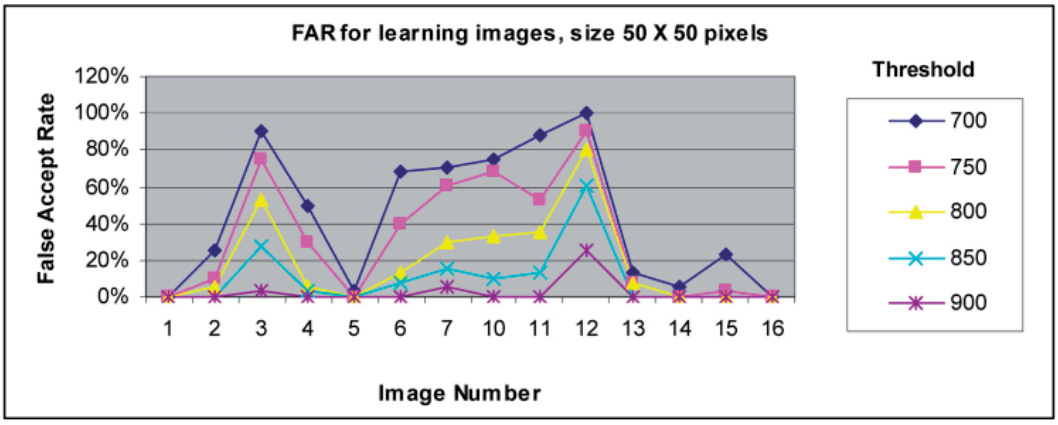

Figure 11. FAR for learning images, size 50 × 50 pixels, at various thresholds

From the above results for FFR and FAR, it is observed that as the threshold value increases, so does the % false rejection, although for the smaller learning images (50 × 50 pixels) the % false rejection is less in comparison to that for the larger learning images (100 × 100 and 200 × 200 pixels). However, no false acceptance was observed (down to threshold of 700) for the learning image sizes of 100 × 100 and 200 × 200 pixels, although for the 50 × 50 pixel learning images a considerable number of false acceptance was observed. The above results are expected as smaller images contain less information in comparison to larger images, and thus the probability of more than one image having the same little information is greater.

Conclusions

An image-based fingerprint verification system has been developed and checked for validity by employing images from FVC2002/Db1_a database. The success rate of the verification system is highly dependent on the threshold value and size of the template used for the learning stage. Smaller- sized learning images have lower false rejection rate and higher false acceptance rate, while larger-sized learning images have higher false rejection rate and lower false acceptance rate. Moreover, the higher the value of the threshold is, the higher the false rejection and the lower the false acceptance become. So, a compromise has to be made between false acceptance and false rejection. The experimental results for different fingerprints and various learning image sizes reveal that a 100 × 100 learning image size and a threshold value of 700 (1000 being the perfect match) is a good compromise for the false acceptance and false rejection rate.

References

1. G. Hribernig, D. Tukulj, and M. Luetic, "Biometric- easy access to networked word", International Conference and Workshop on Telecommunication and Mobile Computing, Graz University of Technology, Austria, 2001.
2. A. K. Jain, L. Hong, S. Pankanti, and R. Bole, "An identity–authentication system using fingerprints", Proceedings of the IEEE, 1997, 85, 1365-1388.
3. A. K. Jain, U. Uludag, and R. L. Hsu, "Hiding a face in a fingerprint image", Proceedings of IEEE International Conference on Pattern Recognition, 2002, 3, 756-759.
4. A. K. Jain, A. Ross, and S. Pankanti, "Biometrics: a tool for information security", *IEEE Transact. Information Forensics and Security, 2006,* 1, 125-142.
5. J. Feng, "Combining minutiae descriptor for fingerprint matching", *J. Pattern Recognition Soc.,* 2008, 41, 342-352.
6. P. Reid, "Biometric for Network Security",1st Indian Reprint, Pearson Education, New Delhi, 2004.
7. E. Spinella, "Biometrics Scanning Technologies: Finger, Facial and Retinal Scanning", SANS Technology Institute, San Francisco, 2002.
8. D. Maio and D. Maltoni, "Direct gray scale minutiae detection in fingerprints", *IEEE Transact. Pattern Analysis and Machine Intelligence,* 1997, 19, 27-40.
9. B. C. Seow, S. K. Yeoh, S. L. Lal, and N. A. Abu, "Image based fingerprint verification", Proceedings of IEEE Conference on Research and Development, Malaysia, 2002, 58-61.
10. A. M. Bazen, G. T. B. Verwaaijen, S. H. Gerez, L. P. J. Veelenturf, and B. Zwaag, "Correlationbased fingerprint verification system", Proceedings of Conference on Research on Integrated Systems and Circuits, Netherlands, 2000, 205–213.
11. J. Travis, "LabVIEW for Everyone", 2nd Edn., Prentice Hall, NJ, 2002.
12. "IMAQ Vision Concepts Manual", National Instruments Corporation, Austin, 2000.

Maejo International Journal of Science and Technology
ISSN 1905-7873
Available online at www.mijst.mju.ac.th

Full Paper

Oilseed rape straw for cultivation of oyster mushroom

Ahmad Norouzi, Gholamali Peyvast *, and Jamalali Olfati
Department of Horticulture, University of Guilan, Rasht, Iran-Islamic Republic

* Corresponding author, e-mail: gpeyvast@gu.ac.ir

Received: 30 May 2008 / Accepted: 22 September 2008 / Published: 25 September 2008

Abstract: Oyster mushroom [Pleurotus ostreatus var. sajor caju (Fr.) Singer] was grown on five substrates: rice straw, rice straw + oilseed rape straw (75:25, 50:50, and 25:75 dw/dw), and oilseed rape straw alone. Rice straw + oilseed rape straw (25:75) and oilseed rape straw were best for fruit body production of P. ostreatus. The time to fruiting for P. ostreatus was also shorter on oilseed rape straw. Protein content of the fruit bodies obtained with oilseed rape straw was highest among all substrates. Oilseed rape straw thus appears to be a suitable substrate for oyster mushroom production.

Keywords: Pleurotus ostreatus, oilseed rape straw, rice straw

Introduction

Oyster mushroom [Pleurotus ostreatus var. sajor caju (Fr.) Singer] cultivation has increased during the last decade [1,2]. This mushroom accounted for 14.2% of the total world production of edible mushrooms produced in 1997 [2]. Although commonly grown on pasteurised straw of wheat or rice, oyster mushroom can be cultivated on a wide variety of substrates containing lignin and cellulose. Oyster mushroom cultivation can play an important role in managing and recycling of organic wastes as an alternative to other methods of disposal [3].

Oyster mushroom can also produce fruiting bodies on straw of goose grass (Eleucine coracana Gaertn.) and kikuyu grass (Pennisetum typhoides S. & H.); stem of sorghum (Sorghum vulgare Pers.) and maize (Zea mays L.) [4,5], as well as on wood and sawdust of poplar (Populus robusta Bartr.), oak (Quercus leucotrichopora L.), horse chestnut (Aesculus indica Colebr.), Acasia sp. [6], chopped pseudostem of banana [Musa paradisiaca subsp. sapientum (L.) Kuntze] [7], cotton (Gossypium sp.) stalk, pea (Pisum satium L.) shells [8,9], and straw of some species of wild plants including Leonotis

sp., Sida acuta Burm, *Parthenium argentatum* Gray, *Ageratum conyzoides* L., *Cassia sophera* L., *Tephrosia purpurea* (Linn.) Pers., and *Lantana camara* L. [3]. The substrate used depends on its availability in a specific region. Rice is an important agriculture crop in the northern part of Iran, and a staple food for many Iranians. Oilseed rape (*Brassica napus* L. var. Hyola 401) as a secondary crop has been on the increase recently after rice harvesting in this region. Oilseed rape straw is considered to be a kind of wastes and is normally disposed of by burning. This project was undertaken to determine if oilseed rape straw can be used as an alternative to the common straw such as rice and other gramineae straw as a substrate for cultivation of oyster mushroom.

Materials and Methods

Oyster mushroom spawn was purchased from Keshtpashohan Laboratory in Tehran, Iran. The substrates were rice straw, rice straw + oilseed rape straw (75:25, 50:50, and 25:75 dry weight/dry weight), and oilseed rape straw. Rice and oilseed rape straw was obtained locally and stored for approximately 6 and 2 months respectively. The straw was chopped into small pieces (1-2 cm), weighed and soaked in water overnight. Excess water present in the substrates was drained and the substrates were spread on clean blotting paper and air-dried for 15 min to remove excess water. The substrates were pasteurised by boiling for 30 min in water.

A sample of each substrate was weighed before and after drying in an oven at 60 ^{o}C for 2 days to determine the dry mater (DM) content. Total nitrogen (N), potassium (K), and ash were determined [10,11] (Table 1). Each substrate (3,000 g) with 85% moisture was mixed with 10% spawn (wet weight/wet weight) and placed in a 50×35 cm polythene bag which was then tightly closed. Pin holes were made through the bags (1/100 cm^2) for drainage. It was kept in a spawn running room at 25±1 °C in the dark until primordia were formed. After primordial formation, large holes were made in the polythene bag to allow normal development of fruiting bodies. Bags were kept at 22±1°C with a 12-hr photoperiod (1,500–2,000 lux) and 85–90% relative humidity. Adequate ventilation was provided to prevent increased CO_2 concentration in the room. The mushrooms were manually harvested three days after primordia initiation.

Biological efficiency were calculated and defined as the ratio of weight (g) of fresh mushrooms harvested to dry weight (kg) of the substrate. Total nitrogen and protein were determined using 0.5 g sample (dry weight) of oyster mushroom by the Kjeldhal method using concentrated H_2SO_4, K_2SO_4 and $CuSO_4$ to digest the sample. Phosphorus (P) was determined by spectrometry [10]. Total carbon (C) was determined by oxidation with potassium dichromate and titration of excess dichromate with ammonium ferrosulfate [12]. A completely randomised experimental design with 15 replications was used. Data were analysed using SAS (ver. 9.00, SAS, Inc., Cary, N.C.). The Tukey-test was performed to separate means.

Results and Discussion

Added oilseed rape straw had the effect of increasing nitrogen and carbon, and decreasing phosphorus, potassium and ash content in the substrate (Table 1). The type of substrate seemed to affect the time to primordial initiation and the biological efficiency of mushroom production (Table 2). Primordia were formed most rapidly on oilseed rape straw alone in the first flush, but in the second and third flush oilseed rape straw increased primordial initiation. Similarly, biological efficiency in the first flush of production was better for fruiting bodies on oilseed rape straw alone and oilseed rape straw + rice straw (75:25). However, it was generally lowest in second and third flushes especially when the substrate was oilseed rape straw.

Table 1. Some determined characteristics of substrates

Substrate	P (mg/100 g DM)	K (mg/100 g DM)	Ash (%)	C (%)	N (%)
Rice straw	84.2	809.5	4.5	55.39	0.804
Rice straw + oilseed rape straw (75:25 dw/dw)	74.6	803.0	4.4	55.63	0.820
Rice straw + oilseed rape straw (50:50 dw/dw)	68.2	780.3	4.2	55.68	0.822
Rice straw + oilseed rape straw(25:75 dw/dw)	66.6	778.4	3.9	55.89	0.828
Oilseed rape straw	57.0	762.5	3.8	55.97	0.830

The type of substrate also affected DM, ash, protein, potassium and phosphorous content of the mushrooms (Table 3). The lowest levels of DM, ash, potassium and phosphorus were obtained from fruiting bodies developed from spawn grown on oilseed rape straw alone. On the other hand, the protein concentration in fruiting bodies was highest when the mushrooms were cultivated on oilseed rape straw. The protein content of fruiting bodies produced on oilseed rape straw alone or mixed with rice straw was higher than that produced on rice straw alone. There was a tendency for potassium, phosphorus, DM and ash level of the fruiting bodies to decrease with decreasing percentage of rice straw in the substrate, the lowest levels thus being found when oilseed rape straw alone was used as substrate.

Table 2. Effect of substrate on days to primordial initiation and biological efficiency of P. ostreatus

Substrate	Days to primordial initiation			Biological efficiency *			
	1st flush	2nd flush	3 rd flush	1st flush	2nd flush	3rd flush	Total
Rice straw	28.25[a]	13.25[c]	14.25[b]	567.01[d]	236.07[a]	108.80[a]	911.88[c]
Rice straw + oilseed rape straw (75:25 dry wt /dry wt)	24.50[b]	14.25[c]	14.50[b]	588.08[c]	233.20[ab]	108.60[a]	929.88[b]
Rice straw + oilseed rape straw (50:50 dry wt /dry wt)	22.75[c]	17.00[b]	14.75[b]	602.52[b]	228.91[ab]	105.22[ab]	936.65[b]
Rise straw + oilseed rape straw (25:75 dry wt /dry wt)	21.00[d]	20.25[a]	16.25[a]	630.00[a]	228.11[ab]	102.04[b]	960.15[a]
Oilseed rape straw	20.50[d]	20.75[a]	16.75[a]	632.33[a]	224.73[b]	99.80[b]	956.87[a]

* Defined as g (fresh weight) of oyster mushroom /kg (dry weight) of substrate
Note: Values in a column followed by the same letter are not significantly different, $P \leq 0.01$, Tukey test.

Table 3. Effect of substrate on nutritive qualities of oyster mushroom

Substrate	DM (%)	Ash (%)	Protein (% DM)	K (mg/100 g DM)	P (mg/100 g DM)
Rice straw	7.99[a]	6.38[a]	18.53[e]	2826.75[a]	952.25[a]
Rice straw + oilseed rape straw (75:25 dw/dw)	7.98[a]	6.26[ab]	18.76[d]	2447.50[b]	931.00[b]
Rice straw + oilseed rape straw (50:50 dw/dw)	7.93[a]	4.14[b]	19.52[c]	2698.75[b]	917.50[c]
Rice straw + oilseed rape straw (25:75 dw/dw)	7.82[ab]	6.11[b]	20.00[b]	2611.75[c]	895.25[d]
Oilseed rape straw	7.52[b]	5.92[c]	20.27[a]	2583.00[c]	837.75[e]

Note: Values in a column followed by the same letter are not significantly different, $P \leq 0.01$, Tukey test.

Conclusions

Production of oyster mushroom on biological-waste substrates can be a highly efficient method for producing protein-rich food. It appears that oilseed rape straw mixed with rice straw can be used successfully as a substrate to benefit some aspects of oyster mushroom cultivation. It should further be determined if the concentrations of certain components of the oilseed rape straw are at optimum levels for use in a substrate. It also remains to be determined why mixing oilseed rape straw with rice straw produced beneficial results regarding biological efficiency, but this was not the case as regards the nutrient content of the mushrooms, which was benefited by the presence of oilseed rape straw.

References

1. D. J. Royse, "Influence of spawn rate and commercial delayed release nutrient levels on *Pleurotus cornucopiae* (oyster mushroom) yield, size and time to production", *Appl. Microbiol. Biotechnol.,* 2002, 58, 527–531.
2. S. T. Chang, "World production of cultivated and medicinal mushrooms in 1997 with emphasis on *Lentinus edodes* (Berk) Sing", *China. Int. J. Med. Mush.,* 1999,1, 291–300.
3. D. Nirmalendu and M. Mukherjee, "Cultivation of *Pleurotus ostreatus* on weed plants", *Biores. Technol.,* 2007, 98, 2723–2726.
4. V. Goswami, S. Sharma, and S. P. Sehgal, "Possibilities of cultivation of *Pleurotus sajor caju* (Fr.) Singer on agricultural waste in Rajasthan", Proc. Int. Conf. on Science and Cultivation Technology of Edible Fungi, Regional Research Laboratory, Jammu Tawi, India, 1987, pp 75–77.
5. Z. Bano, S. Rajarathnam, and N. Nagaraja, "Some important studies on *Pleurotus* mushroom technology", Proc. Int. Conf. on Science and Cultivation Technology of Edible Fungi, Regional Research Laboratory, Jammu Tawi, India, 1987, pp. 53–64.
6. S. K. Pant, J. C. Bhatt, and N. S. K. Harsh, "A suitable substrate for cultivation of Pleurotus ostreatus", Proc. Int. Conf. on Science and Cultivation Technology of Edible Fungi, Regional Research Laboratory, Jammu Tawi, India, 1987, pp. 70–71.
7. R. P. Singh and I. N. Tandon, "Screening of suitable substrate for production of *Pleurotus xabellatus* (Brek & Br) SAAC, Proc. Int. Conf. on Science and Cultivation Technology of Edible Fungi, Regional Research Laboratory, Jammu Tawi, India, 1987, pp. 90–92.
8. A. Philippoussis, G. Zervakis, and P. Diamantopoulou, "Bioconversion of agricultural lignocellulosic wastes through the cultivation of the edible *mushrooms Agrocybe aegerita, Volvariella volvacea* and *Pleurotus* spp.*", World J. Microbiol. Biotechnol.,* 2001, 17, 191–200.
9. G. Zervakis, A. Philippoussis, S. Ioannidou, and P. Diamantopoulou, "Mycelial growth kinetics and optimum temperature conditions for the cultivation of edible mushroom species on lignocellulosic substrates", *Folia Microbiol.,* 2001, 46, 231–234.

10. H. A. Elliot and B. A. Dempsey, "Agronomic effects of land application of water treatment sludges", *J. Am. Waste Water Assoc.,* 1991, 83, 126.
11. S. C. Croan, "Conversion of wood waste value-added products by edible and medicinal Pleurotus (Fr.) P. Karst Species (Agaricales S.I., Basidiomycetes)", *Int. J. Med. Mush,* 2000, 2, 773–780.
12. S. J. Kalembasa and D. S. Jenkinson, "A comparative study of titrimetric and gravimetric methods for the determination of organic carbon in soil", *J. Science Food Agriculture,* 1973, 24, 1085–1090.

Maejo International Journal of Science and Technology

ISSN 1905-7873

Available online at www.mijst.mju.ac.th

Report

Science and technology research in Thailand: Some comparisons from the data regarding Thailand's position in the region based on volume of published work

Terry Commins 1,*, Warinthorn Songkasiri 2, Suvit Tia 1, and Bundit Tipakorn 1

[1] King Mongkut's University of Technology Thonburi, 98 Suksawad Road, Tungkhru, Bangkok 10140, Thailand

[2] National Centre for Genetic Engineering & Biotechnology (BIOTEC), Science Park, Klong Luang, Pathumthani, 12120, Thailand

* Corresponding author, e-mail: thefox@loxinfo.co.th

Received: 24 June 2008 / Accepted: 27 September 2008 / Published: 2 October 2008

Abstract: Three different sources were used to examine the growth or otherwise in the volume of published research from Thailand. One source compares growth over the last two decades, another over the last six years, while a third examines the current status of Thailand's position in relation to neighbouring countries in ASEAN.

All three methods are based primarily on publication in international literature, with an emphasis on science and engineering. The figures do not include publication in local or regional literature and thus do not reflect the total picture in terms of volume. It was not possible using these sources to obtain a publication-per-head-per-researcher to better illustrate output on an annual basis.

Despite these drawbacks, indicators from international sources can be viewed with some confidence and the overall picture is encouraging. Thailand has seen dramatic growth over the last twenty years and consistent growth over the last six. Thailand ranks second in the ASEAN region behind Singapore, in terms of volume of output, and is ahead of Singapore when this output is compared to GDP.

Keywords: science publication, journals, citation index, scientometrics

Introduction

The generally held belief is that Thailand seriously lags behind other countries in the world, particularly the "Asian tigers", in terms of research and development, or even basic science. In GDP terms, funding for R&D remains low and the country is said to have an almost chronic shortage of skilled researchers. Against this picture it was decided to look at international publication by Thai researchers in the science and engineering fields, to see how the country compared with others in the region. A further objective was to form a picture of whether output was increasing or declining and to suggest what might be the possible causes for this.

Some work has been undertaken in building up a Thai Journal Citation Index (TCI) [1-3] which is a commendable effort, although the focus is on quality whereas this study concentrates on quantity. The evidence is clear that the volume of published work from Asia is increasing [4] and the inference is that quality is increasing commensurately, given the desire by researchers to publish internationally [5]. Examining the data from archived journal articles confirms this trend [6]. It is also apparent that publishing in Asia is on the increase and Thailand is active in this regard with some 228 academic journals produced in the country [7].

In our attempt to gain a clear picture of quantity and to ensure the validity of the data, three different sources/approaches were taken.

Methodology

For the first comparison, major journal or literature providers were searched using the country name as the key word. This returned all published work about, or originating from, the country and is thus not exclusively the output of researchers from that country. For example, the figures for Laos are relatively high, given the low number of researchers in that country. This can be explained by the high external interest in Laos in the fields of biodiversity, medicine and social sciences. In the case of Thailand, Singapore and Malaysia, the figures are considered as reflective of work generated within the country and it is estimated that some 20% is external.

In addition, the search engines employed by the publishers were found to vary greatly in their returns. Some employed the most obscure references to the country contained in the text, while others were more precise with weighted results. Since we were only seeking an indication to obtain a better picture of growth, the data is considered to be reliable for this purpose.

For the second comparison, we explored the ISI Web of Knowledge database [8] for records that are freely available dating from 2001. A search was undertaken for the period 2001-2006, using the country name as the key word and covered the following databases:

- Science Citation Index Expanded
- Social Sciences Citation Index
- Arts and Humanities Citation Index

To gain an entry into the Science Citation Index, the paper must be published in a peer-reviewed journal, must have at least an English title and abstract, and authors must be from multiple countries. This excludes a large number of regional and local journals; however, the figures remain a useful indicator. For this exercise, Thailand was ranked alongside Singapore, Malaysia, Indonesia, the Philippines and Vietnam.

For a further comparison we drew on an unpublished study undertaken by Blackwell Publishing in 2006 on the growth of research output in Asia generally. This study uses Blackwell and ISI sources for primary data and the focus is mainly on the growth in output from China and Japan. Nonetheless, the findings are quite useful as some comparison with GDP is also made.

During the course of our study a new journal citation service became available [9] and this was also accessed to assess the validity of our previous findings.

Results

For the initial study, a search of the major journal publishers and technical literature providers was undertaken using the country key words. In the case of Myanmar, we also obtained results using <Burma> as the key word to better reflect the volume of literature for that country. Table 1 shows the total number of records of published work for each ASEAN country held by the major publishers. The search was undertaken on 3 March 2007 and included Blackwell, Cambridge, Elsevier, Oxford, PubMed, Springer, Taylor & Francis and Wiley.

As shown in the table, Thailand ranks second in the region, followed by a cluster of countries with similar results: Indonesia, Malaysia, the Philippines and Vietnam. Since these figures do not indicate growth over time or trends, a second method was employed to determine this using the ISI Web of Knowledge. ISI allows for search on an annual basis back to 2001. Table 2 and Figure 1 show the results of this search undertaken on 20 March 2007, using the country (CU=) parameter.

From Figure 1 it can be seen that the situation for the Philippines, Vietnam and Indonesia remains much the same, as reflected in Table 1 above. However, by using the ISI Web of Knowledge data, Malaysia shows a distinct improvement. While Singapore, Thailand and Malaysia show steady growth, it can be seen that all countries experienced a levelling-off of growth in 2003-2004. The reason for this is not known. It would be particularly useful to measure these figures against data for each country's annual research expenditure – unfortunately such data is not readily available.

As a third measure, data from Blackwell Publishing was examined and compared with the findings above. Selected data was extracted from a Power Point presentation given by Blackwell in 2006. The author of this presentation [4] also used data from the ISI Science Citation Index and applied this to the broader Asian region, focussing on the dynamic growth in science publishing from China, Japan and Taiwan. Some data were provided for Thailand, Malaysia and Singapore and these have been used for our purposes here. Figure 2 shows the percentage increase in science-related papers published over the last two decades from the major Asian regions.

Table 1. Publishers' Records for ASEAN countries

Country	No. of Records
Singapore	119,370
Thailand	64,248
Indonesia	48,198
Malaysia	45,976
Philippines	44,611
Vietnam	40,273
Laos	25,832
Myanmar	18,182
Cambodia	8,682
Brunei	7,512
TOTAL	422,884

Table 2. Number of Entries from ISI for 2001-2006

Country/ Year	Philippines	Vietnam	Indonesia	Malaysia	Thailand	Singapore
2001	388	390	576	1,044	1,576	4,556
2002	506	380	486	1,031	1,867	4,970
2003	576	565	608	1,330	2,407	5,852
2004	517	468	570	1,482	2,445	6,113
2005	657	654	700	1,798	3,075	7,545
2006	640	664	714	2,045	3,498	7,684

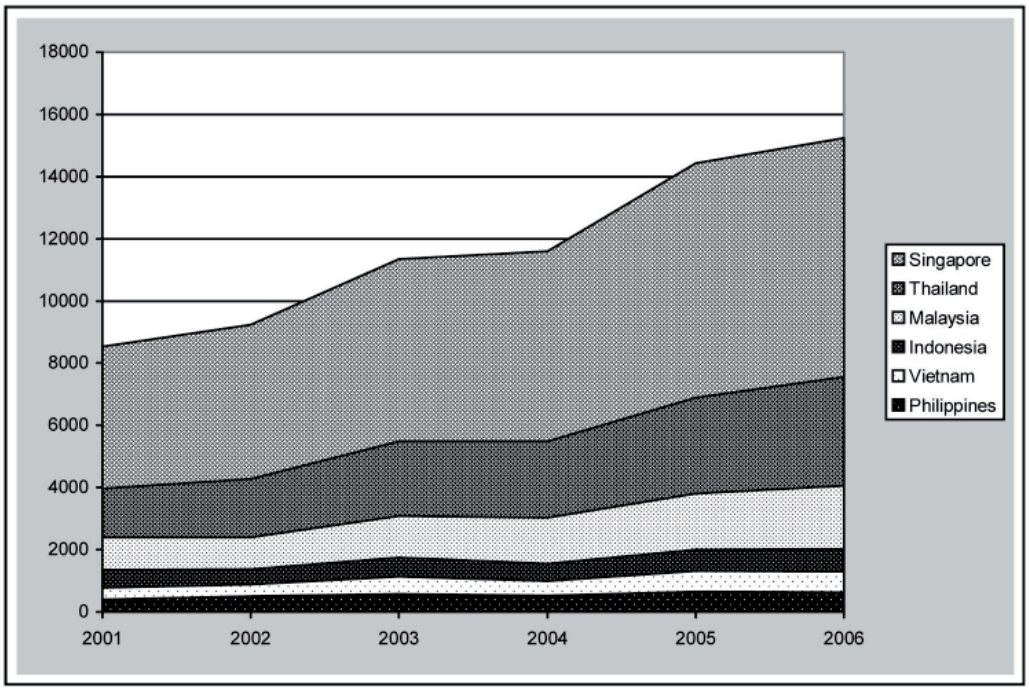

Figure 1. Growth in number of publications in ISI over time (cumulative)

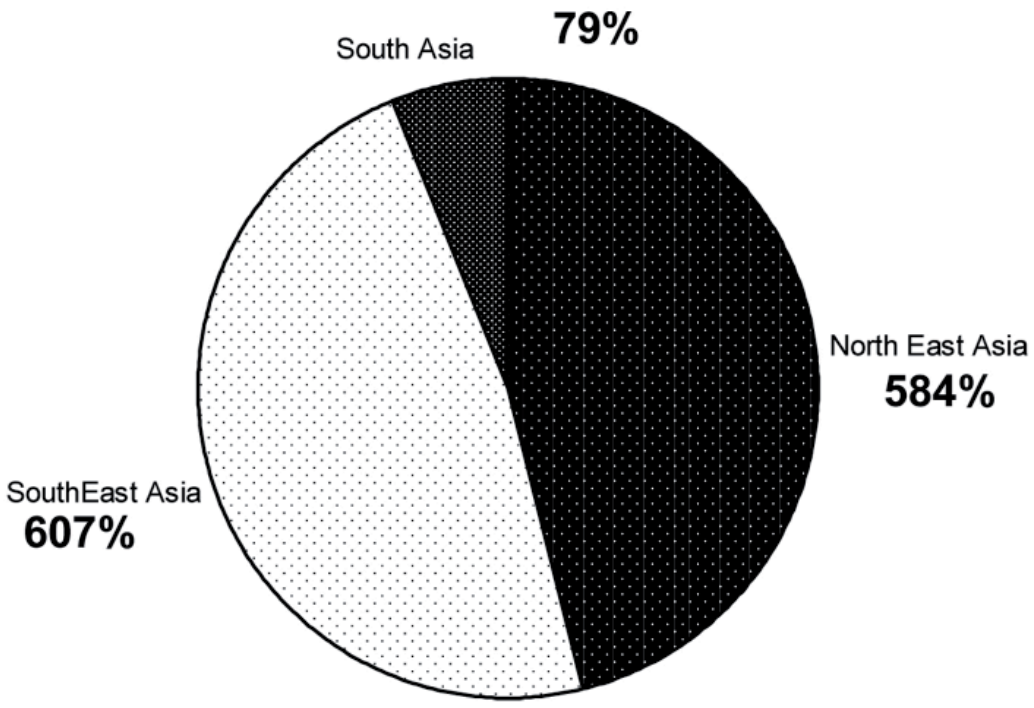

Figure 2. Percentage increase in papers published 1983-2003

It can be seen from Figure 2 that the greatest growth has been in South-East Asia. This has been led primarily by Singapore and Thailand. Given that North-East Asia includes established research leaders such as Japan, Korea, Taiwan, and emerging China, the growth for South-East Asia can be considered remarkable. Figure 3 shows this in terms of the number of science-related articles published from South East Asia over the two decades.

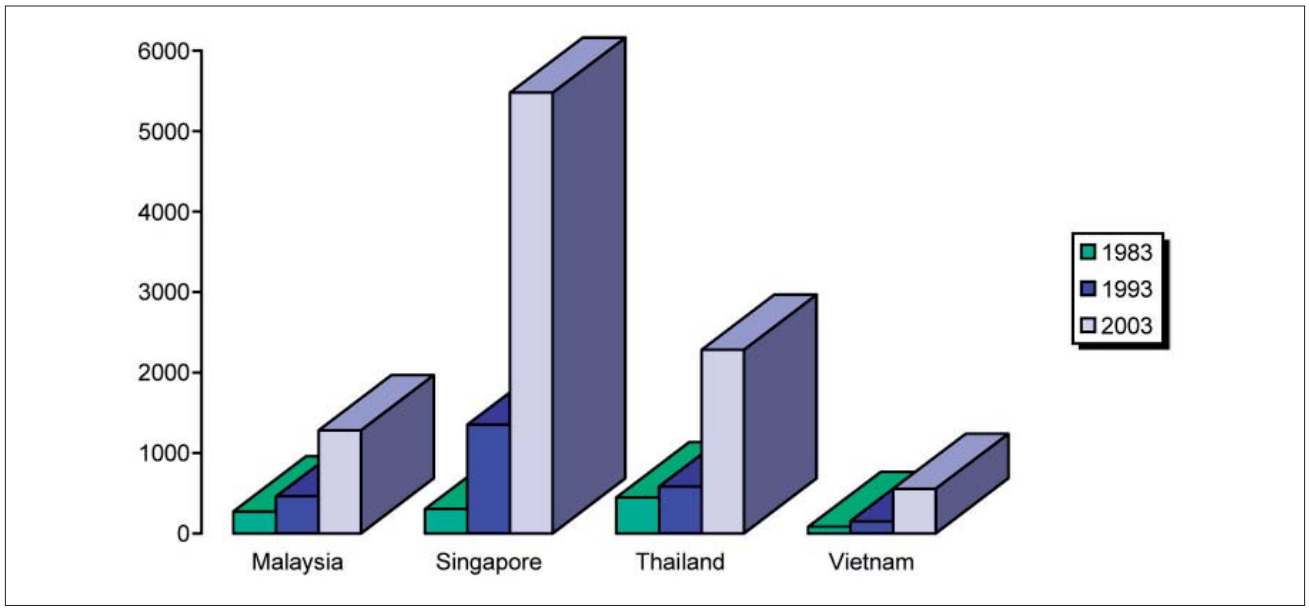

Figure 3. Number of science articles published in 1983-2003

Interestingly, the scientific focus in the Asian region, represented by publication, varies considerably. For example, in Malaysia, Taiwan and Singapore, the focus is mainly on electronics, materials science and the physical sciences. For South Korea, the emphasis is on engineering, life sciences and materials science, whilst for Thailand the growth has been driven by the life sciences and the medical sciences. The Blackwell presentation went on to compare growth in terms of economic factors and some of the relevant data is presented in Figure 4.

Since citation data is made available on a commercial basis and thus difficult to obtain or verify, our findings were tested against data from a new citation service to determine reliability. The SCImago [8] service uses data commencing in 1996 from Scopus (Elsevier) to determine country rankings, based on volume of output:

World Ranking	
Singapore	33
Thailand	42
Malaysia	49
Indonesia	64
Philippines	67
Vietnam	70

This ranking confirms that our findings are in close accord with the international situation for scientific
publishing.

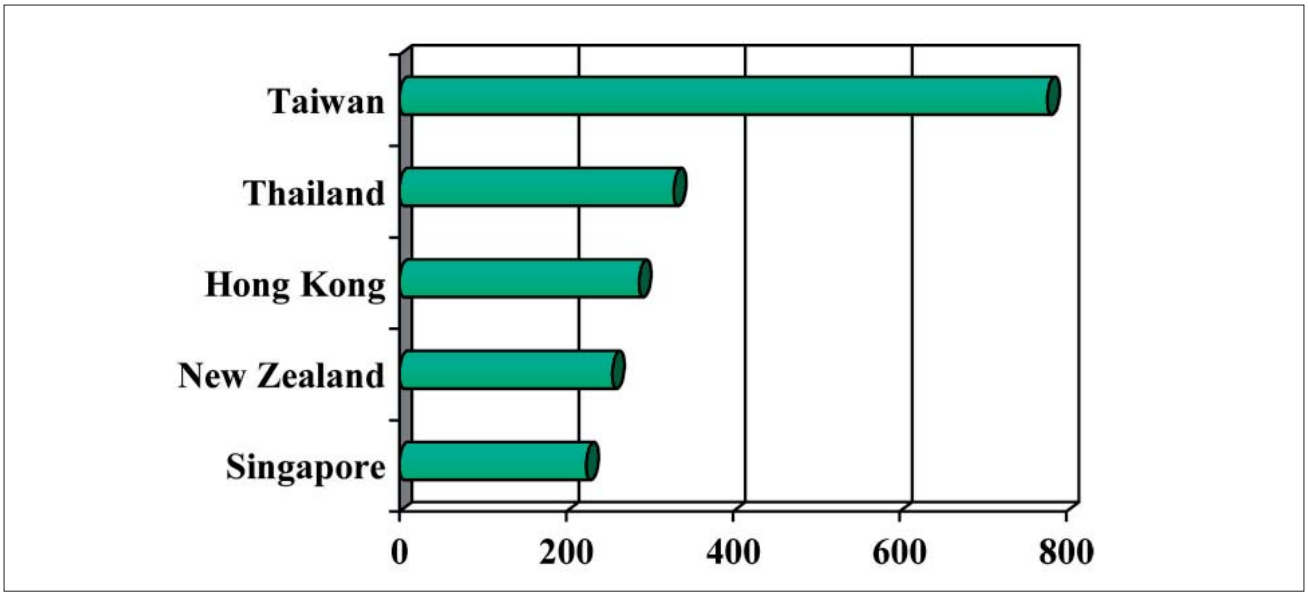

Figure 4. Articles per capita-GDP for selected countries in the region

Conclusions

From the initial study it is apparent that Thailand ranks as second in the ASEAN region in terms of volume of research articles published. This position is confirmed by other studies. Thailand has seen over 400% growth in science research output over the last two decades. Purely in percentage terms, this is on a par with South Korea.

The second study, while confirming Thailand's position, shows steady consistent growth over the last six years. By comparison, growth for the Philippines and Indonesia has been slightly erratic. Since all of the data is based on publications in English, Thailand's reasonably good performance should be viewed in terms of the distinct disadvantage the country has in terms of English when compared to Singapore, Malaysia and the Philippines. Further evidence from SCImago confirms Thailand's ranking as second in the region.

From the third study it can be concluded that Thailand is caught in a major upsurge in research output from the Asian region (Figure 2), and the country's performance is quite creditable when compared to economic factors. Science and technology research in Thailand was given a considerable funding boost when the National Science and Technology Development Agency (NSTDA) came into operation in 1992. Three of the NSTDA major centres, BIOTEC, MTEC and NECTEC have been established since 1983-86. While not conclusive, viewing the data for research output from 1983 until 1993, and from 1993 until 2003, no peaks occur in concert with increased research funding in these key areas. This may in part be due to the current focus on life and medical sciences.

The authors recommend further detailed study be undertaken to attempt to determine the effect scholarships granted by the National Research Council of Thailand have had on raising Thailand's international publications profile. Some examination to determine the particular fields where growth is occurring would also be useful indicators. Unfortunately, factual data on overall government research spending in the region is difficult to obtain.

References

1. N. Sombatsompop, A. Kositchaiyong, T. Markpin, and S. Inrit, "Scientific evaluations of citation quality of international research articles in the ISI database: Thailand case study", *Scientometrics,* 2006, 66, 521-535.
2. N. Sombatsompop, P. Patchatahirun, V. Surathanasakul, N. Premkamolnetr, and T. Markpin, "A citation report for Thai academic journals published during 1996-2000", *Scientometrics,* 2002, 55, 445-462.
3. J. Svasti and R. Asavisanu, "Update on Thai publications in ISI databases (1999-2005)", *Science Asia,* 2006, 32, 101-106.
4. M. Robinson, "The Impact of Asian Science", Unpublished Power Point presentation for Blackwell Publishing/Key Perspectives Ltd, 2006.
5. Y-G. Zhu, P. O'Connor, and J-H. Cao, "Where do Chinese scientists publish their research in environmental science and technology?", *Environmental Pollution,* 2007, 147, 1-3.
6. Data retrieved 12 December 2007 from http://www.thaiscience.info
7. J. Svasti and R. Asavisanu, "Aspects of quality in academic journals: A consideration of the journals published in Thailand", *ScienceAsia,* 2007, 33, 137-143.
8. Data retrieved 4 – 12 February 2007 from: http://apps.isiknowledge.com/
9. Data retrieved 22 November 2007 from: http://www.scimagojr.com/countryrank.php

Maejo International Journal of Science and Technology

ISSN 1905-7873

Available online at www.mijst.mju.ac.th

Full Paper

Effect of Glomus mosseae and plant growth promoting rhizomicroorganisms (PGPR's) on growth, nutrients and content of secondary metabolites in Begonia malabarica Lam.

Thangavel Selvaraj[1],*, Sevanan Rajeshkumar[2], Mathan C. Nisha[3], Lakew Wondimu[2], and Mitiku Tesso1

[1] Department of Plant Sciences, Faculty of Agricultural Sciences, Ambo University College, Post Box No.19, Ambo, Ethiopia

[2] Department of Applied Biology, Ambo University College, Post Box No.19, Ambo, Ethiopia

[3] Department of Botany, Kongunadu Arts and Science College (Autonomous), Coimbatore, Tamilnadu, India

*Corresponding Author, e-mail: tselvaraj_1956@yahoo.com

Received: 31 March 2008 / Accepted: 13 October 2008 / Published: 15 October 2008

Abstract : Begonia malabarica Lam. (Begoniaceae) is one of the important medicinal plants whose main secondary metabolites are luteolin, quercetin and β-sitosterol. The leaves are used for the treatment of respiratory tract infections, diarrhoea, blood cancer and skin diseases. A study was undertaken to determine the effect of arbuscular mycorrhizal (AM) fungus, Glomus mosseae, and some plant growth promoting rhizomicro-organisms (PGPR's) on the growth, biomass, nutrients, and content of secondary metabolites of B. malabarica plant under green house conditions. Various plant growth parameters (total plant biomass, mycorrhizal parameter, shoot and root phosphorus), mineral content (potassium, iron, zinc, and copper), and secondary metabolites (total phenols, ortho-dihydroxy phenols, tannins, flavonoids, and alkaloids) were determined and found to vary with different treatments. Among all the treatments, plants inoculated with 'microbial consortium' consisting of Glomus mosseae + Bacillus coagulans + Trichoderma viride performed better than with other treatments or uninoculated control plants. The results of this experiment clearly indicated that inoculation of B. malabarica with G. mosseae along with PGPR's enhanced its growth, biomass yield, nutrients and secondary metabolites.

Keywords : Begonia malabarica, Glomus mosseae, PGPR's, Bacillus coagulans, Trichoderma viride, secondary metabolites

Introduction

Ecosystems are composed of many organisms interacting in a multiple complex relationships with their environment and with each other. Biological relationships may be antagonistic, neutral or beneficial [1]. Utilisation of biofertilisers in the cultivation of medicinal and aromatic plants is of recent interest. An introduction of arbuscular mycorrhizal (AM) fungi is known to increase the growth of many plant species including medicinal plants. This is attributed to an increased uptake of nutrients, production of growth promoting substances and phytochemical constituents, tolerance to drought, salinity, transplant shock, resistance to plant pathogens, and synergistic interaction with other beneficial soil microorganisms such as N2-fixers and P-solubilisers [2-4]. It has been established that mycorrhizal plants grow better in infertile soils because of improved mineral nutrients through hyphae, which help in exploring a greater volume of soil beyond root hairs [5,6].

With the advent of innovative technologies and the importance being given to sustainable agriculture, AM fungal association is of great economic significance on the growth of agricultural and medicinal crops. Certain plant growth promoting rhizomicroorganisms (PGPRs) have been reported to enhance the activity of mycorrhizal fungi and consequently plant growth [7-13]. Therefore microbial inoculants can help maintain good soil health and fertility that contribute to a greater extent to a sustainable yield and quality of products [1]. However, the information available on the use of these beneficial microorganisms in medicinal plants is meagre.

Begonia malabarica Lam. is one of the important medicinal plants, belonging to the family *Begoniaceae* and commonly called as 'rathasoori' or 'senthandu'. The main secondary metabolites of *B. malabarica* are luteolin, quercetin and β-sitosterol [14]. The leaves are used for the treatment of respiratory tract infections, diarrhoea, blood cancer, and skin diseases [14]. It is found to grow in lateritic and acidic soil. Lateritic soil is, in general, poor in nutritional status and is especially deficient in phosphorus. The present study was undertaken to study the effect of AM fungus, *Glomus mosseae* and the PGPRs, *Bacillus coagulans and Trichoderma viride*, singly and in combination on the growth, biomass, nutrients, and content of secondary metabolites of *B. malabarica* raised under glasshouse condition.

Materials and Methods

B. malabarica seedlings were raised in seed pans containing a sand:soil mix (1:1 v/v). The seedlings after germination were maintained for four weeks. G. mosseae maintained as a pot culture using sterilised sand:soil mix (1:1 v/v) as the substrate and guinea grass (Panicum maximum Jacq.) as the host was used in the present study. The substrate along with the roots of guinea grass was air-dried. The hyphae, spores and root segments in the dried substrate served as the mycorrhizal inoculum. Bacillus coagulans, which is not only a PGPR but also a mycorrhiza helper bacterium (MHB) was grown in nutrient broth and Trichoderma viride in potato dextrose broth each in a 2-L flask containing 800 ml medium. After 3 days of growth for B. coagulans and 7 days for T. viride, the cultures were used for inoculation along with G. mosseae at the time of sowing and the plants were maintained in a glasshouse for 90 days. The microbial cultures were separately mixed with sterile lignite powder and their populations were determined by serial dilution plate method.

Pots of 4.5-kg capacity were filled with a sandy loam soil:sand (1:1 by volume) potting mix. The soil used was of an alfisol-type kaolinitic, isohyperthemic typic kanhaplustafs. The potting mixture had a pH of 6.2 and contained 2.7 ppm available phosphate (NH4F + HCl extractable). A planting hole was made at the centre of the pot. Ten grams each of of G. mosseae (1400 IP g-1), B. coagulans (2.8 X 108 cfu g-1), and T. viride (3.4 X 108 cfu g-1) inocula were added as per the treatment allocation shown in Table 1. One seedling was maintained per pot with 5 replications for each treatment. The plants were kept in a glasshouse and watered regularly.

The plants were harvested 90 days after planting. Growth parameters, viz. plant height, number of leaves and branches were recorded at harvest. Dry weight of shoot and root was recorded after drying the samples at 60ºC to constant weight in a hot air oven. The phosphorus and potassium content of the plants were estimated by vanadomolybdate phosphoric acid and flame photometric method respectively [15]. An atomic absorption spectrophotometre was employed to estimate zinc, copper and iron content of the plant leaf samples, using respective hollow cathode lamps. Acid phosphatase activity was estimated in the root-zone soil as per the procedure given by Tabatabai [16]. The contents of secondary metabolites, i.e. total phenols [17], ortho dihydroxy phenols [18], flavonoids [19], alkaloids [20] and tannins [21] were assayed in the plant leaf samples.

Mycorrhizal root colonisation was determined by grid-line intersect method [22] after staining the root samples with acid fuchsin (0.2%) [23]. Extrametrical chlamydospore numbers in the root-zone soil were enumerated by wet-sieving and decantation method [24]. The data thus generated were

subjected to statistical analysis of completely randomised block design and the means were separated by Duncan's Multiple Range Test [25].

Results and Discussion

In general, inoculants appreciably enhanced plant height especially for B. coagulans treatment (29.2 cm) (Table1), which was significantly superior over other treatments. This was followed by *Glomus mosseae* + *Bacillus coagulans* + *Trichoderma viride* (28.0 cm). There was no significant difference in the number of leaves and branches of PGPR-inoculated and uninoculated control plants. The maximum number of leaves and branches on 90 days after transplanting (DAT) were recorded in plants inoculated with *G. mosseae* + *B. coagulans* + *T. viride* (32.4/plant and 5.2/plant respectively), which was significant over all other treatments, the lowest number of leaves and branches being recorded in control plants (Table 1). Such a response of improved plant growth was also obtained in the investigation of Earanna et al. for Periwinkle [11] and of Sivakumar et al. for Pelargonium graveolens inoculated with *Glomus fasciculatum* and some PGPR's [12].

Single inoculation with G. mosseae or dual inoculation with *G. mosseae* + *B. coagulans* also significantly enhanced the total dry weight of B. malabarica plants. Those similarly inoculated with *G. mosseae* + *B. coagulans* + *T. viride* showed maximum shoot and root dry weight (9.7 g/plant), the lowest biomass being recorded in control (Table 1). This may be due to synergistic interaction of the AM fungi and PGPRs in the rhizosphere of the plants [3,8,12].

Table 1. Effect of AM fungus and PGPRs on growth and biomass of *B. malabarica*

Treatment	90 DAT			Plant biomass (g/plant)		
	Plant height(cm)	No. of leaves	No. of branches	Shoot	Root	Total
Uninoculated control	16.5^{e}	16.2^{e}	3.2^{e}	1.3^{d}	1.4^{d}	2.7^{e}
Glomus mosseae (G.m)	26.8^{c}	25.6^{d}	4.4^{c}	5.4^{c}	4.2^{b}	9.6^{a}
Bacillus coagulans (B.c)	29.2^{a}	20.6^{e}	3.5^{d}	5.5^{a}	2.2^{d}	7.7^{c}
Trichoderma viride (T.v)	16.5^{e}	20.8^{e}	3.6^{d}	1.4^{d}	1.8^{e}	3.2^{d}
G.m + B.c	28.5^{b}	30.1^{b}	4.8^{b}	5.4^{b}	4.2^{b}	9.6^{a}
G.m + T.v	26.5^{c}	29.6^{c}	4.6^{c}	4.8^{c}	4.2^{b}	9.0^{b}
B.c + T.v	20.5^{d}	28.9^{c}	4.8^{b}	4.6^{c}	4.0^{c}	8.6^{b}
G.m + B.c + T.v	28.0^{a}	32.4^{a}	5.2^{a}	5.6^{a}	4.9^{a}	9.7^{a}

Note: Means in the same column followed by the same superscript do not differ significantly according to Duncan's Multiple Range Test ($P< 0.05$).

Maximum per cent root colonisation were recorded in the plants inoculated with *G. mosseae* + *B. coagulans* + *T. viride* (95.2 %) (Table 2). Similarly, spore number was maximum when the plants were inoculated with G. mosseae + B. coagulans (682.4/100g soil) and *G. mosseae* + *B. coagulans* + *T. viride* (585.2/100 g soil), the lowest number being recorded in uninoculated control plants (Table 2). Synergistic interactions have been reported between the free-living rhizosphere bacteria, N2 fixing organisms and mycorrhizal fungi [26,11] with respect to the per cent root colonisation and spore number.

The leaf phosphorus, potassium, zinc, copper and iron content were maximum in the plants treated with *G. mosseae* + *B. coagulans* + *T. viride* (27.14 mg/plant, 15.2 mg/plant, 507.2µg/plant, 89.2 µg/g, and 94.2 µg/g respectively), in contrast with the plants inoculated with *G. mosseae* alone (15.20 mg/plant; 10.5 mg/plant; 160.5 µg/g, 53.6 µg/g and 60.5 µg/g respectively) (Table 2). This is probably due to the enhanced mycorrhizal colonisation. The phosphorus, potassium, zinc, copper and iron content were lowest in the uninoculated control plant. Such an increased P, K, Zn, Cu and Fe uptake due to mycorrhizal inoculation with PGPRs was also reported by earlier workers [3,27].

The acid phosphatase activity in the root-zone soil of all the inoculated seedlings was significantly higher compared to that in the root-zone soil of uninoculated control plants. The highest value was recorded in the root zone of the plants inoculated with *G. mosseae* + *B. coagulans* + *T. viride* (33.5 µ/g soil/hr), followed by that of the *G. mosseae* + *B. coagulans-inoculated plants* (23.03 µ/g soil/hr) (Table 2). Enhanced acid phosphatase activity in the root-zone soil of Neem due to inoculation with AM fungi was also reported earlier [28].

Table 2. Influence of AM fungus and PGPRs on % root colonisation, spore number in the root zone soil, and nutrient status in the leaves of B.malabarica

Treatment	Percent root colonisation	Spore number/ 100 g of soil	Leaf P (mg/plant)	Leaf K (mg/plant)	Leaf Zn (µg/g)	Leaf Cu (µg/g)	Leaf Fe (µg/g)	Acid phosphatase activity(µg/g soil/hr)
Uninoculated control	28.9^{e}	124.0^{e}	1.58^{e}	2.2^{f}	38.6^{f}	18.6^{e}	22.4^{e}	5.06^{e}
Glomus mosseae (G.m)	87.2^{b}	482.6^{b}	15.20^{c}	10.5^{c}	160.5^{d}	53.6^{c}	60.5^{c}	14.40^{c}
Bacillus coagulans (B.c)	30.5^{d}	160.5^{d}	3.40^{d}	2.8^{e}	56.2^{e}	42.5^{d}	48.2^{d}	6.02^{d}
Trichoderma viride (T.v)	31.2^{d}	140.6^{d}	3.08^{d}	2.9^{e}	62.0^{e}	40.2^{d}	41.5^{d}	6.08^{d}
G.m + B.c	83.5^{b}	682.4^{a}	20.22^{b}	12.5^{b}	394.5^{b}	60.8^{b}	92.5^{b}	23.03^{b}
G.m + T.v	62.8^{c}	320.5^{c}	16.56^{c}	11.4^{b}	251.8^{c}	56.8^{c}	90.5^{b}	13.03^{c}
B.c + T.v	45.2^{d}	285.0^{cd}	13.45^{bc}	8.2^{d}	120.2^{d}	38.4^{d}	85.6^{b}	18.05^{c}
G.m + B.c + T.v	95.2^{a}	585.2^{a}	27.14^{a}	15.2^{a}	507.2^{a}	89.2^{a}	94.0^{a}	33.5^{a}

Note: Means in the same column followed by the same superscript do not differ significantly according to Duncan's Multiple Range Test ($P< 0.05$).

The leaf secondary metabolites (total phenols, ortho dihydroxy phenols, flavonoids, alkaloids and tannins) were maximum in the plants treated with G. mosseae + B. coagulans + T. viride (129.8 µg/g, 81.5 µg/g, 3.62 µg/g, 5.08 µg/g, and 0.454 µg/g respectively), followed by the plants dually inoculated with G. mosseae + B. coagulans (124.2 µg/g, 75.6 µg/g, 3.28 µg/g, 4.36 µg/g, and 0.382 µg/g respectively) (Table 3). This is also apparently due to the enhanced mycorrhizal colonisation and nutrient status of the plants. Such an increased content of secondary metabolites due to mycorrhizal inoculation with PGPRs was reported by earlier workers [29,30].

Table 3. Influence of AM fungus and PGPR's on the content of secondary metabolites in the leaves of B. malabarica

Treatment	Total phenols (µg/g fresh wt.)	O-dihydroxy-phenols (µg/g fresh wt.)	Flavonoids (µg/g fresh wt.)	Alkaloids (µg/g dry wt)	Tannins (µg/g dry wt)
Uninoculated control	94.0^{e}	63.5^{e}	3.12^{e}	4.25^{e}	0.285^{e}
Glomus mosseae (G.m)	123.8^{b}	75.2^{b}	3.26^{b}	4.28^{b}	0.380^{b}
Bacillus coagulans (B.c)	118.2^{c}	70.4^{d}	3.21^{c}	4.26^{d}	0.286^{d}
Trichoderma viride (T.v)	110.6^{d}	69.2^{d}	3.16^{d}	4.32^{c}	0.285^{d}
G.m + B.c	124.2^{b}	75.6^{b}	3.28^{b}	4.36^{b}	0.382^{b}
G.m + T.v	112.4^{d}	73.2^{c}	3.24^{c}	4.21^{d}	0.365^{c}
B.c + T.v	110.5^{d}	70.6^{d}	3.18^{d}	4.23^{d}	0.314^{d}
G.m + B.c + T.v	129.8^{a}	81.5^{a}	3.62^{a}	5.08^{a}	0.454^{a}

Note: Means in the same column followed by the same superscript do not differ significantly according to Duncan's Multiple Range Test ($P< 0.05$).

Conclusions

From this study, it can be concluded that the "microbial consortium" consisting of *G. mosseae, B. coagulans* and T. viride seems to be best suited for *B. malabarica.* The results of these experiments clearly indicate that inoculating *G. mosseae* along with plant growth promoting rhizosphere microorganisms encourages the ability of *G. mosseae* and enhances the growth, biomass, nutrients, and content of secondary metabolites of *B. malabarica.*

References

1. S. F. Wright, "Management of arbuscular mycorrhizal fungi", in "Roots and Soil Management: Interactions between Roots and the Soil" (Ed. R. W. Zobel and S. F. Wright), American Society of Agronomy, New York, 2005, pp. 183-197.

2. D. J. Bagyaraj and A. Varma, "Interactions between arbuscular mycorrhizal fungi and plants: Their importance in sustainable agriculture in arid and semiarid tropics", Advances in Microbial Ecology, 1995, 14, 119-122.
3. R. Lakshmipathy, K. Chandrika, B. Gowda, A. N. Balakrishna, and D. J. Bagyaraj, "Response of Calamus thwaitessii var. canaranus Wilde to inoculation with Glomus mosseae, Bacillus coagulans and Trichoderma harzianum", J. Soil Biology & Ecology, 2002, 22, 16-21.
4. P. Jeffries, S. Gianinazzi, G. Perotto, K. Turnau, and J. Bareae, "The contribution of arbuscular mycorrhizal fungi in sustainable maintenance of plant health and soil fertility", Biology and Fertility of Soils, 2003, 37, 1-16.
5. E. George, K. Haussler, S. K. Kothari, , X. L. Li, and H. Marshner, "Contribution of mycorrhizal hyphae to nutrient and water uptake of plants", in "Mycorrhizas in Ecosystem" (Ed. D. J. Read, D. H. Lewis, A. H. Fitter, and I. J. Alexander), C.A.B. International, London, 1992, pp. 42-47.
6. S. K. Rajan, B. J. D. Reddy, and D. J. Bagyaraj, "Screening of arbuscular mycorrhizal fungi for their symbiotic efficiency with Tectona grandis", Forest Ecology and Management, 2000,126, 91-95.
7. A. H. Fitter and J. Garbaye, "Interactions between mycorrhizal fungi and other soil organisms", in "Management of Mycorrhizas in Agriculture, Horticulture and Forestry" (Ed. A. D. Robson, A. K. Abbott, and D. Malazczuk), Kluwer Academic Pub., Amsterdam, 1994, pp.123-132.
8. S. B. Gurumurthy, "Screening and performance of efficient VA mycorrhizal fungi for tree species suitable for Agroforestry", PhD. Thesis, 1997, University of Agricultural Sciences, India.
9. R. Lakshmipathy, K. Chandrika, B. Gowda, A. N. Balakrishna, and D. J. Bagyaraj, "Response of Saraca asoca (Roxb.) de Wilde to inoculation with Glomus mosseae, Bacillus coagulans and Trichoderma harzianum", J. Soil Biology & Ecology, 2001, 21, 76-80.
10. R. Muthuraju, V. U. Boby, V. C. Suvarna, and N. Jayasheela, "Interactive effects of Glomus mosseae, Pseudomonas fluorescens and Azospirillum brasilense on growth and yield of tomato", J. Soil Biology & Ecology, 2002, 22, 8-15.
11. N. Eranna, A. A. Farooqi, D. J. Bagyaraj, and C. K. Suresh, "Influence of Glomus fasciculatum and plant growth promoting rhizomicroorganisms on growth and biomass of periwinkle", J. Soil Biology & Ecology, 2002, 22, 22-26.
12. B. S. Sivakumar, N. Earanna, A. A. Farooqi, D. J. Bagyaraj, and C. K. Suresh, "Effect of AM fungus and plant growth promoting rhizomicroorganisms (PGPR's) on growth and biomass of geranium (Pelargonium graveolens)", J. Soil Biology & Ecology, 2002, 22, 27-30.

13. D. A. Sumana, D. J. Bagyaraj, and J. Arpana, "Interaction between *Glomus mosseae, Azotobacter chroococcum* and *Bacillus coagulans* and their influence on growth and nutrition of Neem", *J. Soil Biology & Ecology,* 2003, 23, 80-86.
14. K. R. Kiritkar and B. D. Basu, "Indian Medicinal Plants", 2nd Edn., Indological and Oriental Publishers, Delhi, 1975, p. 215.
15. M. L. Jackson, "Soil Chemical Analysis", Printice Hall of India, New Delhi, India. 1973, p. 680.
16. M. A. Tabatabai, "Soil enzymes", in "Methods of Soil Analysis: Part 2" (Ed. A. L. Page, R .H. Miller, and D. R. Kennye), American Society of Agronomy, Madison, Wisconsin, USA, 1982.
17. S. McDonald, P. D. Prenzler, M. Autolovich, and K. Robards, "Phenolic content and antioxidant activity of olive extracts", *Food Chemistry*, 2001, 73, 73-84.
18. A. Mahadevan and S. Sridhar, "Methods in Physiological Plant Pathology", Sivakami Publications, Chennai, India, 1996, p. 324.
19. C. Chang, M. Yang, H. Wen, and J. Chern, "Estimation of total flavonoid content in propolis by two complementary colorimetric methods", *J. Food and Drug Analysis,* 2002, 10, 178-182.
20. J. B. Harborne, "Phytochemical Methods", Chapman and Hall, London, 1973, p. 380.
21. M. Zakaria, "Isolation and characterization of active compounds from medicinal plants", *Asia Pacific J. Pharmacology,* 1991, 6, 15-20.
22. M. Giovannetti and B. Mosse, "An evaluation of techniques to measure vesicular-arbuscular infection in roots", *New Phytology,* 1980, 84, 489-500.
23. J. H. Philips and D. S. Hayman, "Improved procedure for clearing roots and staining parasitic and vesicular-arbuscular mycorrhizal fungi for rapid assessment of infection", *Trans. Brit. Mycol. Soc.,* 1970, 55, 158-161.
24. J. W. Gerdemann and T. H. Nicolson, "Spores of mycorrhizal endogone species extracted from soil by wet sieving and decanting", *Trans. Brit. Mycol. Soc.,* 1963, 46, 235-244.
25. T. M. Little and J. F. Hills, "Agricultural Experimentation", John Wiley and Sons, New York, 1978, p. 285.
26. J. R. Meyer and R.G. Linderman, "Response of subterranean clover to dual inoculation with vesicular arbuscular mycorrhizal fungi and a plant growth promoting bacterium Pseudomonas putida", *Soil Biol. and Biochem.,* 1986, 18, 185-190.
27. B. P. Thanuja, "Response on *Datura metal Linn* and *Adathoda vasica* Nees to diverse VA mycorrhizal fungi and some plant growth promoting microorganisms", *MSc. Thesis*, 2000, University of Agricultural Sciences, India.

28. D. A. Sumana, "Influence of VA mycorrhizal fungi and nitrogen fixing and mycorrhization helper bacteria on growth of neem (*Azadirachta indica A. Juss*)", PhD. Thesis, 1998, University of Agriculture Sciences, India.
29. K. V. Elango, "Studies on the effect of native AM fungi and PGPR's on growth and productivity of *Gloriosa superba L.*", PhD. Thesis, 2004, Bharathidasan University, India.
30. N. Mani, "Phytochemical and antimicrobial studies on *Alpinia galanga* and *Coleus amboinicus* as influenced by native AM fungi", *PhD. Thesis*, 2004, Bharathidasan Univiersity, India.

Maejo International Journal of Science and Technology

ISSN 1905-7873

Available online at www.mijst.mju.ac.th

Full Paper

Application of a modified Monte Carlo method for the simulation of heat conduction in a rectangular slab

Ademola. A. Dare* and Olusoji Ofi

Department of Mechanical Engineering, University of Ibadan, Ibadan, Nigeria
* Corresponding author, e-mail: Ademola.dare@mail.ui.edu.ng or Ademola_dare@yahoo.com

Received: 19 April 2008 / Accepted: 13 September 2008 / Published: 20 October 2008

Abstract : Monte Carlo method has been used to study heat conduction problems. It is grid-free in implementation, unlike the conventional Finite Element and Finite Difference Method. However for Monte Carlo method, solutions of desired field of interest can only be obtained one after the other, unlike the others that can be obtained simultaneously. Therefore a modified method has been developed which benefits from the simplicity of the Monte Carlo method and also provides full field description of temperature at one computer run.

The Modified Monte Carlo first obtains sample values of temperature in the domain of interest using the conventional Monte Carlo technique. Thereafter a histogram table is constructed which is then used to predict values for the other parts of the field unknown. The number of clusters obtained from the prediction is noted. The prediction that has minimal clusters is adjudged the best. The technique was tested on grid configurations such as 3 x 3 and 4 x 4 grids. Only isothermal steady-state 2-D cases were considered.

When compared with the results of ordinary Monte Carlo method, the modified technique incurred a maximum error of 4% for 4 x 4 grids. Larger grids were obtained by seamless stitching of smaller grids and as such no growth in errors was noticed. For the 3 x 3 grids, the sample size was about 55% while only 25% of the domain was sampled using 4 x 4 grids.

Using the modified technique, the errors incurred even with the 4 x 4 grids was only 4%. The technique can therefore be used for simulation of steady-state heat conduction.

Keywords : heat conduction, simulation , probability method, Modified Monte Carlo

Introduction

Various heat transfer processes require the knowledge of temperature distribution over the surface where the heat transfer is taking place. This in essence provides for better engineering decision and design. However, because of the mathematical rigour that has to be performed, the governing equations derived are often non-linear. Various numerical methods such as Finite Difference and Finite Element Method have been used extensively to tackle them. Many of such are well documented by Incroprera and DeWitt [1] as well as by Welty et al.[2] and Eckert and Drake [3]. Some recent applications of Finite Element Method and Finite Difference Method include the work of Jing Zhang et al. [4] and Tasarkuyu and Akinoglu [5]. These methods generally require simultaneous solution of domain solution points.

However, a probability method was applied by Haji-Sheikh and Sparrow [6] to obtain temperature of isolated points during heat conduction in a domain. A more recent effort was reported by Grigorin [7]. Leveque and Rezzong [8] carried out thermal studies of a superconductivity current limiter using Monte Carlo method.

Generally, probability methods can be used to obtain a single-point solution in a domain. They are therefore simpler to implement and less demanding on the computer memory. They may however be slower in run time. When a full description of the temperature history of the entire domain is needed, more computational time may be required.

The objective of this work is to preserve the simplicity of the Monte Carlo method by developing a Modified Monte Carlo approach which will make it possible to fully characterise the domain without excessive computational burden. This paper discusses the typical Monte Carlo solution for temperature in a domain and thereafter the Modified Monte Carlo technique is discussed.

Simple Monte Carlo Method

Monte Carlo application to thermal conduction was used by Haji-Sheikh and Sparrow [6] for obtaining temperature history in a rectangular slab. Both unsteady and steady-state cases were treated. In this method a probabilistic approach was adopted which makes single point solution achievable. An abridged description of the method is hereby presented.

Given any domain, the solution of a point in it (e.g. A) is obtained by commencing many random walks from the point of interest. Such walks are terminated whenever an absorbing boundary (a boundary with constant temperature) is encountered. Whenever the walk is terminated, the boundary value is scored. The average of all the scores at the absorbing boundary(ies) gives the solution of the point of interest.

Thus,

$$T_A = \frac{\sum_{i}^{n} T_i}{n}$$

where,

n = number of walks
Ti = temperature score at walk i
TA = temperature of the point of interest in the domain

The procedure is illustrated in Figure 1.

Ogundare [9] used the Monte Carlo technique to solve for temperature distribution in arbitrary surfaces. He reported good agreement with the Finite Difference solution for isothermal cases, but for adiabatic case an error of about 5% was noticed.

Modified Monte Carlo Method

Modified Monte Carlo method is developed to enable full characterisation of a domain, since the Monte Carlo solution can only provide single-point solution at any computational run. An algorithm of this technique is hereby presented.

(1) First divide the entire domain into the desired grid sizes such as 3 x 3 internal grid as in Figure 2.
(2) Select some nodes such as A,B,C, D, E (the selected points are block centred) and designate them as sample points.
(3) Determine the solution values of sample points using the normal Monte Carlo method. For instance, the assumed estimated values of the sample points are shown in Figure 3.
(4) Using the sample values, a histogram is then constructed as shown below.

x	f
1	2
2	3

(5) With the histogram, guess values for the remaining portion of the domain by making use of random numbers between 0 and 1. In the case being considered, if the random number is less than 2/5, a guess value 1 is assigned (x=1 at f =2), otherwise a guess value 2 is assigned.
(6) By comparing guess values , a set of estimated values that minimises cluster formation is chosen. For instance Guess 1 of Figure 4 is chosen.
(7) Steps 1-5 are repeated several times. Thereafter average values at the various grid points are estimated.

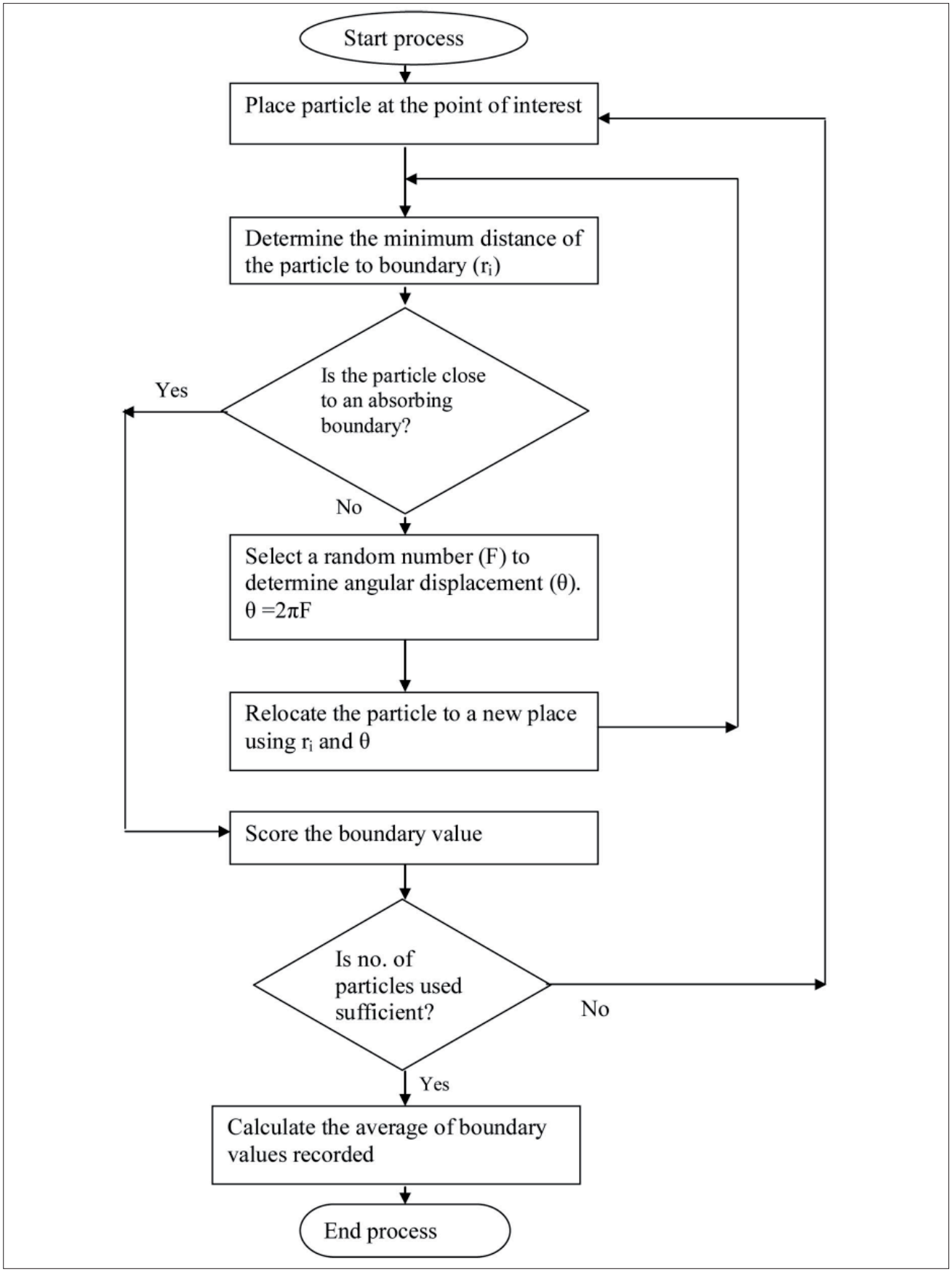

Figure 1. Simple Monte Carlo flow chart

B		**C**
	D	
A		**E**

Figure 2. Domain with sample points

2		1
	2	
2		1

Figure 3. Domain with sample values

Guess 1

2	2	1
2	2	1
2	2	1

Number of clusters = 2

Guess 2

2	2	1
1	2	2
2	1	1

Number of cluster =5

Figure 4. Domain with predicted values

Larger grid solutions are obtained by seamless stitching of smaller grids. For instance, in Figure 5, the 8 x 8 internal grid solutions are obtained as follows:

(i) Divide the 8 x 8 grid into four 4 x 4 internal 'sub-grids.'

(ii) Identify sample points in each of the sub-grids and obtain their values using the simple Monte Carlo technique. Note that sample points solutions must be obtained using the global domain. This enables seamless stitching of the grids.

(iii) Each of the 'sub-grids' is now separately considered. Unknown values in each 'sub-grid' are then obtained using the Modified Monte Carlo procedure.

(iv) All the 'sub-grids' with all the values now known are joined together. No further processing of the results at the grid borders is needed and it is therefore regarded as seamless stitching. Further clarification can be obtained from the accompanying Figure 5.

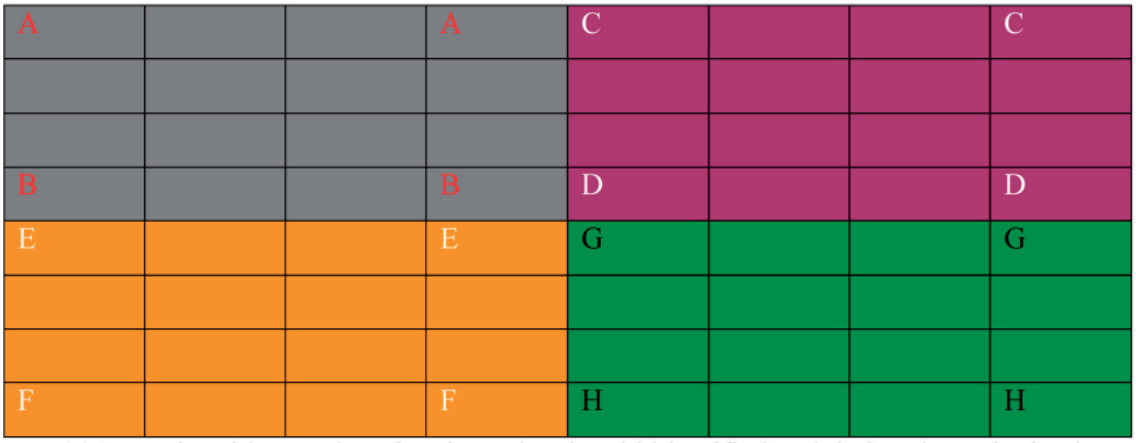

(a) Domain with sample points in each sub-grid identified and their values obtained

A	X	X	A
X	X	X	X
X	X	X	X
B	X	X	B

(b) A sub-grid separately treated with values obtained globally unaltered

Figure 5. Stitching process for 8 x 8 grid (Note: Values of points marked with 'X' in Fig. 5b are predicted using Modified Monte Carlo technique. These values are retained at their corresponding positions in the global domain.)

Application of the Modified Monte Carlo Method to Simple Thermal Conduction Problems

The Modified Monte Carlo method was used to simulate heat conduction in a rectangular slab with thermal conductivity of 0.035 W/m^2 K. This was carried out using different kinds of grid configurations. The results for such grids are hereby presented.

Simulation using 3 x 3 domain

The results for this case is presented in Table 1, which shows no noticeable discrepancies. The sample values are underlined implying that only four other values are simulated using the Modified Monte Carlo technique. In a way this may imply a saving of 45% in computational run when compared to ordinary Monte Carlo technique.

Table 1. Simulation temperature results (K) for 3 x 3 grid using Modified Monte Carlo technique

		400 K		
400 K	*385*	377.6	*373*	**200 K**
	378	*351*	320	
	376	324	*262*	
		200 K		

(Note : All simulated values are for internal grids. Only four new points were predicted using the Modified Monte Carlo technique. The samples (in underlined form) is thus about 55%.)

Simulation using a 4 x 4 grid

The simulated values using the same material properties as for the 3 x 3 grid are presented for the ordinary and Modified Monte Carlo method in Tables 2 and 3 respectively. The sample values are shown underlined for Modified Monte Carlo case. There are thus 12 simulated values obtained using the Modified Monte Carlo technique. The sample size in this case is 25%.

Table 2. Simulated temperature results (K) for 4 x 4 grid using normal Monte Carlo technique

		773 K		
373 K	**557.8**	**773**	**773**	**568.2**
	373	**538.6**	***525.8***	**373**
	373	**417**	**418**	**373**
	373	**373**	**373**	**373**
		373 K		

Table 3. Simulated temperature results (K) for 4 x 4 grid using Modified Monte Carlo method

		773 K		
373 K	**557.8**	**773**	**773**	**555.4**
	373	**538.6**	*503.4*	**373**
	373	**416.2**	**418.6**	**373**
	373	**373**	**373**	**373**
		373 K		

(Notes: 1. Sample values are shown underlined.
2. Except for boundary values, all others are for internal grids.)

Comparison of simulated results of modified and ordinary Monte Carlo method

Inspection of the 3 x 3 grid solution revealed no discrepancies while point-by-point solution comparison for the 4 x 4 grid showed a discrepancy of 4% (discrepancy points in italics).

Simulation results for 12 x 12 grid

The solutions using a 12 x 12 grid were obtained by seamlessly joining solutions for four 4 x 4 sub-grids as earlier highlighted. A sample solution using the same material properties as for the earlier-mentioned cases and with the boundary condition boldly highlighted is presented in Table 4.

Table 4. Simulated temperature (K) results for 12 x 12 grid using Modified Monte Carlo method

591.67	**773**	**773**	**773**	**773**	**773**	**773**	**773**	**773**	**773**	**773**	**579.67**
373	577	626.33	695.67	730.33	725	729	727.67	690.33	594.33	597	**373**
373	531.67	567.67	615.67	671.67	663.67	670.33	663.67	621	542.33	541	**373**
373	438.33	499.67	549	582.33	591.67	587.67	581	555.67	511.67	455.67	**373**
373	399.67	467.67	530.33	531.67	525	526.33	550.33	507.67	458.33	399.67	**373**
373	393	449	486.33	487.67	494.33	510.33	507.67	471.67	442.33	386.33	**373**
373	390.33	431.67	454.33	462.33	487.67	495.67	474.33	427.67	406.33	387.67	**373**
373	391.67	411.67	434.33	438.33	458.33	450.33	439.67	425	411.67	386.33	**373**
373	381	393	403.67	419.67	407.67	401	418.33	405	391.67	378.33	**373**
373	381	382.33	385	405	401	399.67	401	391.67	382.33	374.33	**373**
373	373	374.33	378.33	383.67	379.67	383.67	386.33	379.67	374.33	373	**373**
373	**373**	**373**	**373**	**373**	**373**	**373**	**373**	**373**	**373**	**373**	**373**

(Notes: 1. Boundary values are boldly highlighted.
2. Other values are for internal grids.)

Conclusions

This paper has established the possibility of using a Modified Monte Carlo method for solving heat conduction problems. It shows that by seamless stitching of 4 x 4 grids, a full temperature characterisation of the domain of interest can be obtained. In view of its likely saving in computational time, the method may therefore be explored for numerical studies.

References

1. F. P. Incropera and D. P. deWitt, "Fundamentals of Heat and Mass Transfer", 3rd Edn., John Wiley & Sons, New York, 1990.
2. J. R. Welty, C. E. Wicks, R. E. Wilson, and G. L. Rorrer, "Fundamentals of Momentum , Heat and Mass Transfer", 4th Edn., John Wiley & Sons, New York, 1989.
3. E. R. G. Eckert and R. M. Drake, Jr., "Analysis of Heat and Mass Transfer", McGraw-Hill, New York, 1972.
4. J. Zhang, A. Zavaliangos, M. Kraemer, and J. Groza, "Finite element simulation of thermal and electrical fields in field activation sintering", Proceedings of International Conference on Process Modeling in Powder Metallurgy and Particulate Materials, Newport Beach, CA, November 1-3, 2002.
5. E. Tasarkuyu and B. G. Akinoglu, "Numerical simulation of heat conduction for the growth of anisotropic layered GaSe crystals", *Cryst. Res. Technol.,* 2004, 39, 771-783.
6. A. Haji-Sheikh and E. M. Sparrow, "The solution of heat conduction problems by probability methods", *Transac. ASME, J. Heat Transfer,* 1967, 89,121-130.
7. M. A. Grigorin, "Monte Carlo solution of heat conduction", *J. Heat Transfer,* 2000, 122, 40-45.
8. J. Leveque and A. Rezzong, "Thermal studies of a superconducting current limiter using Monte Carlo method", *Eur. Phys. J. AP.,* 1999, 7, 65-71.
9. M. A. Ogundare, "Monte Carlo modelling of steady state heat transfer in an isothermal arbitrary surface", *MSc. Project Report,* 1990, University of Ibadan, Nigeria.

Maejo International Journal of Science and Technology

ISSN 1905-7873
Available online at www.mijst.mju.ac.th

Full paper

Microscale electrochemical cell using plaster ($CaSO_4$) as liquid junction

Yuthapong Udnan*, Wipharat Chuachuad, and Ratana Sanunmuang

Department of Chemistry Naresuan University, Thailand, 65000
* Corresponding author, e-mail: yuth13@yahoo.com

Received: 7 May 2008 / Accepted: 24 October 2008 / Published: 28 October 2008

Abstract: A microscale apparatus for electrochemical cell in which plaster (CaSO4) was used as liquid junction has been developed. A glass tube (0.5 cm ID x 5.0 cm) was used to prepare each half-cell. The potentials of the resulting galvanic cells were measured by a multimetre and were compared to those of the galvanic cells in which agar was used as liquid junction. It was found that the potentials produced by the galvanic cells with plaster as liquid junction are not significantly different from those of the cells with agar as liquid junction and close to the theoretical values. In addition, when the developed apparatus was used for the study of electrolysis of potassium iodide solution, it was found that the electrolytic cell made from the microscale apparatus with plaster liquid junction can distinctly separate the reactions occurring at the anode and the cathode. Moreover, the lifetime of the plaster liquid junction is much greater than that of the agar liquid junction.

Keywords: plaster, liquid junction, electrochemical cell

Introduction

Microscale chemistry is a teaching method working with small quantities of chemical substances. It has been widely used both at school and at university levels. The method can be applied to many types of experiments. Pioneering development in this area was carried out by Grey and El-Marsafy in Egypt, and Thompson in the US, among others [1]. There are two main strands of the modern approach [1]. One is based on the idea that many of the experiments associated with general chemistry (acids and bases, oxidation and reduction, electrochemistry, etc.) can be carried out in apparatus much simpler

(injection bottles, dropper bottles, syringes, well plates, plastic pipettes) and therefore cheaper than the traditional glassware in the laboratory, thus enabling expansion of laboratory experiences for students in large classes, as well as introduction of laboratory work into institutions too poorly equipped for standard-type equipment. A further application of this idea is to make effective chemical experiments possible for developing countries with schools that lack technical services (electricity, running water) taken for granted in many places. The other strand of idea is the introduction of this approach into synthetic work, mainly in organic chemistry.

There have been many publications [e.g. 2-8] which concern with microscale laboratory. In this work, a microscale apparatus for electrochemistry has been developed. Electrochemistry deals with the production of electricity by chemical reactions (galvanic cell) and with the chemical changes produced by electric current (electrolytic cell). Electrochemical processes require some methods of introducing a stream of electrons into a reacting chemical system and some means of withdrawing electrons. In most applications, the reacting system is placed in a cell and an electric current enters or exits via electrodes [9].

When two miscible aqueous solutions are contacted, they will combine and give a new solution. The way to separate them while some ions can still be transferred from one to the other is to use a liquid junction. In an electrochemical cell, when two half-cells are joined together a liquid junction or salt bridge is used to separate them. Agar has been a material widely used for the liquid junction of the electrochemical cell for many years. The salt bridge serves three functions [9]: 1) it allows electrical contact between the two solutions, 2) it prevents mixing of the electrode solutions, and 3) it maintains the electrical neutrality in each half-cell as ions flow into and out of the salt bridge.

To the best of our knowledge, the use of plaster as liquid junction has not been previously reported. Therefore, a microscale apparatus for electrochemical cells, namely galvanic and electrolytic cells, using plaster as liquid junction is developed and reported in this work, the apparatus being aimed to be used in a first year student laboratory.

Materials and Methods

Apparatus

The micro-electrochemical cell was made from two 3 mm x 5 cm glass tubes. A liquid junction was prepared by mixing 2:1 (by volume) of plaster and saturated (≈ 5 M) potassium chloride solution (Ajax Finechem, AU.) in a 50-ml beaker and stirring. The glass tubes were dipped 0.5 cm into the mixture and left to harden for about 5 minutes, then carefully pulled out. Each tube was then filled with an appropriate solution and an appropriate metal electrode was dipped into the tube. A small cylindricalshaped vial used as cell container was modified from a capillary tube container and a cell holder was modified from the lid of a plastic bottle (Figure 1). A multimeter (model 972A, Hewlett Packard, USA) was used to measure the potential of the galvanic cell. A 9-volt battery was used as a power supply of the electrolytic cell.

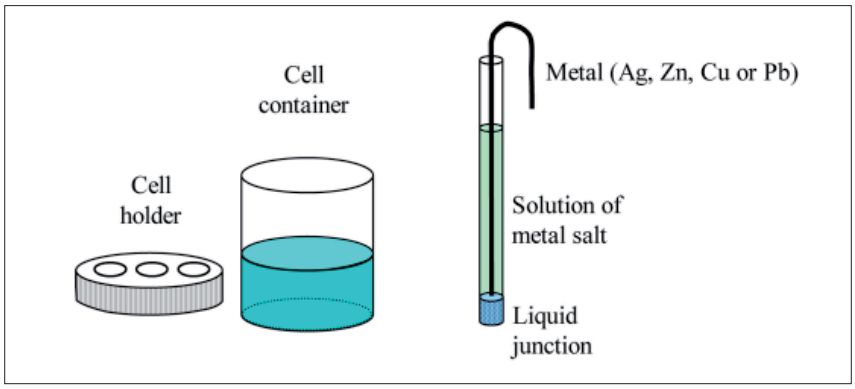

Figure 1. Apparatus used for micro-electrochemical cell

Chemicals

All solutions were prepared from laboratory grade reagents and distilled water. A 0.10 M solution of each metal salt was prepared by dissolving 0.0170 g of $AgNO_3$ (Merck, Germany), 0.0160 g of $Cu(NO_3)_2$ (Merck, Germany), 0.0331 g of $Pb(NO_3)_2$ (Merck, Germany), and 0.0189 g of $Zn(NO_3)_2$ (Merck, Germany) in a portion of water and transferring to a 100-mL volumetric flask before making up to a volume of 100 ml. A 0.1 M solution of KNO_3 (Ajax Finechem, AU) was prepared by dissolving 0.101 g KNO_3 in a portion of water before making up to a volume of 10 ml. A 0.1 M solution of KI (Ajax Finechem, AU) was similarly prepared using 0.17 g KI. Phenolphthalein and starch solution were used as indicators for testing the final products generated from each-half cell.

Study of galvanic cell

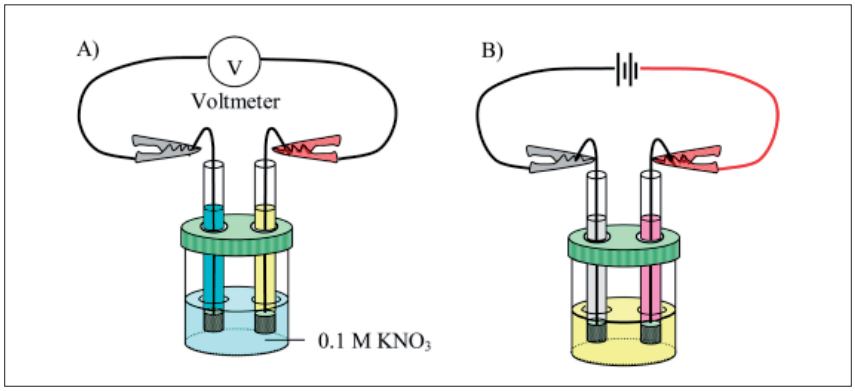

Figure 2. Setup of A) galvanic cell and B) electrolytic cell

The glass tubes with agar and plaster liquid junction were filled with a solution of a metal salt [$AgNO_3$, $Cu(NO_3)_2$, $Pb(NO_3)_2$ and $Zn(NO_3)_2$] to about ¾ of the tube. An appropriate metal was dipped into the glass tubes and the tubes were put into the cell holder as illustrated in Figure 2A. The cell

container was filled up with 1 ml of 0.1 M KNO3 before the cell holder was placed on. The potential produced by each pair of the half-cell was measured using the multimeter.

Study of electrolytic cell

A solution of 0.1 M KI (5 mL), 2 drops of starch solution and 2 drops of phenolphthalein was placed in two glass tubes (about ¾ of the tube) with plaster liquid junction. Graphite rods were dipped into the tubes, which were inserted in the cell holder as shown in Figure 2B. The cell container was filled with 0.1 M KI (1.0 mL) before the cell holder was put in. Each half-cell was connected to a 9-volt battery. The reaction on each half-cell was observed during a period of 5 minutes.

Results and Discussions

Galvanic cell

The potential of each pair of the galvanic cells with plaster and agar as liquid junction was measured and compared to the theoretical value which was calculated from Nernst's equation as follows:

$$E_{cell} = E^0_{cell} - \frac{0.0591}{n} \log \frac{[C]^c[D]^d}{[A]^a[B]^b}$$

where E^0 is the standard reduction potential of each half-cell:

$$Ag^+ + e^- \longrightarrow Ag \qquad E^0 = -0.76\ V$$
$$Pb^{2+} + 2e^- \longrightarrow Pb \qquad E^0 = -0.13\ V$$
$$Cu^{2+} + 2e^- \longrightarrow Cu \qquad E^0 = +0.34\ V$$
$$Ag^+ + e^- \longrightarrow Ag \qquad E^0 = +0.80\ V$$

The results of the potential measured from different types of galvanic cell were shown in Table 1. From the results it was found that the Ecell values produced by the galvanic cells with plaster liquid junction and agar liquid junction were close to the theoretical values, and the relative accuracy of the average values of Ecell (n = 3) was in the range of 94.3-99.9 % and 93.6-100.1% respectively. The precision of the triplicate measurements indicated by the relative standard deviations (%RSD) of the Ecell values was in the range of 0.2-3.0 % and 0.4-5.8 % respectively. Furthermore, it was found that the Ecell values produced by both types of the galvanic cell were not significantly different by paired t-test at 95% confidence level (tcal = 0.1495).

An electromotive force (E_{cell}) is the difference in electrode potential which can be expressed by the following equation:

E_{cell} = E_{cat} - E_{an} + E_j
E_{cat} = Potential of the cathode half-cell
E_{an} = Potential of the anode half-cell
E_j = Junction potential

Table 1. Potential of each pair of galvanic cells

Galvanic cell	E_{cell} (V)			Relative accuracy and % RSD	
	Theoretical value	Plaster junction	Agar junction	Plaster junction	Agar junction
Pb//Cu	0.466	0.465	0.466	99.9 / 3.0	100.1 / 5.8
Pb//Zn	0.637	0.614	0.598	96.3 / 2.6	93.9 / 4.6
Pb//Ag	0.925	0.894	0.895	96.7 / 1.2	96.8 / 3.0
Zn//Cu	1.103	1.079	1.080	97.9 / 0.2	97.9 / 0.4
Cu//Ag	0.459	0.433	0.430	94.3 / 2.1	93.6 / 0.4
Zn//Ag	1.562	1.508	1.509	96.6 / 0.3	96.6 / 0.4

From the equation, the important factor which affects the Ecell value is the junction potential. However, the results show that the Ecell measured from both types of the galvanic cell are not different. This indicates that the junction potentials produced by both plaster and agar liquid junction are quite small and do not affect the Ecell value. As a consequence, the material used in both types of liquid junction or the composition of ions in the liquid junction does not affect the Ecell value.

It was also observed that the plaster liquid junction was harder and more durable than the agar liquid junction. The latter was soft and easy to be penetrated by the metal wire. Besides, the former has a much longer lifetime than the latter after preparing and leaving to contact with air.

Electrolytic cell

The setup for electrolysis of 1.0 M KI solution using the microscacale apparatus for electrolytic cell is shown in Figure 3. From the result of the electrolysis it could be clearly seen that the reactions at both electrodes were different. When the circuit of the electrolytic cell was connected, at the half-cell of the anode, oxidation of the iodide ions occurred as indicated by the dark blue colour of iodine-starch complex:

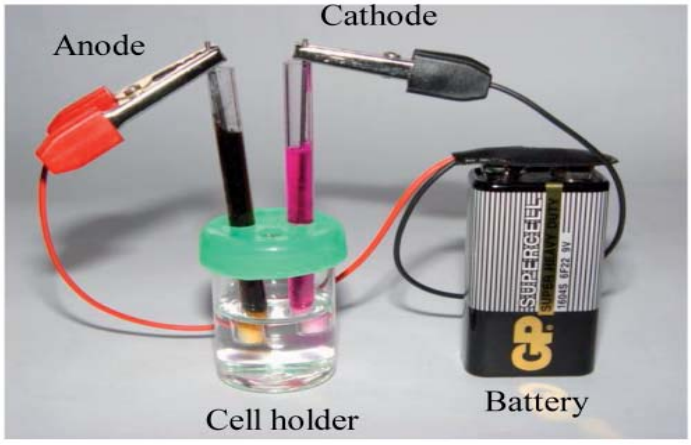

Figure 3. Electrolysis setup of KI using small scale apparatus

$$2I^- \rightarrow I_2 + 2_{e^-}$$

At the half-cell of the cathode, reduction of water took place and hydroxide ions were produced:

$$H2_O + 2e^- \rightarrow OH^- + H_2$$

The generation of hydroxide ions at the cathode half-cell was indicated by the change of colour of phenolphthalein indicator, which turned to pink in the basic solution. In addition, it could be seen that some gas bubbles were also produced at the cathode half-cell.

Conclusions

A microscale apparatus for electrochemical cells has been developed and successfully applied to galvanic and electrolytic cells. It was found that the developed apparatus can reduce the consumption of the solutions involved to less than 5 mL per experiment. This apparatus is environmentally friendly as it produces less amount of waste to the laboratory. Besides, the apparatus works efficiently as the results obtained from the microscale apparatus are not different from those obtained from a large-scale one. The developed apparatus is also inexpensive and can be further applied to small-scale experiments in general chemistry for first-year undergraduate students.

Acknowledgements

Thanks are due to the Faculty of science, Naresuan University for the financial support and to the Department of Chemistry, Naresuan University for equipment support and research facilities.

References

1. Wikipedia, the free encyclopedia, http://en.wikipedia.org/wiki/Microscale_chemistry (accessed 10 December, 2007).
2. R. O. Ragsdale and J. C. Vaderhooft, "Small-scale study of the catalyzed decomposition of hydrogen peroxide", J. Chem. Educ., 1998, 75, 215-217.
3. J. G. Ibanez, M. M. Singh, R. M. Pike, and Z. Szafran, "Laboratory experiments on electrochemical remediation of the environment. Part 3: Microscale electrokinetic processing of soils", J. Chem. Educ., 1998, 75, 634-635.
4. E. Mocellin and T. Goscinska, "Modified carbon electrodes for microscale electrochemistry", J. Chem. Educ., 1998, 75, 771-772.
5. J. N. Richardson, M. T. Stauffer, and J. L. Henry, “Microscale quantitative analysis of hard water samples using an indirect potassium permanganate redox titration”, J. Chem. Educ., 2003, 80, 65 - 67.

6. S. Algirdas, “Demonstrating corrosion using galvanic cells”, J. Chem. Educ., 2003, 80, 1138.
7. E. Per-Odd, G. Truls, and K. Lise, “Small-scale and low-cost galvanic cells”, J. Chem. Educ., 2006, 83, 1201-1203.
8. E. Per-Odd and K. Lise, "Small-scale and low-cost electrodes for standard reduction potential measurements", J. Chem. Educ., 2007, 84, 671-673.
9. K. W. Whitten, K. D. Gailey, and R. E. Davis, “General Chemistry”, 4 Edn., Saunders College, New York, 1988.

Maejo International Journal of Science and Technology

ISSN 1905-7873
Available online at www.mijst.mju.ac.th

Full Paper

Biochemical changes in the liver of Swiss albino mice orally exposed to acrylamide

Asha Sharma [1], Renu Sharma [2],*, and Jyotsna Jain [2]

[1] Department of Zoology, University of Rajasthan, Jaipur, 302004, India
[2] Cell and Molecular Biology Laboratory, Department of Zoology, University of Rajasthan, Jaipur, 302004, India
* Corresponding author, e-mail: renu_sha1982@yahoo.co.in

Received: 19 April 2008 / Accepted: 30 October 2008 / Published: 4 November 2008

Abstract : Acrylamide is a common chemical which is used worldwide to synthesise polyacrylamide. Polyacrylamide and acrylamide both have numerous applications in cosmetic industries, plastic and aesthetic surgeries, ophthalmic operations, waste water treatments, oil recovery processes, and other industrial and laboratory processes. Exposure of mice (Mus musculus) to acrylamide at three dose levels (5, 15 and 25 mg/kg body weight) was investigated for its effects on the liver. Mortality was found to be nil in all the experimental groups. A significant decrease in body weight gain and liver weight was observed but the relative liver weight increased significantly with dose concentration. A significant decrease was observed in protein and GSH levels as compared to those of control, and this reduction was more pronounced at highest dose level. Concentrations of SGOT, SGPT, and serum alkaline phosphatase activity showed a significant increase which was directly proportional to the concentration of the dose.

Keywords : acrylamide, GSH, protein, alkaline phosphatase, SGOT, SGPT

Introduction

Acrylamide (CH_2=CH–$CONH_2$) is a common chemical which is used in both industrial and laboratory processes. The most important use of acrylamide is in the production of high molecular weight polyacrylamide which is produced to give non-ionic, cationic and anionic properties for specific uses [1]. The co-polymers and polymers of acrylamide have a wide range of applications,

e.g. treatment of drinking water, waste water, soil and sand; processing of crude oil, paper, pulp, minerals, concrete, and textiles. They are also used as filler in cosmetic industry, as hydrogel in ophthalmic operations, as an ingredient of microencapsulated gelospheres for drug treatment, in plastic and such aesthetic surgeries as breast augmentation, and in contact lenses, photographic emulsions and adhesives [2-6]. In scientific researches acrylamide is also used to selectively modify –SH groups and as a quencher of tryptophan fluorescence in studies designed to elucidate the structure and functions of proteins [7].

Acrylamide occurs in both solid (crystalline) and liquid (aqueous) forms. The solid monomer is a colorless , free flowing crystal which is soluble in water, methanol, ethanol, dimethyl ether and acetone, and is insoluble in benzene and heptane. Commercially acrylamide is produced by catalytic hydration of acrylonitrile [1,8]. Recent investigations have indicated that it is also formed in heated starchy foods especially potato products via the Maillard-type reaction mainly between the amino acid aspargine and a carbonyl source such as the reducing sugars glucose and fructose [9-10]. It is also a component of tobacco smoke, which indicates that it can also be formed by heating of tobacco-containing products like cigarette, cigar, etc. [11-12]

Although the polymeric form of acrylamide is reported to be nontoxic, its monomeric form has a potential to cause a wide spectrum of toxic effects [13-17]. It is reported to be a multisite carcinogen, which can induce tumours of the adrenal, thyroid, CNS, oral cavity, testis, mammary gland and uterus [18-19]. Genotoxicity of acrylamide has also been reported, which comprised chromosomal aberrations, sister chromatid exchanges, unscheduled DNA synthesis, and dominant lethality [20-26]. Changes in copulatory behaviour, decreased fertility, effects on sperm motility and morphology in treated male, and alterations in the estrogen/progesterone balance in offsprings of treated females are the other reported toxic effects related to the reproductive toxicity of this chemical [27-28]. Acrylamide is also a neurotoxin which induces paraesthesias in fingers, coldness and weakness of hands, numbness in lower limbs, drowsiness, hallucinations, ataxia, convulsions, diffused damage to different sections of the nervous system, lysis in the cerebellum neurons and tibial nerve degeneration [29-33].

The liver plays a central role in the process of detoxification in the body. Glutathione (GSH), a tripeptide present in the liver, kidney, brain, and erythrocyte has a significant binding capacity with toxic substances resulting in the formation of usually non-reactive conjugated products [34]. A large reserve of GSH in hepatocytes makes the liver more efficient in the process of detoxification. However, if the rate of production of the toxic metabolites exceeds the availability of glutathione, hepatotoxicity can occur. Similarly, depletion of the protein store of the liver is also an indicator of hepatic disorders.

Different cells have different enzymes inside them, depending on the function of the cell. When cells die or are damaged, the enzymes leak out causing the blood level of these enzymes to rise. Serum glutamic oxaloacetic transaminase (SGOT), serum glutamic pyruvic transaminase (SGPT), and alkaline phosphatase are some liver-function test enzymes, the elevation of which, in serum, reflects

some hepatic disorders [35]. Therefore, to evaluate the liver damage, estimation of these enzymes in serum is essential.

The aim of the current study is to evaluate the hepatotoxicity in Swiss albino mice orally exposed to acrylamide.

Material and Methods

General

Adult Swiss albino mice (Mus musculus), 8-10 weeks old with body weight of 26 ± 2 gm, were used. They were maintained and bred in animal house as outbred colony as per norms laid down by an Institutional Ethical Committee, given standard mice food and water ad libitum. Acrylamide monomer of 99% purity was obtained from Central Drug House (P) Ltd., Bombay, in powder form. It was dissolved in doubly-distilled water to obtain a 1% solution and kept in a dark brown bottle to avoid polymerisation. The experiment was conducted for the duration of 60 days and divided into three groups, viz. E1, E2, and E3, each with 10 animals that were given 5, 15, and 25 mg respectively of acrylamide/kg body weight. Along with these experimental groups a control group was also set, in which animals were given doubly-distilled water equal to the volume of acrylamide solution given in the experimental group of the highest dose. The dosing of control and all experimental groups was carried out orally with a gavage needle on alternate days for the duration of 60 days and animals were checked daily for any mortality. Mice were autopsied by cervical dislocation after 24 hours of oral administration of the last dose on the 61st day. The serum was obtained by collecting the blood obtained by cardiac puncture in sample bottles without anticoagulant. The blood was centrifuged for 10 minutes at 3000 rpm and the resulting serum was used for analysis. The liver were dissected out carefully, blotted free of blood, weighed, and utilised for the study.

Liver biochemical analysis

Protein concentration in the liver was determined by the method of Lowry et al.[36] and expressed as mg/100mg of tissue weight. Concentration of GSH in the liver was measured using the method described by Moron et al. [37] and expressed as μmol/gm of tissue weight.

Serum biochemical analysis

The activity of alkaline phosphatase in the serum was measured using the method of Fiske and Subarrow [38] and expressed as mg Pi/gm/h. Dete rmin ation of se rum transaminases (SGOT and SGPT) was carried out by the method of Reitman and Frankel [39] and expressed as IU/L. The collected data were statistically analysed by student's t- test and the treatment groups were considered statistically significant at $P<0.001$, $P<0.01$ and $P<0.05$.

Results and Discussion

The mortality rate was observed to be nil in all the experimental groups. A significant reduction ($P<0.001$) in body weight gain and liver weight ($P<0.01$ in E1 and E2, $P< 0.001$ in E3) was observed but the relative liver weight [= (liver weight/body weight)x100] increased nonsignificantly in E1 and E2 and significantly ($P<0.05$) in E3 [Table 1]. Protein and GSH levels in liver decreased significantly ($P<0.001$) in comparison to those of control [Table 2]. Serum SGOT and SGPT concentration and alkaline phosphatase activity showed a significant increase ($P<0.001$) as compared to control, the increase being directly proportional to the concentration of acrylamide dose [Table 3].

Table 1. Changes in body weight and liver weight of Swiss albino mice

Experimental group	Initial body weight (g)	Final body weight (g)	Body weight (g)	Liver weight (g)	Relative liver weight*
Control	26.77 ± 0.281	33.22 ± 0.496	6.556 ± 0.525	2.402 ± 0.056	7.234 ± 0.218
E1	26.98 ± 0.815	27.85 ± 0.774	0.876 ± 0.233 ***	2.105 ± 0.060**	7.564 ± 0.356 NS
E2	26.54± 0.287	27.14 ± 0.326	0.601 ± 0.189 ***	2.078 ± 0.060**	7.658 ± 0.236 NS
E3	26.65± 0.707	25.58 ± 0.344	-1.065 ± 0.534 ***	2.035 ± 0.033***	7.957 ± 0.192*

* = [liver weight/body weight] x 100

Note: Values are depicted as Mean ± SEM. Significance level: **P < 0.05, **P<0.01, ***P<0.001, NS* (not significant)

Table 2. Changes in protein and glutathione (GSH) level in liver of Swiss albino mice

Experimental group	Protein (mg/100mg tissue weight)	GSH (μmol/gm tissue weight)
Control	28.449 ± 0.372	86.465 ± 0.364
E1	16.531 ± 0.534 ***	45.455 ± 0.418 ***
E2	12.589 ± 0.296 ***	40.522 ± 0.577 ***
E3	8.715 ± 0.409 ***	34.352 ± 0.377***

Note: Values are depicted as Mean ± SEM. Significance level: **P < 0.05, **P<0.01, ***P<0.001, NS* (not significant)

Table 3. Changes in alkaline phosphatase (ALP) activity, and SGOT and SGPT concentration in serum of Swiss albino mice

Experimental group	ALP (mg Pi/gm/h)	SGOT (IU/L)	SGPT (IU/L)
Control	5.633± 0.252	29.59 ± 0.260	21.03 ± 0.599
E1	11.699± 0.222 ***	43.647 ± 0.723 ***	32.935 ± 0.565 ***
E2	14.492 ± 0.380 ***	48.102 ± 0.740 ***	35.731 ± 0.453***
E3	17.98 ± 0.724 ***	54.102 ± 0.346***	39.148 ± 0.456 ***

Note: Values are depicted as Mean ± SEM. Significance level: **P < 0.05, **P<0.01, ***P<0.001, NS* (not significant)

The steady decrease in hepatic protein level with higher doses of acrylamide can be attributed to retarded protein synthesis, or to any change in protein metabolism, or to the leaking out of protein reserves from hepatocytes. Previous findings have shown that acrylamide and its metabolite glycidamide have an affinity to bind with DNA and can cause chromosomal aberrations [22-23,40]. Thus, any abnormality in DNA structure can affect transcription and ultimately protein synthesis. As reported [7,41], the acrylamide molecule has two reactive sites, viz. the conjugated double bond and the amide group. Therefore it can conjugate with the –SH group of a sulfur amino acid, the α-NH_2 group of a free amino acid, the ε-NH_2 group of lysine, the ring NH group of histidine, and the N- terminal residue of a protein. The above scenario can explain the unavailability of a few amino acids for protein synthesis, which might consequently be a reason for the depleted protein content in the liver. Further, being an elecrophilic compound, acrylamide can bind with proteins that also can make them undetectable. Hepatocellular necrosis can also lead to the leaking out of protein reserve from the liver to the blood, thereby reducing the protein concentration of the liver.

The low levels of GSH in the present study might be due to the strong affinity of the –SH group of sulfur amino acids like cysteine and methionine for the double bond of such conjugated vinyl compounds as acrylamide, which might have reduced the concentration of these amino acids which are the main components of GSH. Further, the oxidative stress due to acrylamide might also result in oxidation of GSH to GSSG, hence decreasing the GSH concentration. Other studies have suggested that the conjugation of acrylamide to GSH catalysed by glutathione-S-transferase (GST) and excretion as mercapturic acid is a major pathway for the metabolism and detoxification of the same [42-44]. Since a large reserve of GSH is present in the hepatocytes, therefore in the process of detoxification of acrylamide the utilisation of liver GSH would be more pronounced, and thus the detoxification mechanism can also be the cause of the decreased concentration of GSH. Other studies have also shown a significant decrease in protein synthesis and GSH level in neuroblastoma cells on exposure to acrylamide [45-46].

A gradual increase in serum alkaline phosphatase (ALP) activity and also SGPT and SGOT level in this study could be due to the bipolar nature of acrylamide, where the CH_2=CH- part may undergo hydrophobic interactions while the -$CONH_2$ part can form hydrogen bonds with the cell components. This property may enhance its ability to alter the cell membrane structure and make the parenchymal cell membrane of the liver more permeable, thereby ceasing the active retention of enzymes and making them appear first in the extracellular space and then in the blood. These results obtained in the current study are in agreement with other studies which also indicated an increase in activity of the liver enzymes following liver damage in fish and albino mouse [47,48].

Conclusions

The available information based upon human epidemiological and population-based studies on the adverse effects of acrylamide confirms its neurotoxicity, but due to the low statistical power and the limited range of exposure doses, other effects such as reproductive toxicity, genotoxicity and carcinogenicity are still on the verge of potential human health risks. Since absence of evidence is not the evidence of absence, therefore continuing research is needed for the development of models aimed at extrapolating human health risks and the above elementary study is a small step in this direction.

References

1. IARC (International Agency for Research on Cancer), "Some Industrial Chemicals. IARC Monographs on the Evaluation of Carcinogenic Risk of Chemicals to Humans", Vol. 60, WHO Publications, Lyon, 1994, p. 560.
2. T. Patrick, "Polyacrylamide gel in cosmetic procedures: Experience with Aquamid", Seminars in Cutaneous Medicine and Surgery, 2004, 23, 233-235.
3. L. H. Christensen, V. B. Breiting, A. Aasted, A. Jorgensen, and I. Kebuladze, "Long-term effects of PAM hydrogel on human breast tissue", Plastic and Reconstructive Surgery, 2003, 111, 1883-1890.
4. N. X. Cheng, Y. Wang, J. H. Wang, X. M. Zhang, and H. Zhong, "Complications of breast augmentation with injected hydrophilic polyacrylamide gel", Aesthetic Plastic Surgery, 2002, 26, 375-382.
5. E. A. Smith and F. W. Oehme, " Acrylamide and polyacrylamide: A review of production, use, environmental fate and neurotoxicity ", Reviews on Environmental Health, 1991, 9, 215-228.
6. H. Isacoff, "Polyacrylamide in cosmetics", Cosmetics and Perfumery, 1973, 88, 35-37.
7. M. Friedman, "Chemistry, biochemistry and safety of acrylamide. A review", J. Agric. Food. Chem., 2003, 51, 4504-4526.

8. HSDB, "Acrylamide: Hazardous Substances Data Bank", MEDLARS Online Information Retrieval System, US National Library of Medicine, 2003.
9. N. Brunton, R. Grimly, and B. Murray, "Status Report on Acrylamide in Potato Products," Teagasc, The National Food Center, Dublin, 2005.
10. E. Tareke, P. Rydberg, P. Karlsson, S. Eriksson, and M. Tornqvist, "Analysis of acrylamide, a carcinogen formed in heated foodstuffs", J. Agric. Food Chem., 2002, 50, 4998-5006.
11. Public Health Service (PHS), "The Health Consequences of Smoking: a Report of the Surgeon General", Centers for Disease Control and Prevention, U. S. Department of Health and Human Services, 2004. (http://www.cdc.gov/tobacco/sgr/sgr_2004/index.htm)
12. European Commission (EC), "Risk Assessment of Acrylamide (CAS No. 79-06-01, EINEC No. 201-173-7)", Draft risk assessment report prepared by the UK on behalf of the European Union in the framework of Council Regulation (EEC) 793/93 on the evaluation and control of the risks of existing substances, 2000.
13. E. J. Konings, A. J. Baars, J. D. Van Klaveren, M. C. Spanjer, P. M. Rensen, M. Hiemstra, J. A. Van Kooji, and P. W. J. Peters, "Acrylamide exposure from foods of the Dutch population and an assessment of the consequent risks", Food Chem. Toxicol., 2003, 41, 1569-1579.
14. P. Richmont and R. Borrow, "Acrylamide in food", The Lancet, 2003, 361, 361-362.
15. A. Vattem and K. Shetty, "Acrylamide in food: A model for mechanism of formation and its reduction", Innovative Food Science and Emerging Technologies, 2003, 4, 331-338.
16. J. Giese, "Acrylamide in foods", Food Technology, 2002, 56, 71-72.
17. R. Tyl and K. Crump, "Acrylamide in food", Food Standards Agency, 2002, 5, 215-222.
18. C. Pelucchi, C. Galeone, F. Levi, E. Negri, S. Franceschi, R. Talmini, C. Bosetti, A. Giasoca, and C. La Vecchia, "Dietary acrylamide and human cancer", Int. J. Cancer, 2005, 118, 467-471.
19. J. M. Rice, "The carcinogenicity of acrylamide", Mutat. Res., 2005, 580, 3-20.
20. B. I. Ghanayem, K. L. Witt, L. El- Hadri, U. Hoffler, G. E. Kissling, and M. D. Shelby, "Comparison of germ cell mutagenicity in male CYP2E1- null and wild type mice treated with acrylamide: Evidence supporting a glycidamide-mediated effect", Biol. Reprod., 2005, 72, 157-163.
21. H. Glatt, H. Schneider, and Y. Liu, "V79-h CYP2E1-h SULT1A1, a cell line for the sensitive detection of genotoxic effects induced by carbohydrate pyrolysis products and other food-borne chemicals", Mutat. Res., 2005, 580, 41-52.
22. T. Husoy, L. Abramsson-Zetterberg, H. B. Olstorn, J. E. Paulsen, and J. Alexander, "Adenomatous polyphonic coli influences micronuclei induction by PhiP and acrylamide in mouse erythrocytes", Mutat. Res., 2005, 580, 111-118.
23. Center for the Evaluation of Risks to Human Reproduction (CERHR), Meeting Summary, May 20, 2004, National Toxicology Program, Research Triangle Park, N.C.

24. Center for the Evaluation of Risks to Human Reproduction (CERHR), Draft NTP: CERHR Expert Panel Report on the Reproductive and Developmental Toxicity of Acrylamide, National Toxicology Program, Research Triangle Park, N.C, 2004.
25. B. Paulsson, J. Grawe, and M. Tornqvist, "Hemoglobin adducts and micronucleus frequencies in mouse and rat after acrylamide or N-methylolacrylamide treatment", Mutat Res., 2002, 516, 101- 111.
26. B. Paulsson, N. Kotova, J. Grawe, A. Henderson, F. Granath, and B. Golding, "Induction of micronuclei in mouse and rat by glycidamide, genotoxic metabolite of acrylamide", Mutat. Res., 2003, 535, 15-24.
27. H. Zenick, E. Hope, and M. K. Smith, "Reproductive toxicity associated with acrylamide treatment in male and female rats", J. Toxicol. Environ. Health, 1986, 17, 457-472.
28. R. W. Tyl, M. C. Marr, C. B. Myers, W. P. Ross, and M. A. Friedman, "Relationship between acrylamide reproductive and neurotoxicity in male rats", Reprod. Toxicol., 2000, 14, 147-157.
29. B. G. Gold, J. Voda, X. Yu, and H. Gordon, "The immunosuppressant FK 506 elicits a neuronal heat shock response and protects against acrylamide neuropathy", Exp. Neurol., 2004, 187, 160- 170.
30. P. F. Pradat, P. Kennel, and S. Naimi-Sadaoui, "Continuous delivery of neurotrophin 3 by gene therapy has a nueroprotective effects in experimental models of diabetic and acrylamide neuropathies", Human Gene Therapy, 2001, 12, 2237-2249.
31. Y. Kinoshita, H. Matsumura, H. Igisu, and A. Yokota, "Brain of rats intoxicated with acrylamide: Observation with 4.7 tesla magnetic resonance", Arch Toxicol., 2000, 74, 487-489.
32. K. M. Crofton, S. Padilla, and H. A. Tilson, "The impact of dose rate on the neurotoxicity of acrylamide: The interaction of administered dose, target tissue concentrations, tissue damage, and functional effects", Toxicol. Appl. Pharmacol., 1996, 139, 163-176.
33. M. Bachmann, J. E. Myers, and B. N. Bezuidenhout, "Acrylamide monomer and peripheral neuropathy in chemical workers". Am. J. Ind. Med., 1992, 21, 217-222.
34. www.1whey2health.com/glutathione_antioxidant.htm (January, 2002)
35. www.annieappleseedproject.org/whatsomofblo.html (2003)
36. O. H. Lowry, N. J. Rosebrough, A. L. Farr, and R. J. Randall, "Protein measurement with folin phenol reagent". J. Biochem., 1951, 193, 265-275.
37. M. S. Moron, J. W. Depierre, and B. Mannervik, "Levels of glutathione, glutathione reductase and glutathione-S-transferase activity in rat lungs and liver", Biochem. Biophy. Acta. 1979, 582, 67-78.
38. C. H. Fiske and Y. Subbarow, "The colorimetric determination of phosphorus", J. Biochem. , 1925, 66, 375-400.
39. S. Reitman and S. Frankel, "A colorimetric method for the determination of serum glutamic oxaloacetic and glutamic pyruvic transaminases", Am. J. Clin. Pathol. , 1957, 28, 56.

40. K. L. Dearfield, G. R. Douglas, U. H .Ehling, M. M., Moore, G. A. Sega, and B. J Bruisick, "Acrylamide: A review of its genotoxicity and an assessment of heritable genetic risk", Mutat. Res., 1995, 330, 71-99.
41. H. Druckrey, U. Consbruch, and D. Schmahl, "Effect of monomeric acrylamide on proteins", Z. Naturforsch. B. 1953, 86, 145-150.
42. C. Kirman, M. Gargas, R. Deskin, L. Tonner-Navarro, and M. Andersen, "A physiologically based pharmacokinetic model for acrylamide and its metabolite, glycidamide, in the rat", J. Toxicol. Environ. Health, 2003, 66, 253-274.
43. S. C. Sumner, T. R. Fennell, T. A. Moore, B. Chanas, F. Gonzalez, and B. Ghanayem, "Role of cytochrome P450 2E1 in the metabolism of acrylamide and acrylonitrile in mice", Chem. Res. Toxicol., 1999, 12, 1110-1116.
44. V. Molak, "Acrylamide: A review of the literature", NIOH and NIOSH Basis for an Occupational Health Standard, U.S. Department of Health and Human Services, 1991.
45. K. Hashimoto, V. V. Ivanov, K. Inomata, T. Kawai, K. Mizunuma, L. G. Klimatskaya, and Y. A. Fefelova, "Biological monitoring of exposure to alkylating xenobiotics through their determination in the compounds having hemoglobin, plasma proteins, and urinary mercapteuric acids, by using a new analytical approach. II. Acrylamide", Vopr. Med. Khim., 1995, 41, 22-25.
46. I. Odland, L. Romert, C. Clemedson, and E. Walum, "Glutathione content, glutathione transferase activity and lipid peroxidation in acrylamide-treated neuroblastoma NIE 115 cells", Toxicol. in Vitro, 1994, 8, 263-267.
47. N. J. Chinoy and M. R. Memon, "Beneficial effects of some vitamins and calcium on fluoride and aluminium toxicity of gastrocnemius muscle and liver of male mice", Fluoride, 2001, 34, 21-33.
48. J. M. Dheer, T. R. Dheer, and C. L. Mahajan, "Hematological and haematopoitic response to acid stress in an air breathing fresh water fish Channa punctatus Bloch", J. Fish Bio. 1987, 30, 577-588.

Maejo International Journal of Science and Technology
ISSN 1905-7873
Available online at www.mijst.mju.ac.th

Full Paper

Change in dry matter and nutritive composition of Brachiaria humidicola grown in Ban Thon soil series

Jeerasak Chobtang [1],*, Sakda Prajakboonjetsada [2], Supida Watananawin [2], and Auraiwan Isuwan [3]

[1] Animal Nutrition Division, Department of Livestock Development, Ratchathewi, Bangkok 10400, Thailand
[2] Narathiwat Animal Nutrition Research and Development Centre, Takbai, Narathiwat 96110, Thailand
[3] Faculty of Animal Science and Agricultural Technology, Silpakorn University, Petchaburi Campus, Cha-Am, Petchaburi 76120, Thailand
* Corresponding author, e-mail address: jeerasak_lim@hotmail.com

Received: 7 June 2008 / Accepted: 6 November 2008 / Published: 6 November 2008

Abstract: This experiment was conducted to determine the change in dry matter and nutritive composition of Humidicola grass (Brachiaria humidicola) grown in Ban Thon soil series (infertility soil) as a function of growth age. One rai (0.16 ha) of two-year-old pasture of fertilised Humidicola grass was uniformly cut and the regrowth samples were collected every twenty days. The samples were subjected to analysis for dry matter content and nutritive composition, i.e. crude protein, ash, calcium, phosphorus, neutral detergent fibre, acid detergent fibre, and acid detergent lignin. The results showed that while the yields of available forage and leaves increased curvilinearly (quadratic, $p<0.05$), the stem yield increased linearly ($p<0.05$) over sampling dates. The highest biomass accumulation rate was numerically observed between 40-60 days of regrowth. The concentrations of crude protein, ash, calcium and phosphorus decreased curvilinearly (quadratic, $p<0.05$) with advancing maturity and reached the lowest flat after 60 days of regrowth. The cell wall components, i.e. NDF, ADF and ADL, increased over the experimental period and reached the highest plateau at 40 days of regrowth. It was concluded that Humidicola grass should be grazed or preserved at the regrowth age of not over 60 days to maximise the utilisation of the grass.

Keywords: Brachiaria humidicola, Ban Thon soil series, animal nutrition

Introduction

Humidicola grass (Brachiaria humidicola) is a procumbent stoloniferous perennial with lenceolate leaves. The culm is prostrate in the lower part where it roots from the lower nodes. It is distinguished from other species of the genus by its creeping habit. Although containing low crude protein (CP) (3.75-6.25% CP, DM basis), it has good drought tolerance and remains green better than other species [1,2]. It is the common green forage using as the main roughage source for beef cattle and goat production in Narathiwat province, especially in Ban Thon soil series area that covers an area of at least 54,544 rais (8,727 ha).

Ban Thon soil series is very poor physically, chemically and biologically, containing approximately 0.29% organic matter, 1.0 g kg-1 available phosphorus, and 14.5 g kg-1 exchangeable potassium [3]. Sukkasem et al. [2] reported that when four tons of cattle manure were applied to Humidicola grass and the grass was cut every 50 days, it yielded approximately 2 tons of dry matter per year with a content of 6.82% CP, 32.21% acid detergent fibre (ADF), and 66.68% neutral detergent fibre (NDF). Prajakboonjetsada et al. [4] also reported that Humidicola grass hay (harvested at day 70 of regrowth age) contained 4.4% CP, 67.82% NDF and 38.07% ADF. When this grass was fed to beef cattle supplemented with 1% body weight of feed concentrate, it resulted in 4.38 kg/d of dry matter forage intake and 0.542 kg/d of average daily gain of cattle [4].

Forage quality evaluation during the growth cycle would allow us to pinpoint when to harvest the grass at the desired levels of nutritive composition to meet specific animal requirements [5], especially CP concentration [6]. Maintaining appropriate stage of pasture could be a good option in pasture management for improving animal productivity. Although there have been general reports regarding the effect of fertiliser on the quantity and quality of Humidicola grass, there seems to be no scientific evidence on its profile of DM yield and nutritive composition in accordance to its stage of growth. The objective of this study is thus to try to gather this potentially useful information.

Materials and Methods

Soil characteristics and pasture management

The experiment was carried out, starting from 26 September 2006, at Narathiwat Animal Nutrition Research and Development Centre, Takbai, Narathiwat, Thailand. The soil involved in this study was classified as Ban Thon soil series. It was sandy, siliceous, superactive, ortstein, isohyperthermic, Typic Haplorthods [3]. The chemical properties of the soil have been previously reported by Sukkasem et al. [7]. It was considerably acid (pHwater 1:1 = 5.60), low in organic matter content (2.9 g kg^{-1}) with available phosphorus, exchangeable potassium and total sulphur concentration of 1.0, 14.5 and 12.5 g kg^{-1} respectively.

One rai (0.16 ha) of 2-year-old Humidicola grass was cut using a drum mower instrument for a uniform regrowth. The experimental field was equally divided into 4 plots (approximately 0.25 rai or

0.04 ha per plot) and each plot was separated by a 1.5-m spacing, and fertilised once at the beginning of the experiment with N-P-K fertiliser (15-15-15) and nitrogen fertiliser (46-0-0, urea) at 25 kg/rai and 10 kg/rai respectively. No irrigation was practiced over the experimental period. The precipitation accumulation level throughout the experiment was 462.12 mm.

Sample collection and preparation

Starting from 5 October 2006 as day 1, the green yield of Humidicola grass was sampled on day 20, 40, 60, 80, and 100 with 4 replications each. The grass was sampled by clipping five 0.16-m^2 quadrates per plot at approximately 3-cm stubble height. No area within the plot was clipped more than once so that all clipped forage was an original regrowth (plant plus new tillers). All clipped forage samples were weighed and dried individually in a hot-air oven at approximately 60 ^{O}C for 48 hr. The dry weight for each quadrate sample was used to estimate available forage yield. All of weeds and death materials were separated by hand and removed before forage calculation. Dry leaves and stems were separately weighed and ground through a 1-mm screen in a Wiley mill for chemical analysis.

Chemical analysis

All ground samples were subjected to proximate analysis of dry matter (DM), ash, and crude protein (CP) by the methods of AOAC [8]. The detergent fibre composition, i. e. neutral detergent fibre (NDF), acid detergent fibre (ADF), and acid detergent lignin (ADL), was analysed by the procedures described by Goering and Van Soest [9]. The CP was calculated as percentage of nitrogen in the sample multiplied by a factor of 6.25. Calcium and phosphorus were determined by the methods of AOAC [10].

Statistical analysis

Effects of regrowth age on dry matter yield (available forage yield and leaf blade and stem yield) and nutritive composition of grass were analysed as a randomised complete block design with field blocks (n = 4) as replications and the 5 regrowth ages (day 20, 40, 60, 80 and 100) as treatment. This statistical method was described by Ogden et al. [11] and Ogden et al. [12]. Growth age means were separated by single-degree-of-freedom orthogonal contrasts for linear, quadratic and cubic effects of time using SAS statistical package [13].

Results and Discussion

Agronomic traits

Least square means of available forage yield, and leaf and stem yields of Humidicola grass at twenty-day interval sampling from day 20 through day 100 of regrowth are shown in Table 1. The statistical analysis results reveal that the DM yield of available forage (quadratic, p=0.0391), leaf yield

(quadratic, p=0.0044) and stem yield (linear, p<0.0001) increased with sampling dates. The growth rate of the grass reached the peak after day 80 of regrowth.

The curvilinear response of DM yield of available forage and leaf yield might occur because of the emergence of new tillers throughout the sampling period when there was rain. This result was consistent with the reports of Isuwan et al. [14] and Ogden et al. [11], who showed that dry matter yield and leaf percentage of Pangola grass (Digitaria eriantha) and crabgrass (Digitaria ciliaris) reflect significantly the curvilinear effect of the plant regrowth age caused by the release of new immature tillers late in the sampling period. Differing from both traits above, the stem yield linearly increased over the sampling period. This might be due to the emergence of new immature tillers when the grass approached maturity and possessed leaves with less stems.

Table 1. Least square means of available forage, leaf and stem yields of Humidicola grass (kgDM/rai) harvested at different regrowth ages

Regrowth age (days)	Available forage yield[1]	Leaf yield	Stem yield
20	12.72	9.45	3.01
40	42.83	26.90	15.08
60	142.84	81.43	58.86
80	190.73	107.34	78.15
100	356.31	234.91	116.75
SEM[2]	25.26	14.64	9.99
Contrast		*P-value*	
Linear	<0.0001	<0.0001	<0.0001
Quadratic	0.0391	0.0044	0.4592
Cubic	0.5607	0.1884	0.7014

[1] Almost all of weeds and death materials were removed before available forage calculation.
[2] Standard error of the mean (n = 4)

The dry matter yield of grass in this study was obviously lower than those which were reported by Sukkasem et al. (361.45 kgDM/rai/cut at 50 days of growth age) [2] and Thinnakorn et al. (478.3, 844.5 and 1,122.9 kgDM/rai/cut, at 4, 6 and 8 weeks of growth age respectively) [15]. The difference in DM yields may be due to the difference in soil fertility (organic matter content) [15] and organic fertilisation application [2]. Another report [16] concluded that the DM production of this grass is strongly influenced by soil fertility and the productivity ranges from 1.12-5.44 tons/rai/year.

Nutritive composition

The nutritive composition of Humidicola grass at each stage of regrowth is presented in Table 2. While the DM content linearly increased (linear, p = 0.0135), the concentration of CP decreased (quadratic, p<0.0001) when the grass was reaching maturation and both items reached their plateau or flat after day 60 of regrowth. Unlike the trend of CP concentration, the concentrations of NDF, ADF and ADL increased (quadratic, p<0.0001, p=0.0009 and p = 0.0032 respectively) over the experimental period and reached the plateau at about day 40-60. The Ca and P concentration decreased in a curvilinear fashion (quadratic p < 0.0001 and p = 0.0103 respectively) and remained constant after day 60 through the end of the experiment.

Though the results of this study are not different from those of Sukkasem et al. [2], which reported that when four tons of cattle manure were applied, crude protein and cell wall components (NDF and ADF) were 6.82, 66.68 and 33.21% respectively, these are obviously different from the report of Tinnakorn et al. [15], which indicated that grass planting in high fertility soil (Pak Chong soil series) contained 13.87, 12.75 and 8.10% CP, and 62.05, 60.85 and 69.62% NDF, and 38.07, 35.06 and 42.94 % ADF at day 30, 45 and 60 of regrowth respectively. Minson and Wilson [17] suggested that grass should contain at least 6% CP to sustain the activity of microorganisms in the reticulo-rumen of the animal. This study shows that the grass over 60 days of regrowth does not contain the optimum crude protein concentration.

Table 2. Least square means of nutritive composition of Humidicola grass harvested at different regrowth ages

Regrowth age	DM	CP	Ash	Ca	P	NDF	ADF	ADL
(days)	(%)	(%DM)						
20	18.88	13.53	8.34	0.27	0.60	62.96	33.08	3.17
40	18.30	8.52	7.03	0.20	0.49	72.65	37.54	5.35
60	21.91	6.83	5.77	0.06	0.38	78.84	41.19	5.99
80	21.75	5.68	5.34	0.07	0.36	78.81	42.36	5.46
100	23.22	5.17	5.15	0.09	0.34	79.58	43.32	5.26
SEM[1]	0.91	0.44	0.29	0.015	0.024	1.07	0.58	0.44
Contrast		*P-value*						
Linear	0.0135	<0.0001	<0.0001	<0.0001	<0.0001	<0.0001	<0.0001	0.0083
Quadratic	0.9251	<0.0001	0.0159	<0.0001	0.0103	<0.0001	0.0009	0.0032
Cubic	0.4233	0.0786	0.8468	0.0832	0.9480	0.2297	0.7487	0.2438

[1] Standard error of the mean (n = 4)

Generally, as a plant is maturing, the CP decreases while the cell wall components increase and digestibility and energy content decline. These responses are relatively well known and the obvious means to minimise the effects of maturity is to harvest at optimum maturity [18,19]. The decline in protein concentration with advancing maturity occurs because of the decrease in protein both in the leaves and stems. It is also because the stems, with their lower protein concentration, make up a larger portion of the herbage in more mature forage [20]. Van Soest [21] also reported that the decline in forage quality is associated with the stage of maturity of the grass. Forage intake by the animals may be less than optimum for appropriate growth when they feed on low quality forage which contains fibrous bulk. Moreover, the higher the concentration of cell walls in the forage, the lower it is consumed by the animal, resulting in reduction in growth.

Conclusions

Maturity stage or regrowth age is an important factor affecting DM yield and nutritive composition of Humidicola grass. Harvesting the grass at an appropriate stage of maturity will bring about an increase in both quantity and quality of the forage. The quality of Humidicola grass considerably decline with advancing maturity. The regrowth age of the grass at not over 60 days seems to be appropriate for animal grazing and for maximising the utilisation of Humidicola grass grown in Ban Thon soil series.

Acknowledgements

The authors would like to thank Narathiwat Animal Nutrition Research and Development Centre for all facilities and conveniences provided.

References

1. P. J. Skerman and F. Riveros, “Tropical Grasses”, Food and Agriculture Organization of the United Nations, Rome, 1990.
2. P. Sukkasem, K. Dumkongphet, and P. Buakaew, “Response of farm manure and nitrogen fertilizer application rates on yield and chemical composition of Brachiaria humidicola”, Annual Research Report 2000, Animal Nutrition Division, Department of Livestock Development, Ministry of Agriculture and Cooperative, 2000, pp. 36-50 (in Thai with English abstract).
3. Department of Land Development, “Soil of Thailand”, online URL: http://www.ldd.go.th/thaisoils_museum/INDEX.HTM (accessed on July 22, 2006).
4. S. Prajakboonjetsada, J. Ngerndang, and P. Buakaew. “Use of creeping signal grass (*Brachiaria humidicola*) and Thapra Stylo (*Stylosanthes guianensis* CIAT 184) as roughage for beef cattle”, Annual Research Report 2000, Animal Nutrition Division, Department of Livestock Development, Ministry of Agriculture and Cooperative, 2006, pp.192-203 (in Thai with English abstract).

5. M. E. Valente, G. Borreani, P. G. Peiretti, and E. Tabacco, "Codified morphological stage for predicting digestibility of Italian ryegrass during the spring cycle", *Agron. J.,* 2000, 92, 967-973.
6. T. R. Preston, "Nutritional limitations associated with the feeding of tropical forage" *J. Anim. Sci.,* 1982, 54, 877-884.
7. P. Sukkasem, K. Bhokasawat, and K. Dumkongphet, "The effects of macro and micro elements on yield and nutrient content of *Paspalum atratum* grown in Ban Thon and Tha Sae Soil Series", Annual Research Report 2001, Animal Nutrition Division, Department of Livestock Development, Ministry of Agriculture and Cooperative, 2001, pp. 13-31 (in Thai with English abstract).
8. AOAC, "Official Methods of Analysis", 13th Edn., Association of Official Analytical Chemists, Inc., Washington, D.C., 1980.
9. H. K. Goering and P. J. Van Soest, "Forage fiber analysis (apparatus, procedure and some application)", in "United States Department of Agriculture Handbook, No. 379", United States Department of Agriculture, Washington, D. C., 1970.
10. AOAC, "Official Methods of Analysis", 10th Edn., Association of Official Analytical Chemists, Inc., Washington, D.C., 1965.
11. R. K. Ogden, W. K. Coblentz, K. P. Coffey, J. E. Turner, D. A. Scarbrough, J. A. Jennings, and M. D. Richardson, "Ruminal in situ disappearance kinetics of dry matter and fiber in growing steers for common crabgrass forages sampled on seven dates in northern Arkansas", *J. Anim. Sci.,* 2005, 83, 1142–1152.
12. R. K. Ogden, W. K. Coblentz, K. P. Coffey, J. E. Turner, D. A. Scarbrough, J. A. Jennings, and M. D. Richardson, "Ruminal in situ disappearance kinetics of nitrogen and neutral detergent insoluble nitrogen from common crabgrass forage sampled on seven dates in northern Arkansas", *J. Anim. Sci.,* 2006, 84, 669-677.
13. Statistical Analysis System (SAS), "Users Guide", 4th Edn., Version 6.11, SAS Institute, Inc., Carry, N.C., 1998.
14. A. Isuwan, J. Saelim, and S. Poathong, "Effects of levels of sulfur fertilizer on growth of *Digitaria eriantha grass", Silpakorn U. Sci. Tech. J.,* 2007, 1, 13-19.
15. S. Tinnakorn, P. Singthaisong, and I. Kreethapon. "Effects of cutting height and interval on yield of *Brachiaria humidicola grass*", Annual Research Report 1989, Animal Nutrition Division, Department of Livestock Development, Ministry of Agriculture and Cooperative, 1989, pp. 184-211 (in Thai with English abstract).
16. Anonymous, "Tropical Forage: An interactive selection tool. *Brachiaria humidicola*", online URL: http://www.tropicalforages.info/ (accessed on April 13, 2007).
17. D. J. Minson and J. R. Wilson, "Comparative digestibility of tropical and temperate forage – a contrast between grasses and legumes", *J. Aust. Inst. Agric. Sci.,* 1980, 46, 247-249.

18. P. A. Beck, S. Hutchison, S. A. Gunter, T. C. Losi, C. B. Stewart, P. K. Capps, and J. M. Phillips, "Chemical composition and in situ dry matter and fiber disappearance of sorghum x Sudangrass hybrids", *J. Anim. Sci.,* 2007, 85, 545-555.
19. A. Kamalak, O. Canbolat, Y. Gurbuz, A. Erol, and O. Ozay, "Effect of maturity stage on chemical composition, in vitro and in situ dry matter degradation of tumbleweed hay *(Gundelia tournefortii* L.*)", Small Rumin. Res.,* 2005, 58, 149-156.
20. D. R. Buxton, "Quality related characteristics of forage as influenced by plant environment and agronomic factors", *Anim. Feed Sci. Technol.,* 1996, 59, 37-49.
21. P. J. Van Soest, "The Nutritional Ecology of the Ruminant.", 2nd Edn., Cornell University Press, Ithaca, N.Y., 1994.

Maejo International Journal of Science and Technology

ISSN 1905-7873
Available online at www.mijst.mju.ac.th

Communication

Production of Generation-2 Mekong giant catfish (Pangasinodon gigas) cultured with Spirulina sp.

Kriangsak Meng-umphan* and Jaruwan Saengkrachang

Faculty of Fisheries Technology and Aquatic Resources, Maejo University, Chiangmai 50290, Thailand
*Corresponding author, e-mail: kriang12@yahoo.com

Received: 8 February 2008 / Accepted: 10 November 2008 / Published: 12 November 2008

Abstract: The purpose of this study is to evaluate the treatment of Spirulina-supplemented pellet feed to 5-year-old F1 groups of Mekong giant catfish (Pangasinodon gigas) from the brood stock and intended for use as breeders. The effects on their growth and maturation when cultured in an earthen pond were observed. Results revealed that, compared to control, there was more gain in weight while the feed conversion ratio was lower. The number of red blood cells was also higher while that of white blood cells was lower, compared to control. Out of 18 treated fish (9 males and 9 females), 6 males and 2 females gave sperms and eggs while none from control group did. It was concluded that Spirulina supplemented in pellet feed can improve growth and maturation performance to the brood stock of Mekong giant catfish.

Keywords: Pangasinodon gigas, brood stock, breeding, Spirulina

Introduction

The annual catch of the Mekong giant catfish (Pangasinodon gigas or Pla Buek in Thai) in Mekong River at Chiang Kong district in Chiang Rai province of Thailand registered, during 1986-2007, a maximum of 65 fish in 1990. However, in later years (2000 and 2003-2006) this number declined to 1-2, and zero (in 2001, 2002 and 2007) (Figure 1) [1]. This giant catfish in the Mekong River may thus become extinct in the near future. The Mekong giant catfish plays an important role as a valuable fish for the people along the Mekong River. This fish bred in captivity in several rivers, lakes and ponds need at least 10-15 years to reach maturation [1].

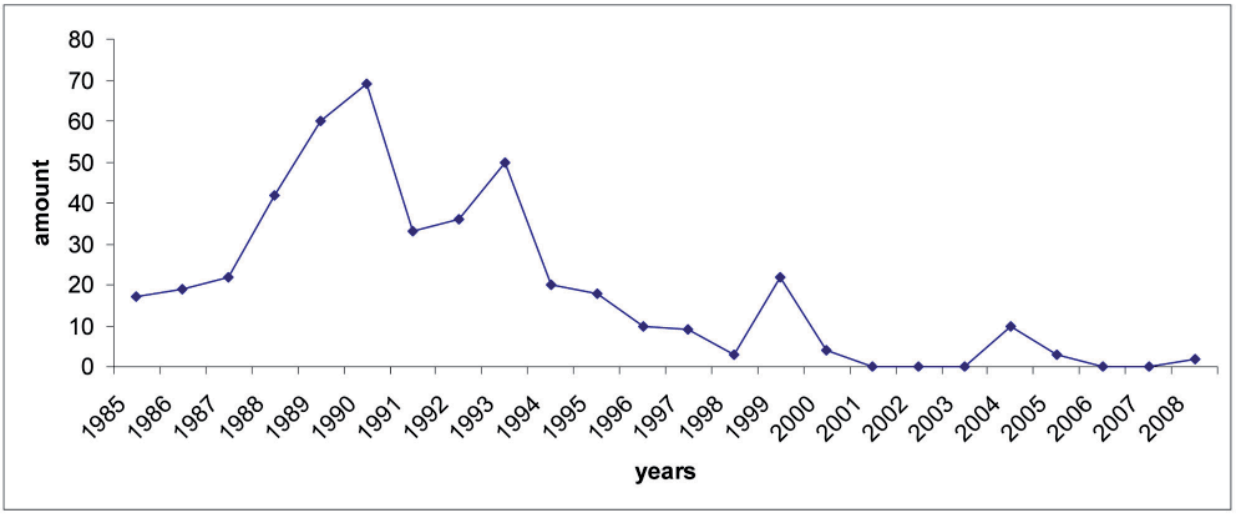

Figure 1. Annual catch of Mekong giant catfish from the Mekong River

Production of quality fry entails the production of good breeders. Since one of the constraints in raising this species is production cost, the feed aspect should be taken into consideration to optimist growth and reproduction with the least possible cost. Of the microalgae and cyanobacteria that have been used as foodstuffs, food supplements and animal feed in many parts of the world, the Spirulina sp. (SP) is the most popular [2]. Among its beneficial properties are its antioxidant [3] and immunostimulant [4] activities and a high protein content. It has been found that raw SP when fed to tilapia produces good flesh quality and gives slightly better sensory evaluations for colour, texture and fattiness [5].

Results of studies utilising SP as sole feed or additive in pellet diet to assess the reproductive performance of different animal species have been variable. The present study is made in order to evaluate the growth performance, blood levels (red and white blood cells), and the number of brood stock of P. gigas prior to breeding. To our knowledge, this study has not been conducted before and its outcome should be beneficial for commercial and conservation purpose.

Materials and Methods

Brood stock and feed preparation

A total of thirty-six 5-year-old P. gigas (Figure 2) with an average weight of 6 kg were randomly treated by one of two treatments with three replications (six fish per replicate) for 8 months (January-August, 2007) in a 55-m2 pen in an earthen pond. In treatment 1 (T1) the fish were fed with ordinary formulated pellets (control), while in treatment 2 (T2) they were fed with pellets which had been incorporated with fresh SP at an amount of 9%. The composition of each formulation of the pellets (Table 1, Figure 3) was analysed by an approximate method.

Data collection

The gain in weight (GW), feed conversion ratio (FCR) and biomass were obtained monthly. Samples of blood were obtained in March for read blood cell (RBC) and white blood cell (WBC) count

using a hemocytometer (Figure 4). In August, the fish brood stocks were checked for sperms and eggs by stripping at the abdomen. The number of mature brood stock was counted in each treatment.

Figure 2. Pangasinodon gigas, 5 years old

Table 1. Components of feed for each treament

Ingredient (% crude protein)	Treatment 1 (control)			Treatment 2 (SP incorporated)		
	Raw material (Kg.)	Protein (%)	Energy (KJ/g)	Raw material (Kg)	Protein (%)	Energy (KJ/g)
Fishmeal (61%)	16	9.7	274.42	7	4.27	120.06
Spirurina (58%)	0	0	0	9	5.22	169.62
Soybean (44%)	40	17.6	604.54	40	17.6	604.54
Rice brand (8%)	21	1.68	322.25	21	1.68	322.25
Broken rice (6%)	21	1.26	271.53	21	1.26	271.53
Oil (0%)	2	0	16.94	2	0	16.94
Total	100	30.3	1,489.68	100	30.03	1,504.94

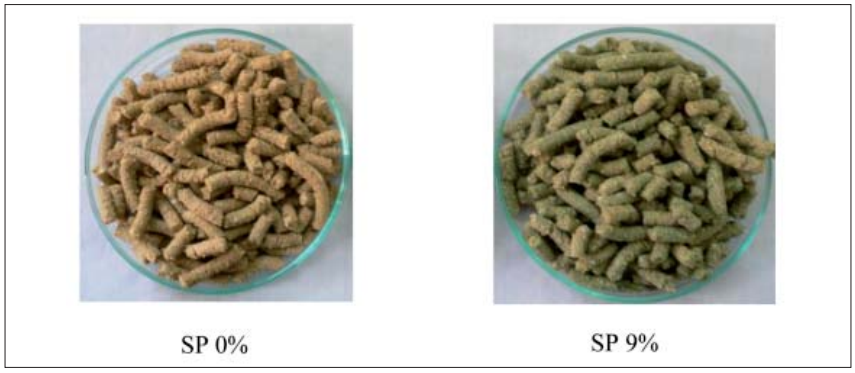

Figure 3. Fish pellets with and without 9% SP

Figure 4. Blood sampling

Statistical analysis

The GW, FCR, RBC and WBC with standard errors were presented in tables and graphs. The variation of treatment was analysed by analysis of variance (ANOVA, $P<0.05$). Significant differences between treatments were analysed using Duncan's Multiple Range Test (DMRT) by SPSS software.

Results and Discussion

GW and FCR

As shown in Table 2 and Figures 5-6, T2 (with 9% SP) gave GW of 872 ± 34 grams/fish whereas the valud for T1 (control) was 711 ± 107 grams/fish. Thus, T2 attained about 20% increase in GW as compared with the control. However, statistical analysis revealed no significant difference. In Figure 5, the FCR was 1.64 ± 0.23 for T1 and 1.33 ± 0.07 for T2, which was lower than that for T1, but statistically no significant difference was observed. In a study by Promkhun-thong and Unchalee [6], they observed an increase in weight, specific growth rate, FCR and antibody level in Clarias sp. supplemented with 10% SP in the feed. Kithja [7] also observed an increasing tendency in weight, specific growth rate and FCR when Pangasius bocourti was supplemented with SP, although no significant differences were observed. Pariwannta [8] reported a FCR level of 2.27 to 2.59 for P. bocourti fed with SP and stocked at different densities.

Table 2. Statistics of the average weight gain, feed conversion ratio, and red and white blood cells from each treatment

Item	Treatment 1 (no SP)	Treatment 2 (9% SP)
Gain in weight (gram)	711 ± 107^a	872 ± 34^a
Feed conversion ratio	1.65 ± 0.13^a	1.34 ± 0.04^a
Red blood cells (cells/mm^3)	$920{,}833 \pm 518{,}461^a$	$995{,}833 \pm 115{,}470^a$
White blood cells (cells/mm^3)	$2{,}167 \pm 381^a$	$1{,}583 \pm 803^a$

Note: Figures that have the same superscript letter are not statistically different ($P>0.05$.) among treatment means.

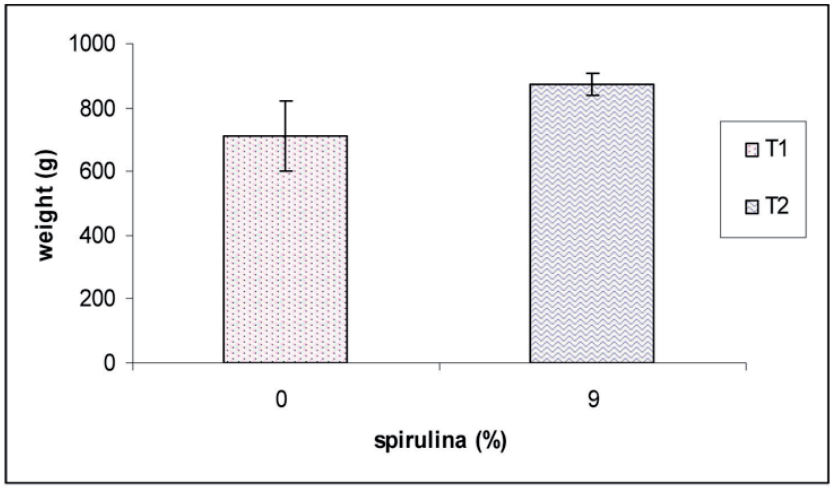

Figure 5. Weight gain/fish from each treatment

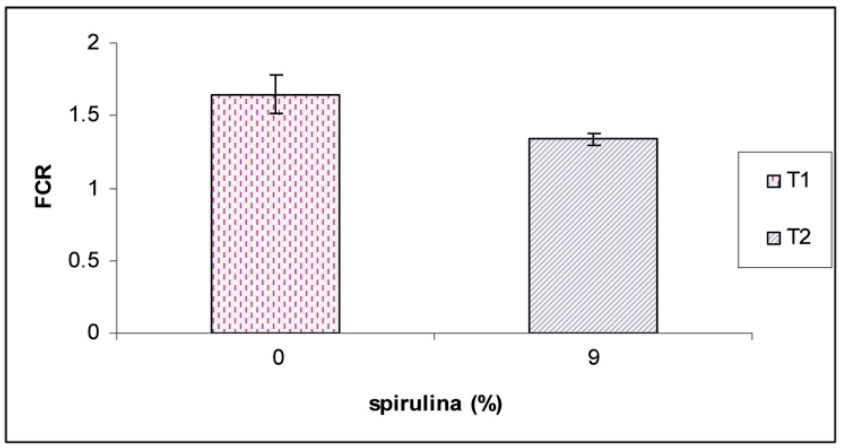

Figure 6. Feed conversion ratio from each treatment

RBC and WBC

As shown in Table 2 and Figures 7-9, although no significant differences were observed between the 2 treatments in terms of RBC and WBC, the higher RBC count was found in T2 (995,833 ± 115,470 cell/mm^3) while T1 (control) registered a lower count (920,833 ± 518,461 cell/mm^3). The WBC, on the other hand, was higher in T1 (2,166 ± 381 cells/mm^3) than T2 (1,583 ± 803 cells/ mm^3). Kithja [7] observed that the supplementation of SP in the feed for *P. bocourti* resulted in an increase of red and white blood cell count. *Spirulina* has a dark blue-green colour because it is rich in a brilliant blue polypeptide called phycocyanin. Studies have shown that phycocyanin affects the stem cells found in the bone marrow. Stem cells are the "grandmother" of both the white blood cells that make up the cellular immune system and the red blood cells that oxygenate the body [7].

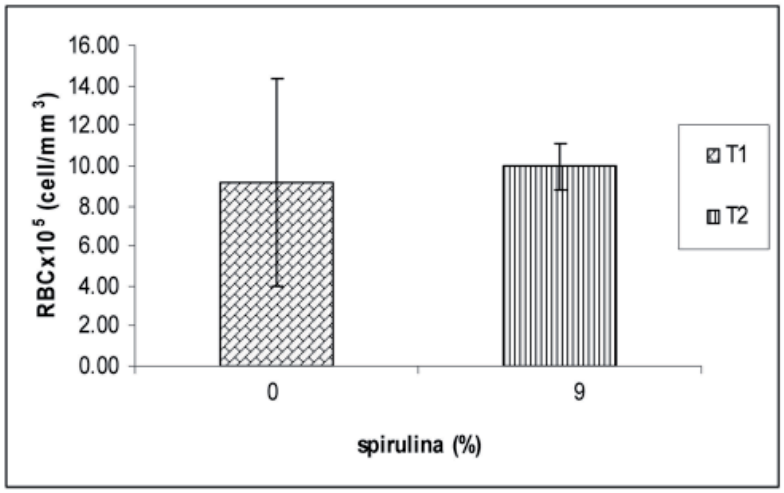

Figure 7. RBC count from each treatment

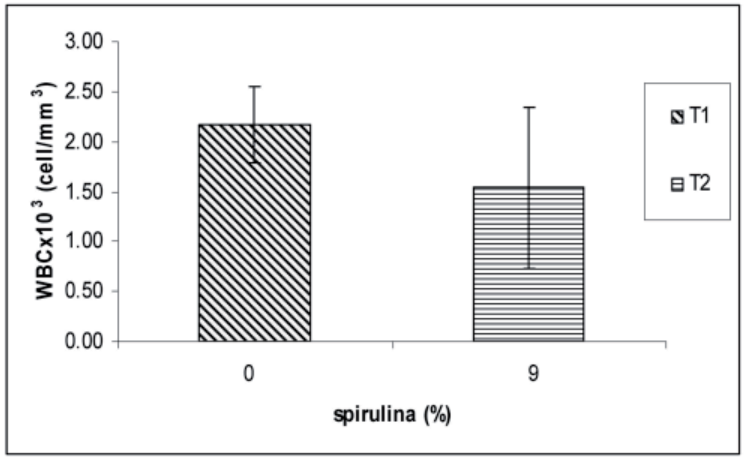

Figure 8. WBC count from each treatment

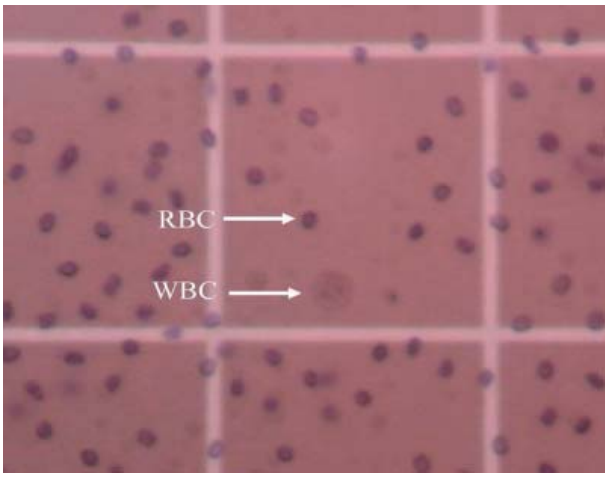

Figure 9. RBC and WBC

Maturation (collection of sperms and eggs)

As shown in Table 3 and Figures10-12, 2 females with eggs and 6 males with sperms were obtained from treatment 2, while none was obtained in treatment 1. The 300 fingerlings (F2) from treatment 2 were also obtained by artificial fertilisation. Pariwannta [8] also observed an increase in the sex hormone level (estradiol) when the feed for *P. bocourti* contained 3% SP. Fecundity in gilthead sea bream (*Sparus aurata*) was found to significantly increase with an increase in dietary level of n-3 HUFA (polyunsaturated fatty acids with 20 or more carbon atoms) up to 1.6% [9]. Other nutrients which have been shown to affect fecundity include vitamin E and ascorbic acid [10].

Table 3. Number of male and female brood stock with sperms and eggs from each treatment (recorded in August 2007)

Treatment	Total number	Number of males	Number of females	Number with sperms	Number with eggs
T1 (control)	18	7	11	-	-
T2 (9% SP)	18	9	9	6	2

Figure 10. Collection of sperms

Figure 11. Collection of eggs

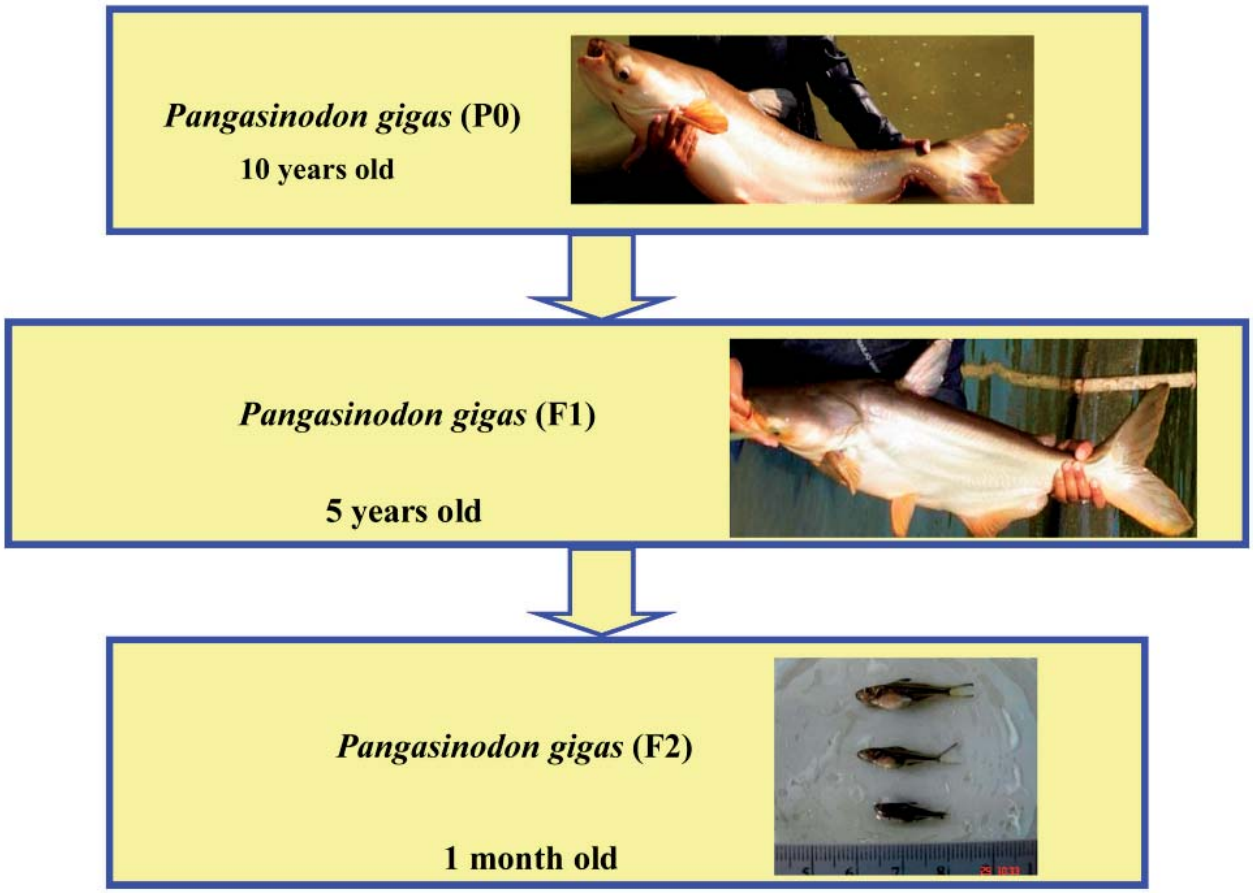

Figure 12. The brood stock of Makong giant catfish from parent (P0) to generation 2 (F2) in earthen pond

Conclusions

Feeding *P. gigas* resulted in a higher GW, RBC and number of mature brood stock. This further suggests that supplementing SP in the feed for this species of fish can have a significant benefit in their reproduction. Our further study will focuss in quantifying both the estradiol and testosterone levels in separate males and females. The quantity and quality of the milt and oocytes will also be taken into consideration.

Acknowledgements

The authors gratefully thank Thailand National Research Council and The Pla Buek Integration Project for all the funding of this research. We also would like to thank Assoc. Prof. Dr. Duang Buddhasukh and Assist. Prof. Chanakun Chitmanat for correcting the manuscript. The Faculty of Fisheries Technology and Aquatic Resources has kindly provided facilities for this research.

References

1. K. Meng-umphan, J. Manosroi, and A. Manosoi, "Successful artificial breeding of the Mekong giant catfish (*Pangasianodon gigas Chevey*) reared in earthen ponds by boosting with gonadotropin releasing hormone analogue (GnRHa)", *Asian Fish. Sci.,* 2006, 19, 149-155.
2. P. R. Anupama, "Value-added food: single cell protein", *Biotechnol. Adv*., 2000, 18, 459-479.
3. M. A. Qureshi, "Immunomodulatory effects of spirulina supplementation in chicken", Proceedings of 44th Western Poultry Disease Conference, North Carolina State University, Raleigh, NC, 1995.
4. H. Watanuki, K. Ota, A. C. Malina, A. R. Tassakka, T. Kato, and M. Sakai, "Immunostimulant effects of dietary *Spirulina platensis* on carp, *Cyprinus carpio*", Aquaculture, 2006, 258, 157-163.
5. T. L. Takeuchi and H. Ogawa, "Flesh quality of tilapia *Oreochromis niloticus* fed solely on raw Spirulina", *Fish. Sci.,* 2003, 72, 529-534.
6. W. Promkhun-thong and P. Unchalee, "Effect of *Spirulina* spp. on growth and antibody level on *Clarias spp" Songklanakarin J. Sci. Technol.,* 1988, 10, 195-203.
7. R. Kithja, "Growth of *Pangasius bocourti* Sauvage fed with different level of *Spirulina* sp. in pellet feed", Special Science Problem, 2005, Faculty of Fisheries Technology and Aquatic Resources, Maejo University, Thailand
8. N. Pariwannta, "Growth, sex hormone profile, red and white blood cells of *Pangasius bocourti* Sauvage (2 years old) Nakornphanom strain fed with different level of *Spirulina* sp. in pellet feed", Special Science Problem, 2006, Faculty of Fisheries Technology and Aquatic Resources, Maejo University, Thailand.
9. P. H. Fernandez, M. Izqierdo, L. Robaina, A. Valencia, M. Salhi, and D. Montero, "The effect of dietary protein and lipid from squid and fish meals on egg quality of brood stock for gilthead seabream (*Sparus aurata*)", *Aquaculture,* 1997,148, 233-246.
10. J. H. Blom and K. Dabrowski, "Reproductive success of female rainbow trout (*Oncorhynchus mykiss*) in response to graded dietary ascorbyl monophosphate levels". *Biol. Reproductive, 1995*, 52, 1073-1080.

Maejo International Journal of Science and Technology

ISSN 1905-7873

Available online at www.mijst.mju.ac.th

Full Paper

Nutritive composition of soybean by-products and nutrient digestibility of soybean pod husk

Sompong Sruamsiri* and Pirote Silman

Faculty of Animal Science and Technology, Maejo University, Sansai, Chiang Mai, 50290, Thailand

* Corresponding author, e-mail: sompong@mju.ac.th

Received: 19 June 2008 / Accepted: 19 November 2008 / Published: 24 November 2008

Abstract: Soybean by-products (soybean germ, soybean milk residue, soybean hull, soybean pod husk and soybean stem) were subjected to proximate analysis, and in vitro digestibility of DM (IVDMD), ADF (IVADFD) and NDF (IVNDFD) were determined after digesting the by-products in buffered rumen fluid for 24 or 48 h in 2 ANKOM^{II} Daisy Incubators using Completely Randomised Design. Four native cattle (body weight 210 ± 13.5 kg) were used to determine nutrient digestibility of soybean pod husk. They were randomly assigned by Cross-over Design to receive two roughage sources, i.e. guinea grass and guinea grass + soybean pod husk (60:40 DM basis), in two experimental periods. Guinea grass was harvested on the 35th day after the first cut of the year and used as green forage. Total collection method was used to determine the digestibility coefficients and digestibility by difference was used to calculate nutrient digestibility of soybean pod husk.

The nutritive composition showed that soybean germ was highest in CP content (42.27% of DM) and EE content (5.07% of DM) but lowest in NDF and ADF content (20.09 and 21.53% of DM respectively). The average CP content of soybean straw, soybean stem and soybean pod husk was low (4.91, 4.67 and 5.04% respectively), while ADF content was high (42.76, 38.01 and 42.08% respectively). In vitro digestibility of DM (IVDMD), ADF (IVADFD) and NDF (IVNDFD) showed that all of them, except soybean stem, can be used as cattle feed, e.g. as supplemented feed or admixture in concentrate feed. Digestibility coefficients of guinea grass were higher in CP, CF and EE when compared to the other groups. The apparent digestibility of CP and CF were highly different ($P<0.01$) and that of EE was significantly different ($P<0.05$). No significant difference was found in digestibility of DM, OM and ADF ($P>0.05$). The digestibility of nutrients (DM, OM, CP, CF, NFE, NDF and ADF) of soybean pod husk were 53.81 ± 4.3, 59.69 ± 4.6, 42.38 ± 3.8, 30.71 ± 3.2, 50.74 ± 4.3, 75.26 ± 4.0, 45.78 ± 3.7 and 30.53 ± 4.2 % respectively. Soybean pod husk was higher in total digestible nutrients (TDN) (51.87 ± 3.3 vs.48.75 ± 3.1 %DM) and digestible energy (DE) (2.11 ± 0.3 vs. 2.08 ± 0.2 Mcal/kg.DM) than guinea grass.

Keywords: apparent digestibility, energy value, soybean by-products, soybean hull, soybean straw, soybean pod husk, soybean germ, soybean milk residue, soybean stem

Introduction

Soybean is one of the major cash crops in Chiang Mai. The products from soybean were usually used as human food and the by-products as animal feed. The harvesting season occurs between March and May, exactly the same time when green forage is short. In the field, soybean straw and soybean pod husk are usually left behind as waste when the seeds have been mechanically or manually harvested and trashed. Soybean straw is a major by-product which is composed of stem, leaf and pod husk. The nutritive value of soybean straw is higher than rice straw but lower than pod husk [4,6]. Therefore, in the dry season it can be well used as alternative or supplemented roughage for cattle both as dry and treated feed even though the crude protein is lower than general roughage. For untreated soybean straw, the palatability is low because of its relative hard stem. Soybean hull, soybean germ (embryo) and soybean milk residue are by-products from soybean industry which farmers also use for cattle feed, practically as supplemented feed or admixture in feed concentrate. However, only a few studies reported on the nutritive composition and the digestibility of nutrients of these by-products in native beef cattle. Therefore, this experiment is aimed to provide a database on the nutritive composition of soybean by-products, and also on the nutrient digestibility of soybean pod husk.

Materials and Methods

Nutritive composition

Soybean hull, soybean germ and soybean milk residue, which are by-products from soybean industry in Chiang Mai province, were collected and sampled for analysis. To obtain a sufficient and uniform sample, each by-product was repeatedly sampled from several bags and mixed thoroughly before randomly taken for analysis. Soybean straw was collected from ten areas in San Sai district, Chiang Mai. Stem and pod husk were separated and samples were mixed throughly prior to analysis of dry matter (DM), crude protein (CP), crude fiber (CF), ether extract (EE), nitrogen free extract (NFE), calcium (Ca), phosphorus (P), and gross energy (GE) according to the methods described in AOAC [1]. The analysis of neutral detergent fibre (NDF) and acid detergent fibre (ADF) was carried out according to Detergent method [17].

Digestibility study

In vitro digestibility

Dried and ground (1mm) samples of soybean by-products (soybean stem, soybean pod husk, soybean hull, soybean germ (embryo) and soybean milk residue)(Figure 1) were analysed for DM, NDF and ADF. In vitro digestibility of DM (IVDMD), NDF (IVNDFD), and ADF (IVADFD) wer determined after incubating the samples in buffered rumen fluid for 24 h and 48 h using ANCOM^{II} Daisy Incubators (ANKOM Technology, Macedon, NY). The buffer was prepared according to the ANKOM Technology procedure. Rumen fluid was obtained before feeding from 2 fistulated native beef cattle fed with guinea grass + soybean pod husk at 60:40 DM basis (1.5-1.9%BW). The experimental design was a completely randomized design.

Apparent digestibility

Four native beef cattle at three years of age with an average body weight of 210 ± 13.5 kg were randomly allocated to one of the two dietary treatments in 2 experimental periods according to Cross-over Design. The treatments were (1) guinea grass and (2) guinea grass + soybean pod husk at 60:40 DM basis. The roughage was fed to the animal as single feed twice daily at 1.5- 1.9 % of the body weight (DM basis). Water and mineral blocks were freely available throughout the experimental periods. The experiment was conducted at Maejo University during July to September 2007. Soybean pod husks used in this experiment were collected from ten areas in San Sai district, Chiang Mai, and mixed thoroughly prior to use as experimental diet. Guinea grass (*Panicum maximum*) was harvested from the university farm on the 35th day after the first cut of the year. The grass was prepared by chopping to pieces of 2 - 4 cm. long before feeding. Total collection method was assigned for the determination of apparent total tract digestibility of nutrients.

Each digestibility period lasted 21 days with preliminary period taking place in the first 14 days and collection period being in the last 7 days. Feed intake was recorded daily throughout the entire experiment. Roughage DM intake was calculated on DM basis. Feces and leftover feed were collected and used for the calculation of nutrient digestibility. Digestibility by difference was used to calculate nutrient digestibility of soybean pod husk. Total digestible nutrients (TDN) were calculated using the equation: TDN = digestible CP + digestible CF + digestible NFE + digestible EE × 2.25 [10]. Gross energy of feed and feces were determined using adiabatic bomb calorimetre (IKA calorimetre system C 5000). Digestible energy was then calculated. The data were analysed according to Completely Randomised Design and Cross-over Design [13]. The significant differences between the treatments were analysed based on Duncan' new multiple range test [12].

Results and Discussion

Nutritive composition of soybean by-products

The dry matter content of soybean milk residue was lowest among the soybean by-products. This might be due to the cooking method of the seeds during soybean milk processing. The low average CP content and high NDF and ADF content (Table 1) showed that soybean straw, soybean stem and soybean pod husk are not good roughage sources and should not be used as the main roughage for ruminants. However, their nutritive values are higher than rice straw, which are usually used as roughage in the dry season. To improve the nutritive value of soybean straw and soybean pod husk, chemical treatment with urea (fertiliser grade) or spraying with urea molass solution are also suggested [14,15].

Among all by-products, soybean germ was highest in CP content (42.27% of DM) and EE content (5.07% of DM) but lowest in NDF and ADF content (20.09 and 21.53% of DM respectively). Apparently this is because it is the reserve food for germ growth. As for the nutritive composition of soybean hull in this experiment, especially CP content (12.65%), this was comparable to that reported (11.42%) by Gerngang [3]. In practice, the farmers also use soybean germ and soybean hull as supplemented feed or admixture in feed concentrate even though soybean hull are light, flaky and bulky. Soybean milk residue was relatively high in CP and EE content but low in NDF and ADF content when compared with soybean hull (27.88 vs. 12.65%, 4.98 vs. 2.82%, 30.80 vs. 43.79%, and 23.11 vs. 33.66% respectively). Farmers also use soybean milk residue, the soybean seed by-product which is left after the filtration of soybean milk, as supplemented feed for cattle because it contains relatively high content of protein and energy.

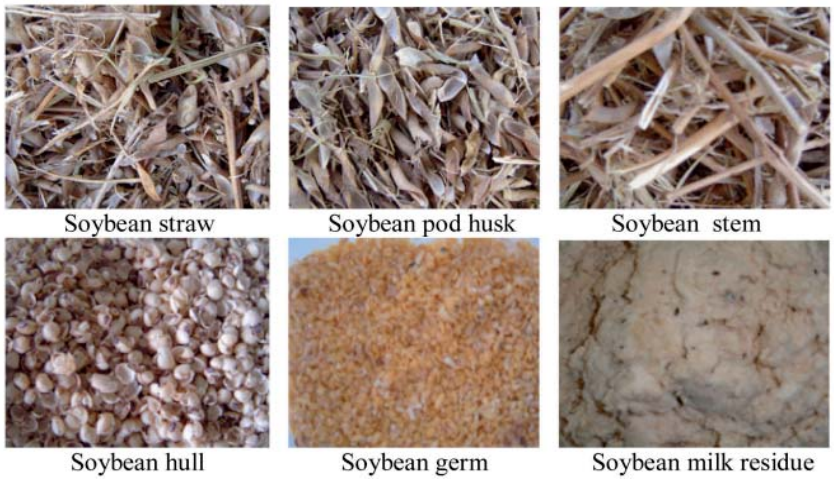

Figure 1. By-products from soybean field and soybean industry

Table 1. Chemical composition of soybean by-products used in the experiment

Item	DM (%)	% of DM						GE (kcal/g.DM)
		CP	EE	NDF	ADF	Ca	P	
Soybean straw	89.76	4.91	1.21	54.24	42.76	1.21	0.07	3.90
Soybean stem	93.59	4.67	1.84	56.41	38.01	0.81	0.08	3.86
Soybean pod husk	91.11	5.04	1.65	60.15	42.08	1.21	0.06	3.98
Soybean hull	92.37	12.65	2.82	43.79	48.66	0.55	0.18	4.22
Soybean milk residue	59.96	27.88	4.98	30.80	23.11	0.53	0.37	4.88
Soybean germ	92.19	42.27	5.07	20.09	21.53	0.22	0.70	5.14

In vitro digestibility of soybean by-products

Among the soybean by-products, soybean germ was highest in IVDMD and IVADFD values ($P>0.01$) at 24 and 48 h, and soybean hull was highest in IVNDFD value ($P>0.05$) (Tables 2-3). Unlike the other soybean by-products, soybean stem was lowest in IVDMD value ($P>0.01$) at 24 and 48 h. The increase in IVDMD value at 24 and 48 h in soybean by-products, except soybean stem, suggests that these by-products could be used as feed for ruminants. The in vitro digestibility of nutrients (DM, ADF and NDF) increased with incubation time. The in vitro digestibility of ADF (IVADFD) and NDF (IVNDFD) followed the same pattern as that of DM digestibility. The IVADFD values of the by-products were highly different ($P<0.01$) while IVNDFD values were

significantly different (P<0.05) as influenced by the nutritive composition. Fibre digestibility values (IVADFD and IVNDFD) of soybean stem were not found in this in vitro digestibility experiment. Thus, soybean stem is not recommended for ruminant feeding.

Table 2. In vitro DM and fibre digestibility (%) of soybean by-products at 24 h

Item	IVDMD**	IVADFD**	IVNDFD*
Soybean germ	46.83^{A}	27.79^{A}	9.74^{B}
Soybean milk residue	24.77^{B}	8.13^{B}	6.62^{BC}
Soybean hull	26.11^{B}	9.04^{B}	13.16^{A}
Soybean pod husk	27.03^{B}	0.50^{C}	6.75^{BC}
Soybean stem	4.76^{C}	-	-

* Means with different superscripts differ significantly (P<0.05).
** Means with different superscripts differ highly (P<0.01).

Table 3. In vitro DM and fibre digestibility (%) of soybean by-products at 48 h

Item	IVDMD**	IVADFD**	IVNDFD*
Soybean germ	68.95^{A}	58.01^{A}	58.59^{A}
Soybean milk residue	57.03^{B}	38.07^{B}	29.75^{C}
Soybean hull	52.89^{B}	31.71^{B}	38.85^{B}
Soybean pod husk	45.07^{C}	18.79^{C}	28.71^{C}
Soybean stem	6.14^{D}	-	-

* Means with different superscripts differ significantly (P<0.05).
** Means with different superscripts differ highly (P<0.01).

Apparent digestibility of nutrients

The data from the nutritive composition (Table 4) show that guinea grass cut on the 35th day (after the first cut of the year) had a higher nutritive value than soybean pod husk, especially CP, EE, NDF and ADF (10.12 vs. 5.11%, 2.98 vs. 1.79%, 68.82 vs. 58.64%, and 49.64 vs. 41.09% respectively). The crude protein content of soybean pod husk in this experiment was similar to that reported by Cheva-Isarakul et al. [2] and Sruamsiri et al. [16], but was lower than the value reported by Sanitwong et al. [11]. The difference might be attributed to variation in cultivar, cultivation area, water supply and management during their growth, as well as the amount of contained stem or branch particles.

Table 4. Nutritive composition of guinea grass and soybean pod husk

Item	DM	% of DM						GE
	(%)	CP	CF	EE	NFE	NDF	ADF	(kcal/g.DM)
Guinea grass	22.33	10.12	32.68	2.98	42.70	68.82	49.64	3.94
Soybean pod husk	89.96	5.11	35.07	1.79	50.62	58.64	41.09	3.99

It was observed that cattle fed with guinea grass + soybean pod husk consumed slightly lower dry matter than the guinea grass-fed group (3.72 vs. 4.15 kg/h/d which is equal to 1.76 vs. 1.89%BW respectively). This might be due to physical characteristic of soybean pod husk which is

bulky and provides less nutrients, especially nitrogen for microbial growth and activities in the rumen. The negative effect of the group fed with guinea grass + soybean pod husk was thus due to the nutritive value of the pod husk, which was low in CP but high in CF content. The result from this experiment agrees with that of Oldham [9], who found that increasing CP content of the diet tended to increase dry matter intake.

Table 5 shows that the digestibility values of CP, CF and EE in cattle fed with guinea grass were higher than those of guinea grass + soybean pod husk group. The apparent digestibility values of CP and CF were highly different ($P<0.01$) while the digestibility value of EE was significantly different ($P<0.05$). The result agrees with that of Hoover [5], who reported that fibre digestibility of the diet decreased with increasing fibre intake, and that of Van Soest [18], who found that nutrient digestibility decreased with increased fibre intake. Guinea grass was lower in digestibility of DM, OM, NFE, NDF and ADF than guinea + soybean pod husk. The apparent digestibility of NFE and NDF were highly different ($P<0.01$). No significant difference was found on the apparent digestibility of DM, OM and ADF ($P>0.05$). The positive effect of digestibility of DM, OM, NFE, NDF and ADF in the group fed with guinea + soybean pod husk was due to the pod husk being lower in cell wall and lignin content (ADF) than guinea grass. Lignin is an undigestible cell wall component in plant and feedstuff, thus tending to limit nutrient digestibility especially of carbohydrate components [7,8].

Table 5. Apparent digestibility of guinea grass and guinea grass + soybean pod husk (60:40)

	Apparent digestibility (%)	
Nutrient	Guinea grass	Guinea grass + Soybean pod husk (60:40)
DM	52.21 ± 4.8	53.28 ± 5.1
OM	51.83 ± 4.2	53.29 ± 4.8
CP**	62.99^{A} ± 2.4	57.19^{B} ± 2.2
CF**	40.88^{A} ± 4.2	33.26^{B} ± 4.8
EE*	68.22^{A} ± 3.2	55.32^{B} ± 2.4
NFE**	46.55^{B} ± 4.2	65.48^{A} ± 3.3
NDF**	41.42^{B} ± 4.4	48.43^{A} ± 4.1
ADF	38.16 ± 3.8	39.53 ± 4.6

* Means with different superscripts differ significantly ($P<0.05$).
** Means with different superscripts differ highly ($P<0.01$).

The results of nutrient digestibility of soybean pod husk calculated by different methods showed that it was high in digestibility of DM, OM, NFE and NDF, but low in that of CP, CF and ADF (Table 6). Calculated TDN from the equation showed that soybean pod husk was higher in the average value of TDN than guinea grass (51.87 ± 3.3 vs. 48.75 ± 3.1%). The digestible energy (DE) content of soybean pod husk in native cattle was 2.11 ± 0.42 Mcal/kg DM (Table 7).

Table 6. Apparent digestibility of nutrients in soybean pod husk

Nutrient	Apparent digestibility, %
DM	53.81 ± 4.3
OM	59.69 ± 4.6
CP	42.38 ± 3.8
CF	30.71 ± 3.2
EE	50.74 ± 4.3
NFE	75.26 ± 4.0
NDF	45.78 ± 3.7
ADF	30.53 ± 4.2

Table 7. Total digestible nutrients (TDN) and digestible energy (DE) of guinea grass and soybean pod husk

Item	TDN (% of DM)	DE (Mcal / kg DM)
Guinea grass	48.75 ± 3.1	2.08 ± 0.3
Soybean pod husk	51.87 ± 3.3	2.11 ± 0.4

Conclusions

The nutritive composition analysis of soybean by-products showed that those from the field, i.e. soybean straw, soybean pod husk and soybean stem, were low in CP and high in CF and ADF content, while by-products from soybean industry, i.e. soybean germ, soybean milk residue and soybean hull, were high in CP but low in NDF and ADF. In vitro digestibility of DM (IVDMD), ADF (IVADFD) and NDF (IVNDFD) showed that all of them, except soybean stem, can be used as cattle feed in the form of supplemented feed or admixture in feed concentrate (soybean hull, soybean germ and soybean milk residue), or supplemented roughage (soybean pod husk and soybean straw).

The digestibility coefficients of DM, OM, CP, CF, NFE, NDF, and ADF of guinea grass were 52.21 ± 4.8, 51.83 ± 4.2, 62.99 ± 2.4, 40.88 ± 4.2, 68.22 ± 3.2, 46.55 ± 4.2, 41.42 ± 4.4, and 38.16 ± 3.8% respectively. Calculation by different methods showed that guinea grass was high in digestibility of CP and EE but low in NDF and ADF. The digestibility coefficients of DM, OM, CP, CF, NFE, NDF, and ADF of soybean pod husk were 53.81 ± 4.3, 59.69 ± 4.6, 42.38 ± 3.8, 30.71 ± 3.2, 50.74 ± 4.3, 75.26 ± 4.0, 45.78 ± 3.7, and 30.53 ± 4.2% respectively. Soybean pod husk was high TDN and DE content when compared to guinea grass (51.87 ± 3.3 vs. 48.75 ± 3.1% and 2.11 ± 0.4 vs. 2.08 ± 0.3 Mcal/kg DM respectively).

Acknowledgement

This study was supported by a grant from "Establishment of Feeding Standard of Beef Cattle and Feedstuff Database for Indochinese peninsula research fund" of Japan International Research Centre for Agricultural Sciences.

References

1. AOAC, "Official Methods of Analysis", 16th Ed., Association of Official Analysis Chemists, Gaithergurg, 1998.
2. B. Cheva-Isarakul, I. Poupaisarn, B. Cheva-Isarakul, and S. Promma, "Digesbility and calculated net energy of soybean pod husk in cows and sheep", Proceedings of the Symposium in Animal Science Conference", Chiang Mai University, Chiang Mai, 1999, pp.141-150.
3. S. Gerngang, "Use of soybean hulls as dairy feed", *Master Thesis,* 2003, Chiang Mai University, Thailand.
4. B. S. Gupta, D. E. Johnson, F. C. Hinds, and M. C. Minor, "Forage potential of soybean straw", Agronomy J., 1973, 65, 538-541.
5. W. H. Hoover, "Chemical factors involved in ruminal fiber digestion", J. Dairy. Sci. 1986, 69, 2755-2766.
6. D. L. Krieder, P. Chaisatanayute, L. Shields, and D. T. Stallcup, "Proximate analysis and digestibility of soybean refuse", *J. Anim. Sci.,* 1979, 49 (supplement), 75(abstract).
7. T. Klopfenstein and F. G. Owen. "Value and potential use of crop residues and by-products in dairy rations", *J. Dairy. Sci.,* 1981, 64, 1250-1268.
8. P. McDonald, R. A. Edwards, J. F. D. Greenhalgh, and C. A. Morgan , "Animal Nutrition", 6th Ed., Longman Scientific and Technical, New York, 2002.
9. J. D. Oldham, "Protein-energy interrelationships in dairy cows", *J. Dairy. Sci.,* 1984, 67, 1090- 1097.
10. W. G. Pond, D. C. Church, and K. R. Pond, "Basic Animal Nutrition and Feeding", 4th Ed., John Wiley & Sons, New York, 1995.
11. C. Sanitwong, O. Naksakul, and S. Intalit, "Utilization of soybean pod husk as feed supplement for milking cow in dry season", Proceedings of the Symposium in Animal Science Conference, Chiang Mai University, Chiang Mai, 1997, pp.241-250.
12. SAS, "Statistical Analysis System User Guide", 4th Ed., Version 6, SAS Institute Ins., Carry, N.C., 1994.
13. R. G. D. Steel and J. H. Torrie, "Principles and Procedures of Statistics", 2nd Ed., McGraw-Hill, New York, 1980.
14. A. Siri, P. Niumsup, P. Seetakoses, and S. Sruamsiri, "Study on the ration of soybean straw in urea treatment on performance of cattle", *J. Agric. Res. Extension,* 1994, 11, 68-75.
15. S. Sruamsiri, P. Seetakoses, P. Niumsup, and A. Siri, "The use of soybean straw as roughage source for dairy replacement heifer", *J. Agric.,* 1994, 10, 148-157.

16. S. Sruamsiri, "The use of soybean pod husk as supplemented roughage in calf's ration", "Proceedings of the Symposium in Animal Science Conference", Chiang Mai University, Chiang Mai, 1999, pp.163-174.
17. P. J. Van Soest, J. B. Robertson, and B. A. Lewis, "Methods of dietary fiber, neutral detergent fiber and nonstarch polysaccharides in relation to animal nutrition", *J. Dairy. Sci.,* 1991, 74, 3583-3597.
18. P. J. Van Soest, "Nutrition Ecology of Ruminant", 2nd Ed., Cornell University, New York, 1994.